Ministère de l'Enseignement Supérieur et de la Recherche Scientifique

Université Hassiba Benbouali de Chlef

Faculté de Technologies

Département d'électrotechnique

THÈSE

Présentée pour l'obtention du diplôme de

DOCTORAT

Filière : électrotechnique

Spécialité : Electrotechnique des Energies renouvelables

Par

Maamar SOUAIHIA

Thème:

ETUDE ET DIAGNOSTIC DES BATTERIES DEDIES AUX SYSTEMES PHOTOVOLTAIQUES

(Study and diagnosis of batteries dedicated to photovoltaic systems)

Soutenue le 04/06/2020, devant le jury composé de :

Abdelkader DJAHBAR	Professeur	Université de Chlef	Président
Bachir BELMADANI	Professeur	Université de Chlef	Rapporteur
Rachid TALEB	Professeur	Université de Chlef	Examinateur
Abdallah ZEGAOUI	MCA	Université de Chlef	Examinateur
Youcef BOT	MCA	Université de Khemis Miliana	Examinateur
Toufik TAHRI	Professeur	Université de Chlef	Examinateur

Anneé universitaire : 2019/2020

ABSTRACT

The increasing demand for Photovoltaic energy has led to technological advancements in the field of battery technology. State of charge (SOC) estimation is a fundamental function of the battery management system, which is a key to modelling, managing the Lithium-ion battery system. Numerous methods have been developed to estimate the SOC based on the terminal voltage and current measurements of battery.

The purpose of this thesis is to establish a robust mapping between open circuit voltage (OCV) and SOC, beside that developing a performed algorithm for SOC estimation with less parameters based on simple electrical circuit model (ECM). An algorithm is capable to track SOC with high precision, take in consideration of low memory and flexible with initial uncertainties.

To solve the previous problem, an adaptive extended Kalman filter (EKF) have been adopted and compared with a sliding mode observer (SMO). The results show better speed tracking performance at dynamic and steady state. However, the SMO algorithm provides a better performance, acceptable estimations errors, robustness in different tests compared to the Kalman filter.

Keywords: State of charge, Battery management system, Kalman filter, Sliding mode observer, Lithium-ion battery, Photovoltaic.

RESUME

La demande croissante en énergie photovoltaïque nous a conduit envers des technologies développées dans le domaine de batterie. L'estimation de l'état de charge (SOC) est une fonction essentielle du système de la gestion de la batterie, qui est considéré comme un élément clé de la modélisation, de la gestion du système de batterie lithium-ion. De nombreuses méthodes ont été développées pour estimer le SOC basées sur des mesures de tension et de courant aux bornes de la batterie.

Le but de cette thèse est d'établir une cartographie robuste entre la tension en circuit ouvert (OCV) et le SOC, en plus de développer un algorithme pour l'estimation du SOC avec moins de paramètres basé sur un simple modèle de circuit électrique (ECM). Un algorithme capable de suivre le SOC avec une grande précision, en tenant compte de la faible mémoire et flexible avec les incertitudes initiales.

Pour résoudre le problème précédent, un filtre de Kalman adaptatif étendu (EKF) a été adopté et comparé à un observateur en mode glissant (SMO). Les résultats montrent de meilleures performances de la vitesse de suivi à l'état dynamique et stable. Cependant, l'algorithme SMO offre de meilleures performances, des erreurs d'estimation acceptables, une robustesse dans différents tests par rapport au filtre de Kalman.

Mots clé : Etat de charge, Système de gestion de batterie, Filtre de Kalman, Observateur en mode glissant, Lithium-ion batterie, Photovoltaïque

ملخص الدراسة

أدى الطلب المتزايد على الطاقة الكهروضوئية إلى التقدم التكنولوجي في مجال تكنولوجيا البطاريات. تقدير حالة شحن البطارية (**SOC**) هي وظيفة أساسية في جهاز نظام تسيير البطارية ، وهي مفتاح نمذجة ، وتسيير بطارية ليثيوم أيون. تم تطوير العديد من الطرق أو الأنماط لتقدير حالة الشحن (**SOC**) استنادًا إلى قياسات الجهد الطرفي (فرق الكمون) و شدة التيار للبطارية.

الغرض من هذه الأطروحة هو إنشاء خريطة قوية تربط جهد الدارة المفتوحة (**OCV**) مع حالة الشحن للبطارية (**SOC**). الى جانب ذلك، تطوير خوارزمية لتقدير حالة الشحن (**SOC**) بإعدادات أقل بناءً على نموذج دارة كهربائية بسيطة. خوارزمية قادرة على تتبع حالة الشحن بدقة عالية، مع مراعات سعة ذاكرة منخفضة و مرونة التعامل مع الحالات الابتدائية غير المؤكدة.

لحل المشكلة السابقة ، تم اعتماد مرشح كالمان الموسع المتكيف (**EKF**) و مقارنته بنظام مراقبة ذو النمط الإنزلاقي (**SMO**). حيث تظهر النتائج سرعة تتبع أفضل في الحالتين الديناميكية والثابتة. ومع ذلك ، توفر خوارزمية (**SMO**) أداء أفضل وأخطاء تقديرات مقبولة ومتانة في الاختبارات المختلفة بالمقارنة مع مرشح كالمان.

الكلمات المفتاحية : حالة الشحن، نظام تسيير البطارية ، مرشح كالمان ،مراقب ذو النمط المنزلق ، بطارية ليثيوم-إيون ، خلية ضوئية

ACKNOWLEDGMENTS

Praise to **"Allah"** who gave me the faith, courage and patience to complete this research in better and good conditions.

First of all, I would like to thank my supervisor **Pr. Bachir BELMADANI**, lecturer at the department of electrical engineering of Chlef University and director of laboratory of research: 'Laboratory of Electrical Engineering and Renewable Energy' for giving me all the help to do this research, for all patience, guidance and support during the realization of this work.

I express my sincere gratitude to the members of my graduate study committee: President of committee member, **Pr. Abdelkader DJAHBAR** lecturer at the University of Chlef, and the members of the jury: **Dr. Abdallah ZEGAOUI** lecturer at the University of Chlef, and **Pr. Toufi TAHRI** lecturer at University of Chlef, and **Dr. Youcef BOT** lecturer at the University of Khemis Miliana, for taking the time for revise my thesis and to serving on my committee and for their valuable advice and help. I am thankful that in the midst of all their activities, they accepted to be members of the reading committee.

I would also express my very great appreciation to **Pr. Rachid TALEB** lecturer at Department of Electrical Engineering of Chlef University, for his invaluable help and for his willingness to give me his time whenever I need his help from him.

Finally, I especially thank **my parents**, for their unconditional support throughout these long years of study.

DEDICATION

This thesis is dedicated to my great parents who have raised me to be the person I am today. Thank you for your unconditional and never ending love, and for your support that you have always given to me, thank you for everything.

To my dear wife for her help and support. To my dear brothers: **Yahia, Aissa, M'hammed, Ahmed and Abdelkader.**

I would also mention and send a special Thanks to my nephew **Abdelkader BOUCHAHDA** who has supported me endlessly with his love. I would like to thank my nieces who continually remind me to enjoy the little things in life and never give up.

To my close friends for theirs supports and caring.

To my dear sisters for their love and support.

To all my nephews and sweet nieces.

To all my family Souaihia, Bouchahda, Toumir and Hassainia.

To all my relatives, friends and colleagues.

To all my teachers throughout my career of study.

To all lecturers in the Department of Electrical Engineering of Chlef university.

To my parents, I dedicate this thesis.

SOUAIHIA Maamar

TABLE OF CONTENTS

ABSTRACT ..... **I**

ACKNOWLEDGMENTS ..... **IV**

DEDICATION ..... **V**

TABLE OF CONTENTS ..... **VI**

LIST OF FIGURES ..... **XI**

LIST OF TABLES ..... **XVI**

LIST OF ABBREVIATIONS ..... **XVII**

LIST OF SYMBOLS ..... **XIX**

General introduction **2**

Thesis motivation **2**

Scope and objectives **3**

Thesis organization **3**

Chapter 1

Photovoltaic and batteries generalities

1.1. Introduction **6**

1.2. Photovoltaic system architecture **7**

1.2.1. Stand-alone system PV **7**

1.2.2. Hybrid PV systems **8**

1.2.3. Grid-connected PV systems **10**

1.3. Solar cells **11**

1.4. Photovoltaic generator **11**

1.5. Modelling a photovoltaic cell **12**

1.5.1. Single diode model **12**

1.5.2. Double diode model **14**

1.6. Overview of battery technologies **15**

1.7. Construction of battery **15**

1.8. Battery electrochemical principle **18**

1.9. Battery type and potential **19**

1.9.1. Lead-Acid batteries **19**

1.9.2. Nickel-Cadmium battery 20
1.9.3. Lithium-Ion battery 21
1.10. Battery classification 22
1.10.1. Primary batteries 22
1.10.2. Secondary batteries 23
1.11. Specifications by battery chemistry 23
1.12. Batteries comparison 25
1.13. Battery terminology 26
1.13.1. Terminal voltage 26
1.13.2. Open circuit voltage 26
1.13.3. Capacity 26
1.13.4. Internal resistance 26
1.13.5. Usable power 27
1.13.6. Cut off voltage 27
1.13.7. Full voltage 27
1.13.8. Stored Energy 27
1.13.9. Self-discharge phenomenon 27
1.13.10. Life cycle 27
1.13.11. Charge rate 28
1.13.12. Notion cell, module and packs 28
1.14. State of charge (SOC) 29
1.15. Depth of discharge 30
1.16. State of health (SOH) 30
1.17. Conclusion 30

Chapter 2

SOC estimation review

2.1. Introduction 33
2.2. Battery management system 33
2.3. Profile of charge and discharge batteries 35
2.3.1. Constant Voltage Charge (CV) 36
2.3.2. Constant current (CC) charge 36

2.3.3. Combined charge Protocol CC-CV 37
2.3.4. Discharge regime 37
2.4. Internal states relationships 37
2.5. State of charge estimation methods 39
2.5.1. Coulomb-counting method 39
2.5.2. Open circuit voltage method 39
2.5.3. Model-based methods 41
2.5.3.1. Kalman filter based methods 42
2.5.3.2. Sliding-mode observer 43
2.5.3.3. Particle filter 44
2.5.3.4. H-infinity observer 45
2.5.3.5. Proportional-Integral observer 46
2.5.4. Machine learning methods 47
2.5.4.1. Artificial neural network 47
2.5.4.2. Support vector machine 48
2.5.4.3. Fuzzy logic 49
2.6. Conclusion 50

Chapter 3

Battery modelling

3.1. Introduction 53
3.2. What's the importance of modelling a battery? 54
3.3. Battery models 54
3.3.1. Electrochemical models 55
3.3.2. Thermal model 59
3.3.3. Mathematical models 60
3.3.3.1. Behavioural model 60
3.3.3.2. Shepherd model 62
3.3.3.3. Electrical equivalent circuit models 62
3.3.3.3.1. Simple battery model 63
3.3.3.3.2. Partnership for a new generation of vehicle (PNGV) model 65
3.3.3.3.3. Thevenin Model 66

3.3.3.3.4. Dynamic model 68
3.3.3.3.5. Second-order Thevenin model 69
3.3.3.3.6. Third-order Thevenin model 70
3.3.3.3.7. N-order Thevenin model 71
3.3.3.3.8. Resistor-Capacitor (RC) model 72
3.3.3.3.9. Hybrid model 73
3.4. Conclusion 73

Chapter 4

Battery SOC estimation based on EKF and SMO observers

4.1. Introduction 75
4.2. Estimation technique 75
4.3. Kalman filter observer 76
4.3.1. Kalman filter 77
4.3.2. The extended Kalman filter (EKF) 79
4.3.3. The adaptive extended Kalman filter (AEKF) 82
4.3.4. State of Charge Estimation using KF 84
4.3.4.1. Partnership for a new generation of vehicle (PNGV) model 85
4.3.4.2. 1st order Thevenin model 86
4.3.4.3. 2nd order Thevenin model 86
4.3.4.4. 3rd order Thevenin model 86
4.3.5. OCV-SOC mapping 86
4.3.5.1. Partial derivatives 87
4.3.5.2. Proposed model 95
4.4. Sliding mode observer 106
4.5. Sliding mode control history 106
4.5.1. Basic of sliding mode concepts 106
4.5.2. Sliding surface choice 108
4.6. Conditions of existence and convergence of the sliding mode 109
4.7. Drawback of sliding mode control 109
4.8. Sliding Mode Observer structure 110
4.9. Solving the chattering problem 111

4.10. Application of sliding mode in battery SOC estimation 112
4.10.1. Conventional sliding mode observer design 113
4.10.2. Modified sliding mode observer design 116
4.11. Comparison between EKF and SMO 118
4.12. Conclusion 121
General conclusion 123
Summary of research 124
Recommendations and future work 125
Appendices 126
Appendix A 127
Appendix B 130
References 133

LIST OF FIGURES

FIGURE (1-1): APPLICATION OF PHOTOVOLTAIC SYSTEM [5]. 6

FIGURE (1-2): GENERAL SCHEMATIC OF A PV SYSTEM 8

FIGURE (1-3): CONNECTION DIAGRAM FOR A HYBRID INSTALLATION [7]. 9

FIGURE (1-4): DIAGRAM OF AN AUTONOMOUS INSTALLATION OF SOLAR WATER PUMPING TYPE [9]. 9

FIGURE (1-5): DIAGRAM OF A PV SYSTEM CONNECTED TO THE GRID, WITH BATTERIES [10]. 10

FIGURE (1-6): PHOTOVOLTAIC CELL BASIC OPERATION [11]..... 11

FIGURE (1-7): CONCEPT OF CELL, MODULE, AND PHOTOVOLTAIC PANEL [12]. 12

FIGURE (1-8): SCHEMATIC OF THE SINGLE DIODE MODEL [13]..... 13

FIGURE (1-9): SCHEMATIC OF THE DOUBLE DIODE MODEL [15]. 14

FIGURE (1-10): EXPLODED PRISMATIC STRUCTURE USED FOR LEAD ACID BATTERY (TYPE VRLA)[19]. 17

FIGURE (1-11): EXPLODED CYLINDRICAL STRUCTURE VIEW OF THE DIFFERENT ELEMENTS OF LI-ION CELL (ALSO USED FOR NI-CAD AND NI-MH BATTERIES) [18]. 18

FIGURE (1-12): DIAGRAM OF BATTERY CHEMICAL OPERATIONS 19

FIGURE (1-13): RAGONE PLOT OF VARIOUS ENERGY STORAGE TECHNOLOGIES [36] 25

FIGURE (1-14): BATTERY PACKS CONNECTIONS. 28

FIGURE (1-15): STATE OF CHARGE. 29

FIGURE (2-1): BLOCK DIAGRAM OF BATTERY MANAGEMENT SYSTEM. 34

FIGURE (2-2): BMS MAIN FUNCTIONS. 35

FIGURE (2-3): CHARGE PROFILE CONSTANT CURRENT (CC), CONSTANT VOLTAGE (CV)..... 36

FIGURE (2-4): RELATIONSHIPS OF BATTERY STATES..... 38

FIGURE (2-5): THE OCV-SOC CURVE OF A LEAD-ACID BATTERY CELL..... 40

FIGURE (2-6): SCHEMATIC OF BATTERY MODEL-BASED SOC ESTIMATION METHODS..... 41

FIGURE (2-7): CLASSIFICATION THE APPROACHES FOR SOC ESTIMATION 49

FIGURE (3-1): BASIC REACTIONS DIAGRAM OF A LITHIUM-ION CELL..... 55

FIGURE (3-2): SCHEMATIC OF A LITHIUM-ION BATTERY ELECTROCHEMICAL MODEL..... 56

FIGURE (3-3): SCHEMATIC OF THERMAL MODEL [105]..... 59

FIGURE (3-4): AVAILABLE CAPACITY AT PEUKERT'S COEFFICIENT 1.08-1.5 [107]..... 61

FIGURE (3-5): SCHEMATIC OF SIMPLE BATTERY MODEL..... 63

FIGURE (3-6): THE AVERAGE HYSTERESIS BETWEEN CHARGE AND DISCHARGE..... 64

FIGURE (3-7): SCHEMATIC OF HYSTERESIS MODEL. 65

FIGURE (3-8): SCHEMATIC OF PARTNERSHIP FOR A NEW GENERATION OF VEHICLE MODEL [113]. 66

FIGURE (3-9): SCHEMATIC OF THE FIRST-ORDER THEVENIN MODEL..... 67

FIGURE (3-10): SCHEMATIC OF THE DYNAMIC MODEL..... 68

FIGURE (3-11): SCHEMATIC OF THE SECOND-ORDER THEVENIN MODEL (DP). 69

FIGURE (3-12): THE THIRD-ORDER THEVENIN MODEL..... 70

FIGURE (3-13): THE N-ORDER RANDLE MODEL..... 71

FIGURE (3-14): RESISTOR-CAPACITOR MODEL. 72

FIGURE (3-15): SCHEMATIC OF HYBRID MODEL WITH TWO STAGES..... 73

FIGURE (4-1): GENERAL BLOCKS OF STATE ESTIMATOR. 76

FIGURE (4-2): BLOCK DIAGRAM OF DISCRETE KALMAN FILTER SYSTEM. 77

FIGURE (4-3): OVERVIEW OF PREDICTOR-CORRECTOR TECHNIQUE. 78

FIGURE (4-4): OVERVIEW ON GENERAL EXTENDED KALMAN FILTER EQUATIONS..... 81

FIGURE (4-5): PRESENTATION OF INTERNAL STATES ESTIMATION. 84

FIGURE (4-6): OCV-SOC RELATIONSHIP MAPPING FOR LITHIUM-ION BATTERY. 87

FIGURE (4-7): PARTIAL DERIVATIVE OF VOC WITH RESPECT TO SOC CURVE. 88

FIGURE (4-8): THE TRANSIENT RESPONSE FOR A PULSE DISCHARGE CURVE. 89

FIGURE (4-9): THE PLATFORM OF THE EXPERIMENT. 90

FIGURE (4-10): PULSE CURRENT DISCHARGE. 91

FIGURE (4-11): THE TERMINAL VOLTAGE RESPONSE LI-ION BATTERY. 92

FIGURE (4-12): THE TRANSIENT RESPONSE FOR A PULSE DISCHARGE. 92

FIGURE (4-13): THE CALCULATED Rs VALUE VERSUS SOC..... 94

FIGURE (4-14): THE $R1$ VALUE VERSUS SOC. 94

FIGURE (4-15): THE $C1$ VALUE VERSUS SOC. 95

FIGURE (4-16): FITTED OCV RESULTS AT 25°C. 98

FIGURE (4-17): EKF SIMULATION BASED ON OCV MODELS. 98

FIGURE (4-18): COMPARISON BETWEEN EXPERIMENTAL SOC AND AEKF ESTIMATED SOC UNDER DISCHARGE TEST. 99

FIGURE (4-19): COMPARISON BETWEEN EXPERIMENTAL SOC AND EKF ESTIMATED SOC UNDER PULSE CURRENT 0.4 C..... 100

FIGURE (4-20): COMPARISON BETWEEN EXPERIMENTAL SOC AND EKF ESTIMATED SOC UNDER PULSE CURRENT 0.5 C..... 100

FIGURE (4-21): COMPARISON BETWEEN EXPERIMENTAL SOC AND EKF ESTIMATED SOC UNDER PULSE DISCHARGE CURRENT 1C..... 101

FIGURE (4-22): THE SOC ESTIMATION WITH INITIAL VALUE OF 0.6 FOR FIRST ORDER THEVENIN MODEL 102

FIGURE (4-23): THE SOC ESTIMATION ERROR OF FIRST ORDER THEVENIN MODEL..... 102

FIGURE (4-24): THE SOC ESTIMATION WITH INITIAL VALUE OF 0.6 FOR SECOND ORDER THEVENIN MODEL 103

FIGURE (4-25): THE SOC ESTIMATION ERROR OF SECOND ORDER THEVENIN MODEL..... 103

FIGURE (4-26): THE SOC ESTIMATION FOR INITIAL VALUE OF 0.6 OF THIRD ORDER THEVENIN MODEL..... 104

FIGURE (4-27): THE SOC ESTIMATION ERROR OF THIRD ORDER THEVENIN MODEL..... 104

FIGURE (4-28): THE TERMINAL VOLTAGE AND ERROR OF ESTIMATION. 105

FIGURE (4-29): PRINCIPLE CONCEPTS OF THE SLIDING MODE CONTROL. 107

FIGURE (4-30): PROBLEM OF CHATTERING PHENOMENON. 110

FIGURE (4-31): SLIDING MODE OBSERVER STRUCTURE..... 110

FIGURE (4-32): CSMO BASED SOC ESTIMATION WITH LARGE GAINS. 115

FIGURE (4-33): CSMO BASED SOC ESTIMATION WITH LOW GAINS..... 116

FIGURE (4-34): SATURATION FUNCTION 118

FIGURE (4-35): SOC ESTIMATED UNDER 1C-RATE CURRENT PROFILE. 119

FIGURE (4-36): SOC ESTIMATED UNDER 1C-RATE PULSE CURRENT PROFILE. 119

FIGURE (4-37): SOC CONVERGENCE FOR BOTH ALGORITHMS AT DIFFERENT INITIAL SOCS. 120

FIGURE (A-1): SCHEMA BLOCK OF THE BATTERY MODEL IN MATLAB/SIMULINK. 127

FIGURE (A-2): A VIEW OF THE ACQUISITION PROGRAM USED IN COLLECTING EXPERIMENTAL DATA. 127

FIGURE (A-3): PHOTO OF THE TEST BENCH OF THE EXPERIMENT 128

FIGURE (A-4): MATLAB/SIMULINK SCHEMATIC BLOCKS OF EXPERIMENT. 129

FIGURE (B-1): DATASHEET OF CURRENT SENSOR LA55..... 130

FIGURE (B-2): DATASHEET OF CURRENT VOLTAGE SENSOR LA55..... 131

LIST OF TABLES

TABLE (1-1): CLASSIFICATION OF DIFFERENT BATTERY TYPES IN PRIMARY OR SECONDARY CELLS 22

TABLE (1-2): COMPARATIVE SPECIFICATIONS BETWEEN DIFFERENT BATTERIES TYPES [18].24

TABLE (2-1): THE COMPARISON OF DIFFERENT SOC ESTIMATION METHODS REGARDING TO THEIR COMPLEXITY AND ACCURACY [1]. 50

TABLE (3-1): THERMAL MODEL PARAMETERS. 60

TABLE (4-1): ALGORITHM FOR COMPUTING THE PARTIAL DERIVATIVE $\partial Voc/\partial SOC$. 88

TABLE (4-2): VALUES OF RELATIONSHIP BETWEEN Voc-SOC OF LI-ION BATTERY..... 91

TABLE (4-3): OCV MODELS OVERVIEW 96

TABLE (4-4): CANDIDATE OCV MODELS. 96

TABLE (4-5): THE COEFFICIENTS OF THE FITTED OCV MODELS. 97

TABLE (4-6): COMPARISON BETWEEN THE OCV MODELS' ERROR PRECISION. 97

TABLE (4-7): THE RMSE OF SOC ESTIMATED FOR THIRD MODEL-BASED 105

TABLE (4-8): COMPARISON BETWEEN EKF AND MSMO TECHNIQUES. 120

TABLE (4-9): CONVERGENCE TIME AT DIFFERENT INITIAL SOCS..... 121

LIST OF ABBREVIATIONS

Abbreviation	Definition
AEKF	Adaptive extended Kalman filter
Ah	Ampere hour
ANFIS	Adaptive neuro fuzzy interface system
ANN	Artificial neural network
AUKF	Adaptive unscented Kalman filter
BMS	Battery management system
CC	Constant current
CDKF	Central difference Kalman filter
C-rate	Capacity rate
CSMO	Conventional sliding mode observer
CV	Constant voltage
DC	Direct current
DOD	Depth of discharge
DP	Dual polarity
ECC	Electrical equivalent circuit
ECM	Electrical circuit model
EKF	Extended Kalman filter
EM	Electrochemical model
EMF	Electromotive force
EOL	End of life
EV	Electric vehicle
FL	Fuzzy logic
GPV	Grid connected photovoltaic
HEV	Hybrid electrical vehicle
KF	Kalman filter
LA	Lead acid battery
LCD	Linear current decay load
Li-NMC	Lithium nickel manganese cobalt
Lithium-Ion	Li-ion battery
LTV	Linear time varying

mAh	Milli-ampere hour
MLCD	Modified Linear current decay load
Ni-Cd	Nickel cadmium battery
Ni-Mh	Nickel metal hydride battery
OCV	Open circuit voltage
PC	Personal computer
PDE	Partial differential equation
PF	Particle filter
PHEV	Plug-in Hybrid electrical vehicle
PI	Proportional integral observer
PNGV	Partnership for new generation of vehicles
PV	Photovoltaic
RBFNN	Radial basis function neural network
RC	Resistor capacitor
RMSE	Root mean square error
SLA	Sealed lead acid battery
SMC	Sliding mode control
SMO	Sliding mode observer
SOC	State of charge
SOE	State of energy
SOH	State of health
SOP	State of power
SPKF	Sigma point Kalman filter
SVM	Support vector machine
SVR	Support vector regression
UKF	Unscented Kalman filter
UPF	Unscented particle filter
UPS	Uninterruptible power supply
VRLA	Valve regulated lead acid battery

LIST OF SYMBOLS

Symbol	Definition
A	Ideality factor of diodes
A_k	Discrete system matrix
B	Boltzmann constant
B_k	Discrete system input matrix
C_c	The heat capacity of the battery core
C_e	Electrolyte concentration
C_s	Concentration of solid phase lithium
C_k	Discrete output system matrix
C_s	The heat capacity of the battery surface.
C_{surf}	The concentration of Lithium ions on the surface of the intercalation of electrode
C_{max}	The maximum concentration of Lithium ions in the intercalation of electrode
C_1	Polarisation capacitance
D_k	Discrete system input matrix
D_s	Solid phase diffusion coefficient of Li-ions for each electrode
e_k	The difference between y_k and the predicted observation $\hat{y}_k$
e_{VL}	Estimation errors
$f(.)$	Nonlinear function
F	Faraday's constant
F_k	Jacobian matrix of partial derivative of function f
$g(.)$	Nonlinear function
g_1	Switching gain
G_k	Jacobian matrix of partial derivative of function g
H_k	Innovative matrix of AEKF
I	The identity matrix
I_b	The charging current
I_{cc}	Constant current of charging
I_{dis}	Current of discharge
I_d	Current of diode
I_L	Applied current of the load
I_{ph}	Photo current
I_{sh}	Current of shunt

I_0	Current of saturation of diode
J	Current density at the surface of the spherical particle
k	Time step
K_1	Parameter related to temperature and discharge battery
L_k	Kalman gain
M	The size of moving estimation windows
pk	Peukert number
P_k	Matrix covariance
q	Charge of electron
Q_k	Matrix of system noise covariance of w_k
Q_n	Nominal capacity of battery
Q_r	Remaining battery capacity available
q_s	The instantaneous stored charge of battery
Q_{th}	Theoretical capacity of battery
R	Radius of particle for each electrode
R_c	Conduction resistance between T_c and T_s.
R_{em}	Empirical resistor
R_{gas}	Gas constant
R_k	Matrix of measurement noise covariance of v_k
R_s	Ohmic resistance
R_u	The convection resistance between T_f and T_s
R_1	Polarisation resistances
$S(x)$	Sliding surface
$sat(.)$	Saturation function
$sign(.)$	Signum function
$sigma$	The boundary of width for saturation function
$SOC(t)$	Actual or estimate state of charge
SOC_0	Initial state of charge
t	Sampling time
T	Ambient temperature
T_c	Temperature of core
t_{dis}	Total time of battery discharge
T_f	The ambient or coolant temperature of the system
T_s	Temperature of surface
u_k	Input vector of the system

V_{full}	Constant voltage of full charge
v_k	The measurement noise
V_L	Voltage of the load
$\hat{V}_L$	Estimated battery terminal voltage V_L
V_{oc}	Open circuit voltage
$V_{oc}(z)$	Open circuit voltage as a function of state of charge
$\hat{V}_{oc}$	Estimated open circuit voltage V_{oc}
V_r	Lyapunov function
$\hat{V}_1$	Estimated polarisation voltage V_1
$\hat{x}_{k+1/k}$	Approximate states vectors
y_k	Output vector of the system
$z(t)$	Actual state of charge
z_0	Initial state of charge
α_i	Slope for certain range of state of charge
β_i	Intercept for certain range of state of charge
η	Coulomb efficiency
μ	Constant number
δ	Specific interfacial area
$\Phi_s(0^+, t)$	Electric potential at the anode
$\Phi_e(0^-, t)$	Electric potential at the cathode

General introduction

General introduction

Recently, battery cells are increasingly used in many applications affecting our daily life, such as laptops computers, cell phones, digital cameras, other portable electronic devices also with stand-alone systems, and in the industry like Lead-acid and Lithium-Ion batteries. Batteries have gained attention in the past ten years because of their high energy density, slow loss of charge when it is free of use and lack of higher requirement for independent systems of the network.

Therefore, nowadays they use in new second generation of Hybrid Electric vehicles (HEV), Plug-in Hybrid Electrical Vehicles (PHEV) and hybrid stand-alone systems. As battery applications and usage increase, accurate management, monitoring and control techniques are needed to enhance the performance, efficiency, safety, reliability and long cycle of life for battery packs. Especially in the case of stand-alone systems, a battery management systems (BMS) play a fundamental role due to the battery operating conditions are subjected to fast transients and frequent charging and discharging cycles result of sudden power demand [1, 2].

Battery Management Systems (BMS) must be able to provide an accurate real-time estimate for the Battery State of Charge (SOC) and State of Health (SOH). The SOC value is so critical information for the BMS especially if the battery is the only source of power and the system is not connected to the network.

Since the SOC is not directly measurable or captured, it causes the main challenge of finding and proposing different estimation methods. In the literature, various strategies are settled for accurate SOC estimation based on different algorithms and techniques [1].

Thesis motivation

The motivation for this research thesis is guided by the world's need to reduce emission of carbon by using sustainable and renewable energy sources. Important considerations for photovoltaic energy and its integration into stand-alone systems or electric vehicles pay attention to energy storage and battery management systems.

Basically, homes can be fed by network electricity while countryside house or electric vehicle necessitates reliable power sources. Therefore, these power sources are formed by collecting batteries (battery packs). However, measuring the amount of useful energy remaining inside battery packs is becoming a challenge due to considering the battery as a black box [1].

Accordingly, this energy remaining is known as the SOC. It is not easy to measure since there is no sensor able to do that or the battery facing fast transients in terms of charging and discharging due to mission profile for a stand-alone system or the driving cycle in electrical vehicle.

Therefore, an accurate mathematical model for battery along with a robust technique for SOC estimation is necessary [3]. Another substantial consideration of the battery is the state of health (SOH), due to the importance of battery operation and management factors in extending and remaining useful battery life, which they often released by using model-based strategies [1, 3].

Scope and objectives

In this thesis, different battery modelling circuits and SOC estimations strategies are considered and compared with respect to their performances. The research objectives can be stated as follows:

- Battery cell models are selected, refined, implemented and validated using measured and simulated test data. The models considered can be categorized as: behavioural, equivalent circuit. However, experimental data used for model validation were obtained from prototype design in laboratory research.
- Estimation strategies were used for obtaining the SOC. These included the extended Kalman Filter (EKF) and sliding mode observer (SMO).

A comparative study of the battery models with estimation strategies lead to better performance of SOC.

Thesis organization

After the general introduction, which it gives an overview about the state of charge, existing methods of estimation and proposed strategies, which they will be treated in this

thesis concerning the estimation of the SOC. Therefore, the main body of the thesis is divided into four chapters:

Chapter 1 presents a literature review of the different types of photovoltaic systems. In addition, it highlights battery technologies, structure and application, followed by its famous terminologies.

Chapter 2 is dedicated to an overview on the various methods which has been used to estimate the state of charge of a battery, discussed and compared.

Chapter 3 presents the dissimilarity of variety of electrical circuit models of battery followed by their equations.

Chapter 4 presents analyse of the battery as a physical system that depends on the selected electrical circuit model, which involves the state of charge and the polarization effects. The polarization effects have been calculated by using mathematical model. The adaptive extended Kalman filter has been used to estimate the state of charge. Afterward, the sliding mode control has been applied and compared with the Kalman filter to show the highest precision algorithm.

Lastly, the thesis will be finished by a general conclusion, which is presenting the different results obtained and the constraints encountered. In addition, for the continuation of this research some potential applications of the proposed techniques and future perspectives are discussed.

Chapter 1
Photovoltaic and batteries generalities

1.1. Introduction

Photovoltaic energy is a promising solution to dispense with other forms of energy, which is known as a source of pollution and non-renewable. However, it has the disadvantage of having a low conversion yield of materials, the lack in pieces of information about the mastery part of storage device, which is usually presented by battery packs, and the cost which considers the highest comparing to other forms.

In addition, the increasing of this energy and high demand for it open another huge market concerning batteries sales due to their importance as portable energy storage devices and their eco-friendly characteristic.

In order to appreciate the implication of this energy and its advantages, we will try to enumerate the different domains that use this energy and the devices (subsystem or module) that allow its exploitation. Moreover, we will try to give a relevant overview of batteries terminologies with great focus into battery type's technology and provide an extended explanation on its terminologies and charge/discharge cycle [4].

The term "photovoltaic" comes from "photo" meaning light and word "Volt" named by Italian physicist Alessandro Volta (1745-1827), which means the production of electricity. Therefore, the process "photovoltaic" means the production of electricity directly from sunlight or light. The term "photovoltaic" is often referred to as "PV" [4].

Figure (1-1): Application of Photovoltaic system [5].

Nowadays, PV systems are installed by government or specific persons that are interested in the environment. Often, PV systems are embedded in many applications (Figure 1-1). For some applications where small amounts of electricity are needed, such as emergency boxes.

Therefore, PV systems are used even when the network is not very far for applications that necessitate larger amounts of electricity and they are located far from existing power lines. So, PV systems can be in many cases the most practical, and cheaper option.

However, the applications of energy generated using photovoltaic generators are extremely varied. In general, they can be classified in three major:

- Stand-alone PV systems
- Hybrid systems
- Grid-connected PV systems.

Other fields can use photovoltaic technologies as:

- Embedded systems (Phone, Net book, Tablet ... etc.)
- Space systems (satellites, Space Telescopes).

1.2. Photovoltaic systems architecture

Photovoltaic systems are generally categorized into three main systems. Their capacities range from a few kilowatts to hundreds of megawatts.

1.2.1. Stand-alone system PV

Stand-Alone PV stands for any system that relies solely on solar energy as a source of electrical energy and can range from milli-watts to kilowatts or more. These systems may include accumulators that store the energy produced by the PV modules during the day (sunshine phase) and serve during the night (dark phase) or during periods when solar radiation is insufficient. A general scheme of its installation is depicted in Figure (1-2). They can also meet the needs of an application without recourse to accumulators (for example, house PV installation) [6].

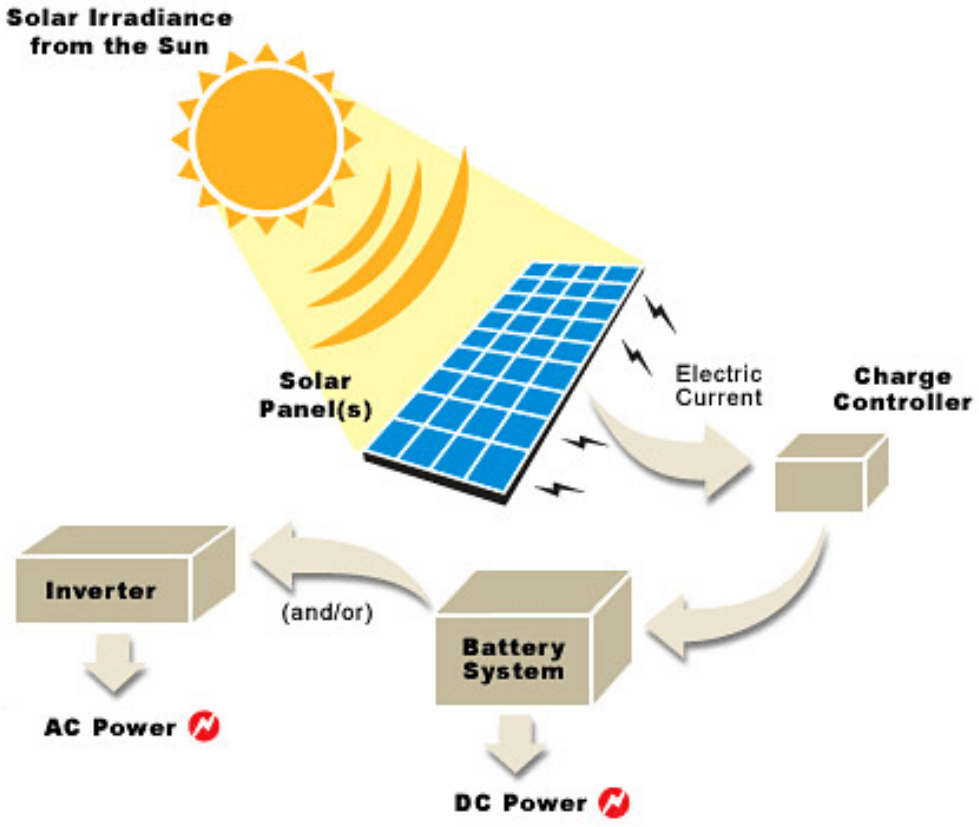

Figure (1-2): General schematic of a PV system

1.2.2. Hybrid PV systems

The hybrid systems, which are composed of a grid-connected photovoltaic (GPV) combined with a wind turbine or a fuel generator, or both. They are also isolated from electricity distribution systems.

They are such good choices for applications that require a continuous supply of relatively high power when there is not enough sunlight at certain times of the year, or if we want to reduce our investment in photovoltaic module fields and/or storage batteries as shown in Figure (1-3) [6, 7].

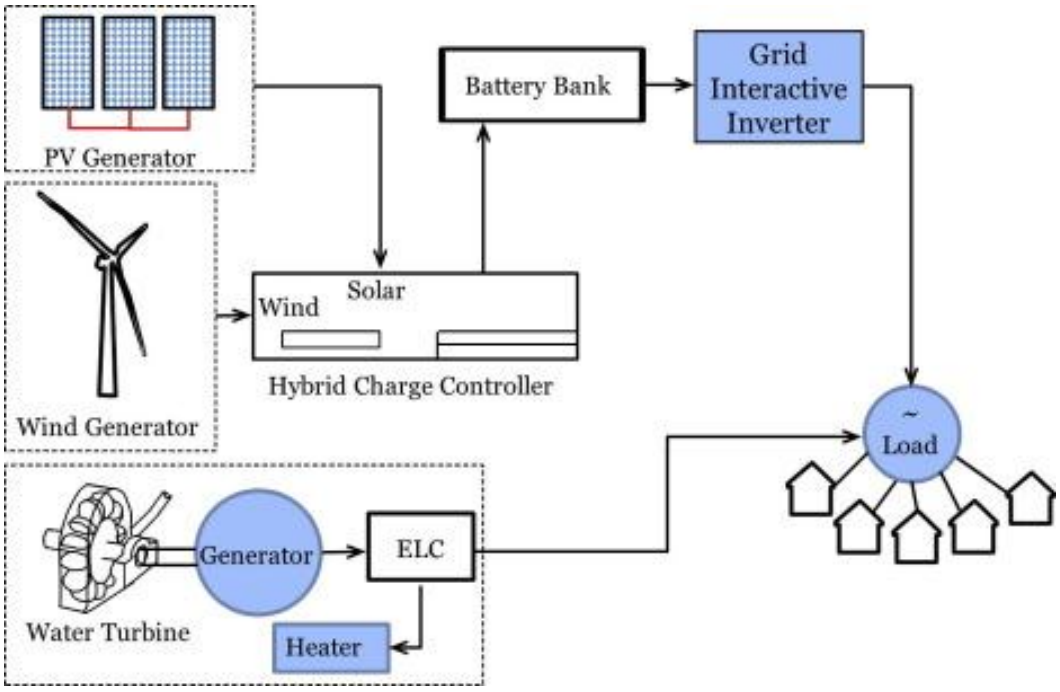

Figure (1-3): Connection diagram for a Hybrid installation [7].

Other photovoltaic systems can be also considered autonomous as the case of solar pumping water for irrigation or drinking. They can be also considered hybrid if the installation combines the system with another source of electrical energy as depicted in Figure (1-4) [8].

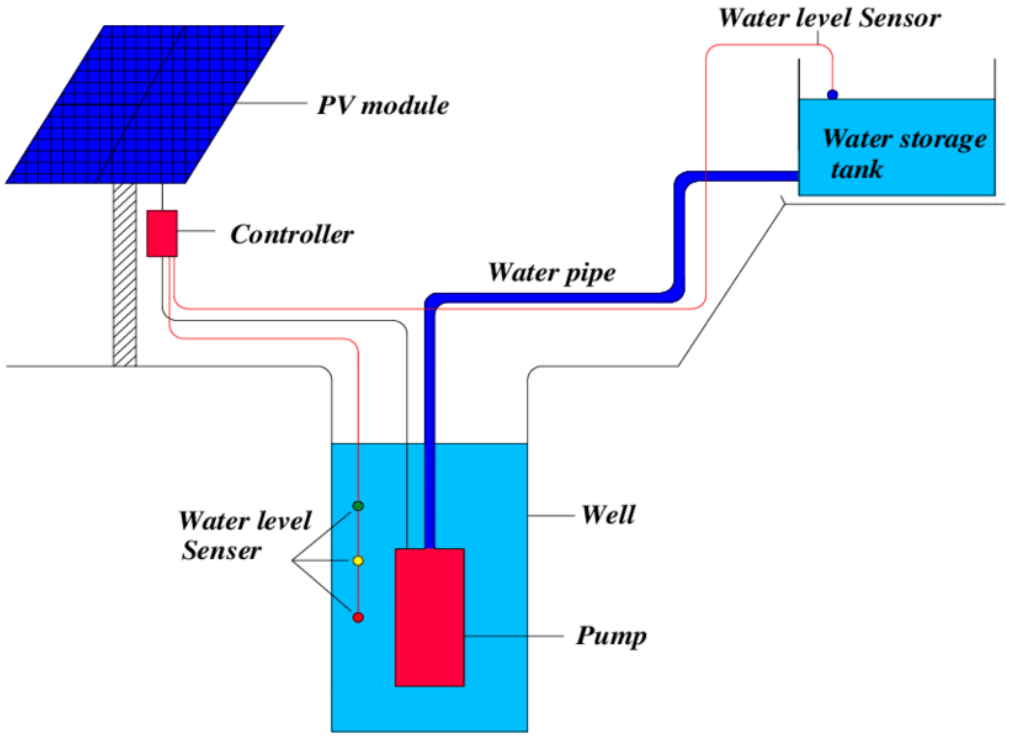

Figure (1-4): Diagram of an autonomous installation of solar water pumping type [9].

1.2.3. Grid-connected PV systems

Photovoltaic power systems connected to the grid, which are known as On-grid systems too, they are recent and innovative systems. They consist of a farm of photovoltaic panels and an inverter capable of transforming the energy supplied by the panels.

In this type of systems, the electric power is closer to the place of consumption. As well, they have the advantage of increasing the capacity of transmission and reducing the distribution lines. The injection of photovoltaic power into the grid needs such special installations where the inverter must contain a certain number of protections against bidirectional situation occur into the electricity grid as illustrated is Figure (1-5).

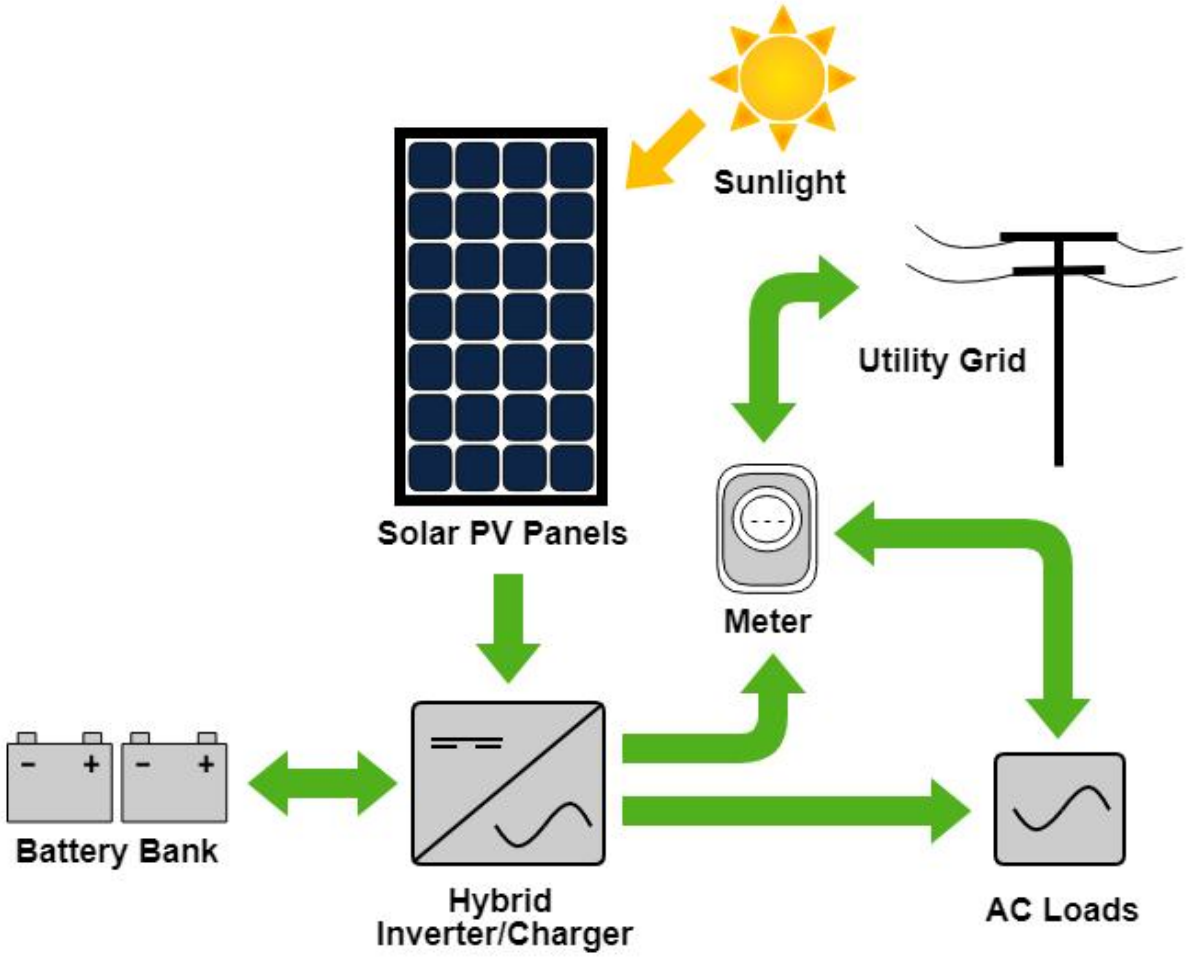

Figure (1-5): Diagram of a PV system connected to the grid, with batteries [10].

As a system connected to the grid, it produces its own electricity and sends its excess energy to the grid and gets supplies if necessary. Therefore, it is always possible to use these batteries as backup power when a network failure occurs.

1.3. Solar cells

At the heart of any photovoltaic system there is a solar cell, which also called photovoltaic cell. The cell consists of a photodiode, which works without external polarization. By converting the light directly into electricity, the cell delivers direct current (DC) into the load as shown in Figure (1-6). In addition, its generator has very low reverse breakdown voltage.

The diagram below depicts the operation of a basic solar cell. From physical view, solar cells made by a thin semiconductor wafer, which is specially treated to form an electric field, positive on one side and negative on the other. When light energy strikes the solar cell, electrons are knocked loose from the atoms in the semiconductor material [11].

If electrical conductors are attached to the positive and negative sides, forming an electrical circuit, the electrons can produce an electric current. That current is electricity. This electricity can then be utilized to power a load as illustrated in Figure (1-6).

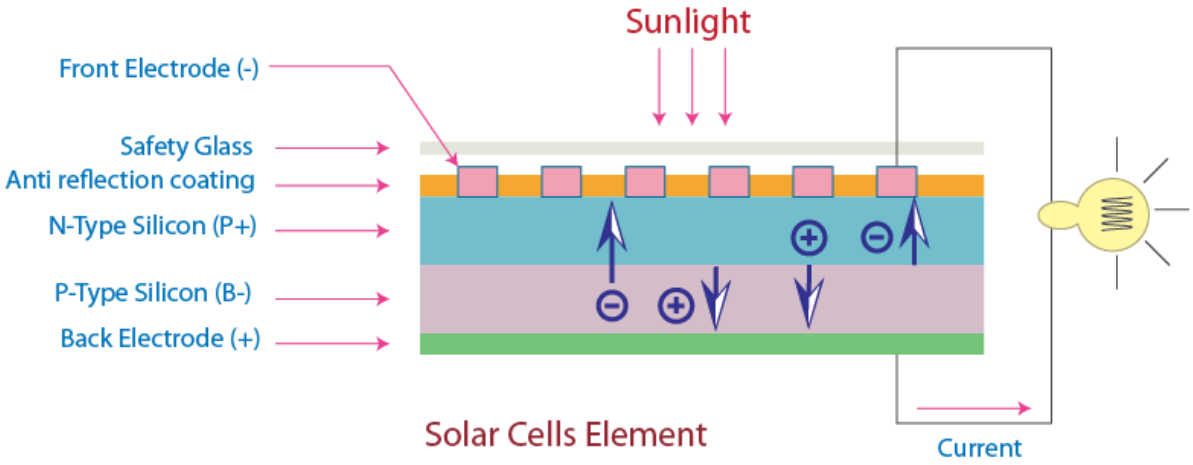

Figure (1-6): Photovoltaic cell basic operation [11].

1.4. Photovoltaic generator

A photovoltaic generator is a set of solar cells electrically connected in series and/or in parallel to generate the desired current and voltage. Depending on the application, a GPV can compose from a simple cell, module, and array until reaching the level of a photovoltaic field as depicted in Figure (1-7).

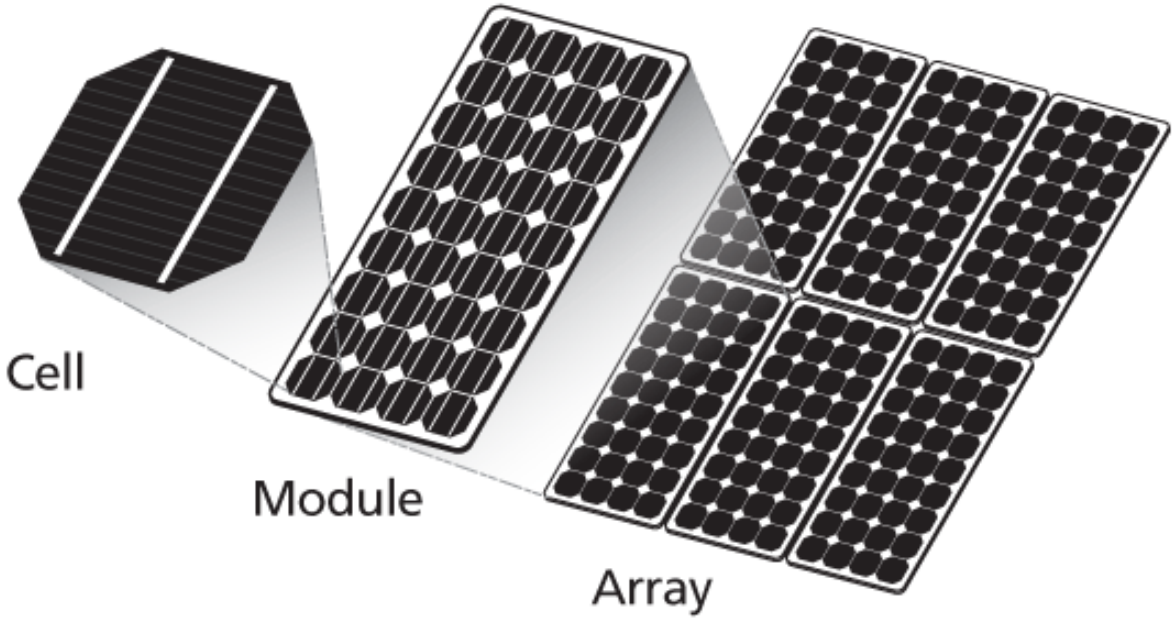

Figure (1-7): Concept of cell, module, and photovoltaic panel [12].

The serial connections of several cells increase the voltage for the same current, while the paralleling increases the current while maintaining the voltage. It is possible that the current of a cell can exceed 3A. However, the voltage remains low; it becomes obvious the use of serial connection to have a usable voltage [12].

1.5. Modelling a photovoltaic cell

The PV module can be modelled by modelling a cell, which can be represented by two different models.

1.5.1. Single diode model

In the model shown in Figure (1-8), the PV cell is represented by a current source parallel to a diode. The current source is represented by a current generated by the light I_{ph}. This current varies linearly with the variation of the solar radiation [13, 14].

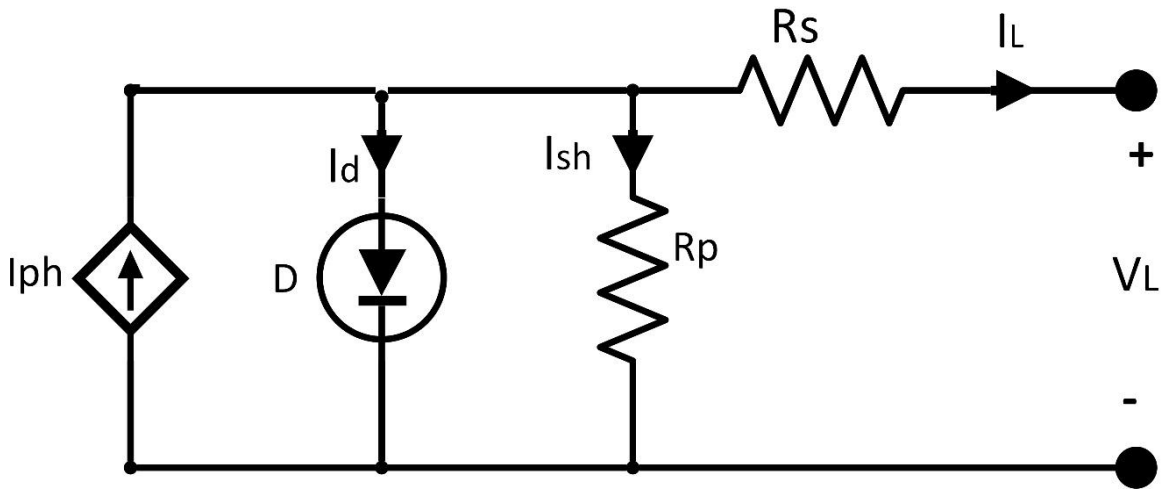

Figure (1-8): Schematic of the single diode model [13].

In accordance with the single diode model, the current I_{ph} can be expressed by the equation:

$$I_{ph} = I_d + I_L + I_{sh} \tag{1.1}$$

and the current across the diode by equation given:

$$I_d = I_0(exp\left(\frac{q(V_L + R_s I_L)}{ABT}\right) - 1) \tag{1.2}$$

where I_0 is the current of saturation of the diode (D). V_L is the solar cell output voltage and I_L is the current of the load.

By applying Kirchhoff's voltage law, we get the equation:

$$I_{sh}R_p = V_L + I_L R_s \tag{1.3}$$

To get the load current I_L we should substitute between (1.2) and (1.3), the final equation of the single diode model is:

$$I_L = I_{ph} - I_0\left(exp\left(\frac{q(V_L + R_s I_L)}{ABT}\right) - 1\right) - \frac{V_L + R_s I_L}{R_p} \tag{1.4}$$

where $\boldsymbol{q}$ is charge of the electron and its value is $1.602 * 10^{-19}$ C, $\boldsymbol{B}$ is the Boltzmann constant and its value is $1.380 * 10^{-23}$ J/K, and the $\boldsymbol{T}$ is the temperature of the solar cell that is 33° C which means 306.15 in Kelvin. $\boldsymbol{A}$ is the diode ideality factor.

1.5.2. Double diode model

This model contains, in addition, a second diode placed in parallel with the current source. This diode is included to improve the accuracy characteristics of the PV cell. In addition, it takes into account the difference in the current flow when the current is low due to the charge recombination in the region of depletion of the semiconductor. Figure (1-9) shows this model [15, 16].

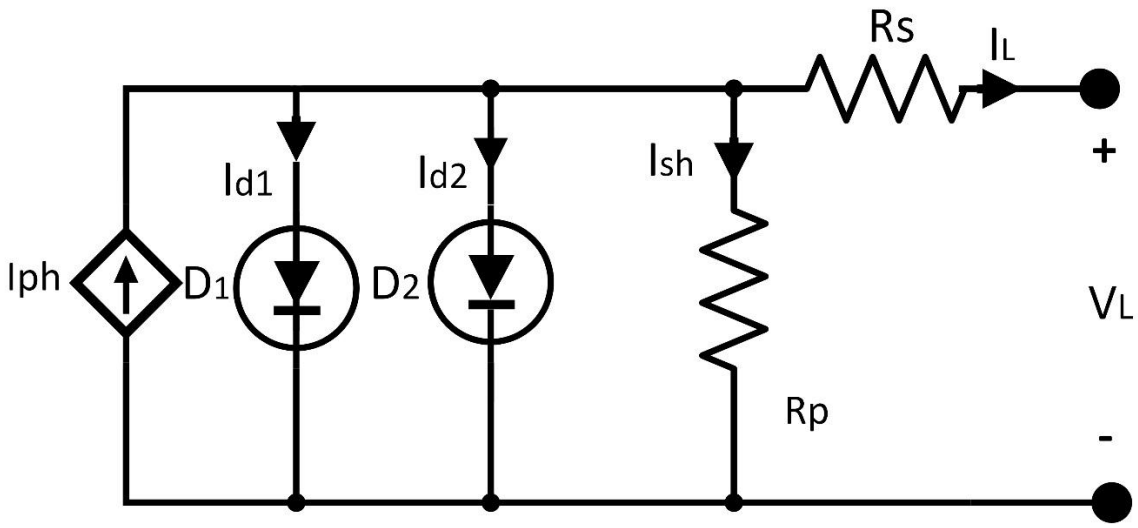

Figure (1-9): Schematic of the double diode model [15].

In accordance with the double diode model (D1) and (D2), the current I_{ph} can be formed by the equation:

$$I_{ph} = I_{d1} + I_{d2} + I_L + I_{sh} \tag{1.5}$$

and the current across the diodes their equations given:

$$I_{d1} = I_{01}(exp\left(\frac{q(V_L + R_s I_L}{A_1 BT}\right) - 1) \tag{1.6}$$

$$I_{d2} = I_{02}(exp\left(\frac{q(V_L + R_s I_L}{A_2 BT}\right) - 1) \tag{1.7}$$

I_{01} and I_{02} are the current of saturation of the two diodes respectively I_{d1} and I_{d2}. V_L is the solar cell output voltage and I_L is the current of the load.

The voltage of the load gets by applying Kirchhoff's voltage as:

$$I_{sh}R_p = V_L + I_L R_s \quad (1.8)$$

The final equation of the double diode model is:

$$I_L = I_{ph} - I_{01}\left(exp\left(\frac{q(V_L + R_s I_L)}{A_1 BT}\right) - 1\right) - I_{02}\left(exp\left(\frac{q(V_L + R_s I_L)}{A_2 BT}\right) - 1\right) - \frac{V_L + R_s I_L}{R_p} \quad (1.9)$$

where A_1 and A_2 represent the diode ideality constants.

1.6. Overview of battery technologies

Since the first development by Gaston Planté in 1859 of a rechargeable lead-acid battery, batteries have revolutionized the way in which energy is stored. Nowadays they have allowed a great mobility and independence for different sectors and applications were previously immobile like telecommunication, measuring instruments, medical equipment …etc. On the other hand, batteries are unavoidable solutions for aeronautics, space (satellites) and newly for smart phones, tablets and electric vehicles (EV) [17].

Through the almost worldwide encouragement of sustainable development and the exploitation of renewable energies to replace other forms of energy (fossil fuels, nuclear energy … etc.), batteries (accumulators) are put in value as a solution of storage of energy that can be easily recovered in electrical form by an induced discharge phase, and subsequently regenerate it during a charging phase.

Today's batteries have the advantage of being recycled because the majority of constituent components are recovered at their end of life (EOL) and can be reused to manufacture other.

1.7. Construction of battery

The battery consists of several electrochemical cells (element). Although the terms battery and cell are often used interchangeably, cells are modules (blocks) with which batteries are built.

The cells are assembled according to prismatic, cylindrical or other structures to end up having the elementary module or specific battery, which is designed in voltage, current and lifetime standards or for a determined application [18, 19].

The essential constituents of a battery are:

- **The galvanic cell:** This is the basic electrochemical block in a battery, consisting of a set of positive and negative plates divided by separators, immersed in the electrolyte solution and included in a tank. Each cell has a nominal voltage, for example 2.1Volts for a lead-acid battery, so there are six cells in series in a lead-acid battery of nominal voltage 12 Volts [20]. (see Figure (1-10))

- **Active ingredients:** This is forming the positive and negative plates. The energy released during their chemical reactions, allows the production of electrical energy. In a lead-acid battery, the active ingredients are lead dioxide (PbO_2) in the positive plates and lead (Pb) in the negative plates.

- **The grids:** whose role in a battery is to support the active ingredient in the plate, so it represents the support of this material to ensure the distribution of the current. In a lead-acid battery, the grid is an alloy of lead and antimony or calcium. These last two are used to strengthen the lead grid [19].

- **The electrolyte:** it represents the Conductive Channel in which the plates are immersed, and which allows the ionic exchanges between them. In the case of an open lead-acid battery, the electrolyte is a solution of sulfuric acid (30% H_2SO_4). This electrolyte can be gelled, as is the case of sealed lead-acid batteries (SLA) [20]. (see Figure (1-11))

- **The plates:** they are the basic elements of a battery, composed of grids and the active ingredient, sometimes called electrodes [19].

- **The plugs:** which allow the filling of the battery and the departure of the gases formed during the charge for the open batteries, in their places one can have valves in the case of the batteries of type "VRLA".

- **Separators:** These are micro porous sheets whose role is to prevent short circuits between plates of opposite natures; they complement the support of the active ingredient [18, 19].

- **Terminals:** Connect the battery to the external circuit.

- **Tray:** Made from a variety of materials, acid-resistant insulators, like plastic, ebonite or other materials.

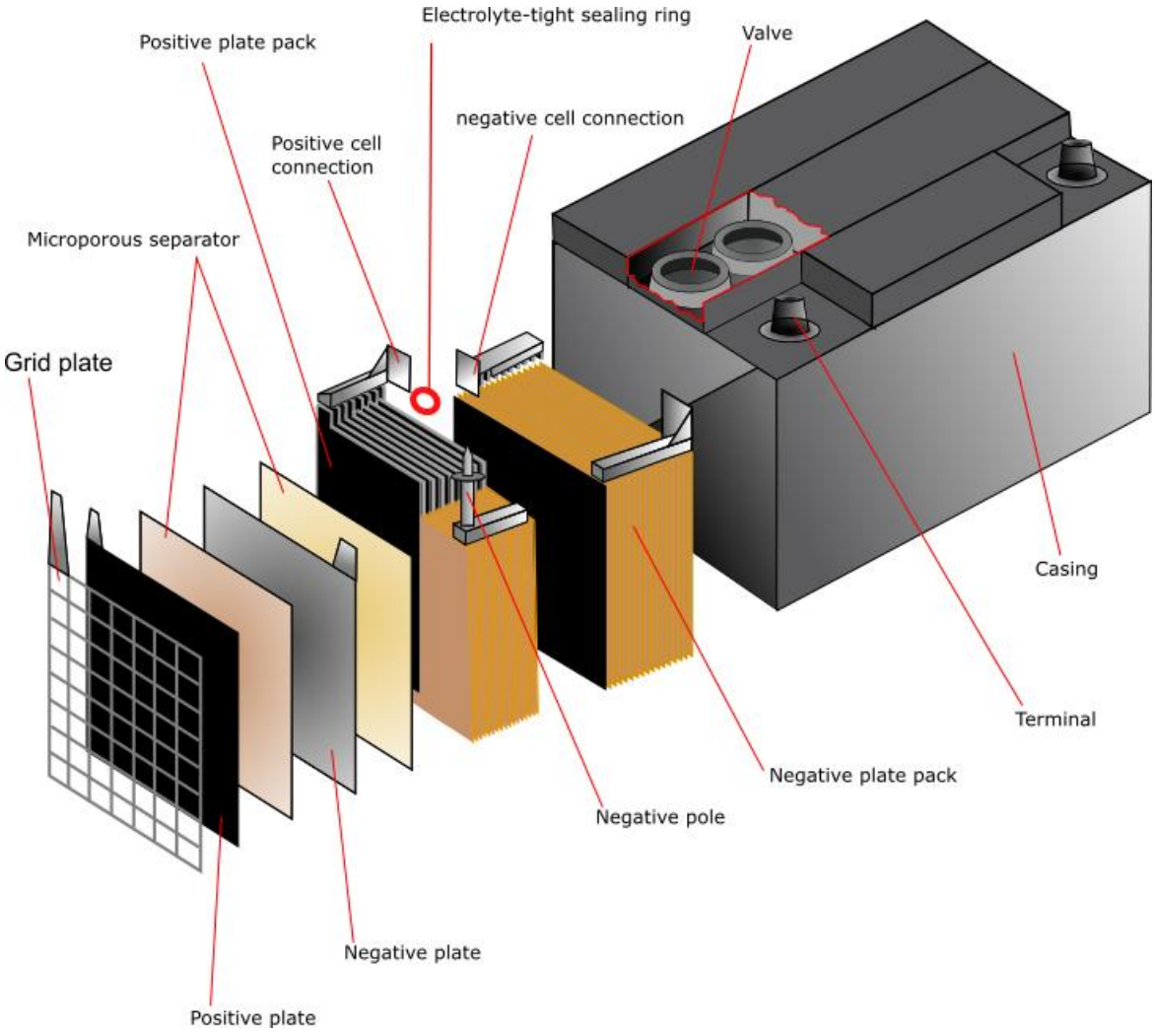

Figure (1-10): Exploded prismatic structure used for lead acid battery (Type VRLA)[19].

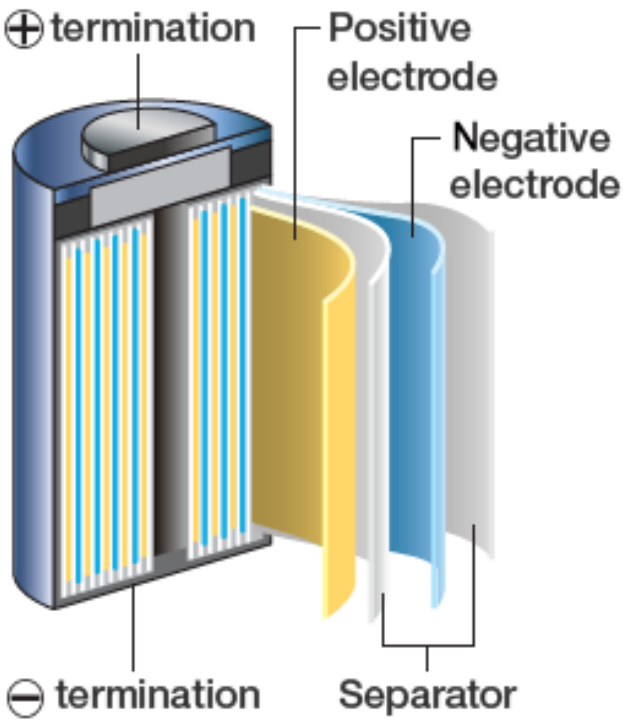

Figure (1-11): Exploded cylindrical structure view of the different elements of Li-Ion cell (also used for Ni-Cad and Ni-Mh batteries) [18].

1.8. Battery electrochemical principle

It is necessary to understand the basic chemical phenomena governing the operation which occur inside batteries in order to justify the choice of methods, models, and subsequently better interpret the results of these interactions. The schematic diagram of an electrochemical cell is shown in Figure (1-12).

During a discharge of the accumulator, the oxidation reaction that occurs at the anode releases one or more electrons in the external circuit. These electrons then circulate to the cathode where they participate in the reduction reaction (gain of one or more electrons). Simultaneously, the anions and cations migrate into the electrolyte solution between the two electrodes to preserve the charge balance. When the anode is completely oxidized (or the cathode completely reduced), these reactions are completed and the battery is discharged. As for the charge, it is carried out by applying an electric current to the electrodes in order to generate the opposite reactions [21, 22].

In discharge, the anode is the negative terminal of the battery and the cathode is the positive terminal. On the other hand, in the charging phase, the negative electrode is the

cathode and the positive is the anode, the electrons then flowing in the other direction [23].

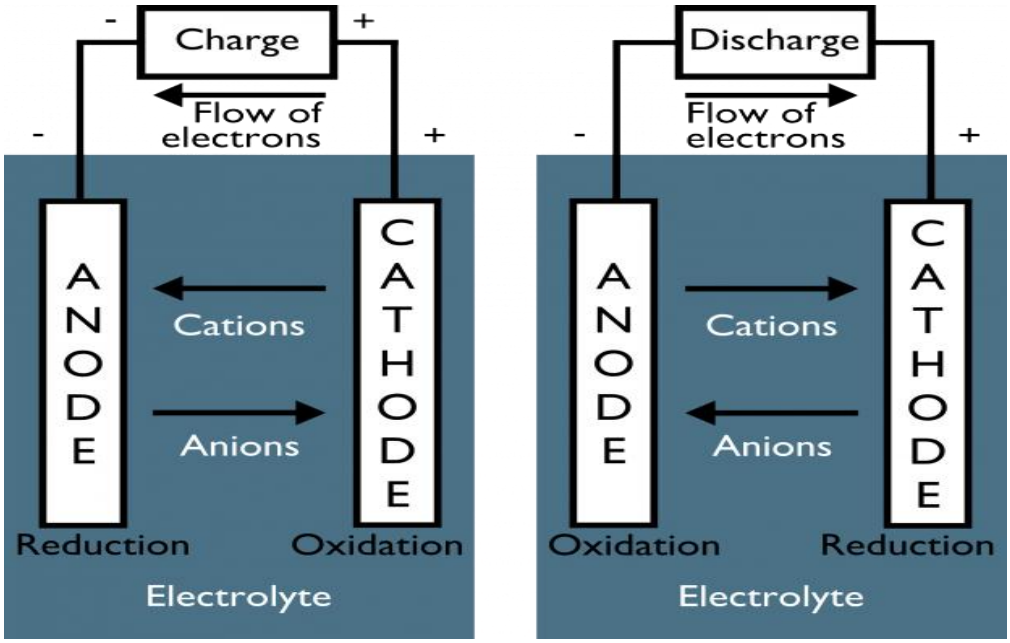

Figure (1-12): diagram of battery chemical operations

1.9. Battery type and potential

The battery potential reflects to the voltage nominal of the terminal voltage of battery cell, which is related to the cell cathode and anode type.

1.9.1. Lead-Acid batteries

Lead-acid batteries are one of the most popular and the oldest technology in batteries. In today's time, Lead-acid batteries have high reliability and low cost due to their mature technology [21]. Among the disadvantages of this technology are the low specific energy and the short service life [24].

Moreover, Lead-Acid batteries are in the foreground, at 65%, of the world battery market, given their involvement in the automotive sector, industrial traction applications and in isolated and emergency energy installations.

Lead-acid batteries are one of the most common secondary batteries, used primarily for storing large cell potential. These are commonly found in automobile engines. Its advantages include low cost, high voltage and large storage of cell potential; and disadvantages include heavy mass, incompetence under low-temperatures, and inability to

maintain its potential for long periods of time through disuse [25, 26]. The reactions of a lead-acid battery are shown below:

- cathode (reduction):

$$PbO_2 + HSO_4^- + 3H^+ \rightarrow PbSO_4 + 2H_2O$$

- Anode (oxidation)

$$Pb + HSO_4^- \rightarrow PbSO_4 + H^+ + 2e^-$$

- Overall

$$Pb + PbO_2 + 2HSO_4^- + 2H^+ \rightarrow 2PbSO_4 + 2H_2O$$

Discharging occurs when the load is connected and where the cell potential equals **2.02V**. Therefore, charging occurs when the car is in motion and where the electrode potential equals **-2.02V**, a non- spontaneous reaction which requires an external electrical source. The reverse reaction takes place during charging.

1.9.2. Nickel-Cadmium battery

The nickel-cadmium (Ni-Cd) pair was first exploited in 1890 by Waldemar JUNGER, which start in service as a battery at the beginning of the 20th century. It is another common secondary battery that is suited for low-temperature conditions with a long shelf life [27].

However, the nickel-cadmium batteries are more expensive and their capacity in terms of watt-hours per kilogram is less than that of the nickel-zinc rechargeable batteries [26, 28]. It has a potential equal to **1.29V**.

Nickel-cadmium battery has high specific energy with no degradation for deep charge/discharge cycles. However, cadmium is very toxic and it has high recycling cost, which is why its application has been limited. Besides, there exist other non-toxic compositions of nickel batteries, nevertheless, they suffer from memory, high self-discharge, high cost and shortened life [29].

The Ni-Cd memory effect, affected cells that were repeatedly only partially discharged. The result was that after multiple partial discharges the cell would only discharge to the level it had been repeated discharged to [29].

Furthermore, Nickel-Cadmium dominated portable and aerospace applications. Besides, more performance with even lighter and less bulky batteries is beneficed. Therefore,

research work has been conducted to allowing the implementation of other couples such as (Nickel-Metal-Hydride and Nickel-Hydrogen).

- cathode (reduction):

$$2NiO(OH) + 2H_2O + 2e^- \rightarrow 2Ni(OH)_2 + 2OH^-$$

- anode (oxidation):

$$Cd + 2OH \rightarrow 2Cd(OH)_2 + 2e^-$$

- overall:

$$Cd + 2NiO(OH) + 2H_2O \rightarrow 2Cd(OH)_2 + 2Ni(OH)_2$$

1.9.3. Lithium-Ion battery

Lithium-Ion (Li-ion) is the newest technologies, which is still under research and development. Among other different batteries technologies, Li-Ion shows promising application to electric vehicle (EV) due to their high specific energy, high voltage operation and long cycle of life.

Despite that, the cost still remains high and their life is significantly compromised by deep discharge cycles and is significantly affected to temperature [29, 30].

However, Lithium-ion batteries are ubiquitous in our daily lives. Most of us carry one around in our phone. There are several types of lithium-ion batteries. The main difference between them is their cathode chemistry such as:

- Lithium cobalt oxide (LiCoO2)
- Lithium iron phosphate (LiFePO4)
- Lithium manganese oxide (LiMn2O4),
- Lithium polymer
- Lithium nickel manganese cobalt oxide (LiNiMnCoO2 or NMC)

Different kinds of lithium-ion batteries offer different features, with trade-offs between cost, efficiency and safety. It has two attractive characteristics; light (6.94g / mol) and high energy density (3860 mAh / g), the latter has been studied since the 1950s.

However, the first commercial batteries in Li-Ion have emerged only since the beginnings of 1997. Today, several varieties are available, the most frequently used are Lithium-Ion (Li-Ion) and Li-Polymers (Li-Po), while the terminal voltage varies between **3 to 4.2V**.

- anode:

$$LiC_6 \rightarrow Li^+ + e^- + C_6$$

- cathode:

$$LiFe(III)PO_4 + xLi^+ + xe^- \rightarrow LiFe(II)PO_4$$

$$FePO_4 + Li^+ + e^- \rightarrow LiFePO_4$$

- The overall:

$$LiFePO_4 + 6C \rightarrow LiC_6 + FePO_4$$

1.10. Battery classification

The batteries are grouped under two main classes: primary (non-rechargeable) and secondary (rechargeable) accumulators. There are also other types of classifications based on a particular structure (technological design) or a defined field of use. In Table (1-1), it is shown a classification with several examples of both kinds of batteries [31].

Table (1-1): Classification of different battery types in primary or secondary cells

Primary batteries	Secondary batteries
Zinc Carbon, Lithium, Alkaline	Sealed Lead Acid, Lithium-Ion, Lithium-Polymer, Nickel Metal-Hydride, Nickel Cadmium

1.10.1. Primary batteries

They are unable to be electrically charged. They are used only once times, after they must be changed because the chemical reactions that governs them are irreversible. Besides, their price is relatively high.

However, primary batteries are very convenient for certain applications such as flashlight, instrumentation apparatus, toys, and launchers in the space field. The main advantages of a primary battery are a very high specific energy, appreciable service life, no

maintenance required, and ease of use.

1.10.2. Secondary batteries

A secondary battery is an electrochemical device for storing electricity and then restoring it on demand. This kind of battery can be electrically charged once discharged by the passage of an electric current through these electrodes in the opposite direction of the discharge current. This gives it its appearance as an electrical energy storage device known as the "Accumulator".

First application

In first case, the accumulators are used as a means of storing energy, which are generally connected to an electric source to be charged (alternator, electrical network, GPV system, etc.), a charge that consumes the energy delivered by the power supply. Also as an accumulator in discharge mode, for example, car, airplane electrical installations, satellite, uninterruptible power supply (UPS) [31].

Second application

In this case, they are used in place of primary batteries in discharge regime, thereby, the benefit of being rechargeable multiple times (cycles) rather than disposable is attained. By way of example, it can avoid changing them each time for certain stages, so this choice is a fort point made for certain stages of the launcher in order to cover the phases of the pre-launch tests and also to avoid changing them in the event of delayed launch [32, 33].

1.11. Specifications by battery chemistry

Batteries come with a good deal of specifications which you would find with their specs, or datasheet. Common specifications include the type of cell the battery is in, its standard voltage, its AH or mAH rating, its standard charge (for rechargeable), and its rapid charge.

The technological characteristics of batteries as well as the chemical phenomena governing their operation are common for all electrochemical systems. In this sense, we group together the parts dealing with the structures, the principles and the control of charge and / or discharge. By other parts, we highlight the specificities of each battery.

Table (1-2): Comparative specifications between different batteries types [18].

Specifications	Lead Acid	Ni-Cd	Ni-MH	Li-ion		
				Cobalt	Manganese	Phosphate
Specific Energy Density (Wh/kg)	30-50	45-80	60-120	150-190	100-135	90-120
Life Cycle (80% discharge)	200-300	1000	300-500	500-1,000	500-1,000	1,000-2,000
Fast-Charge Time	8-16h	1h typical	2-4h	2-4h	1h or less	1h or less
Self-Discharge/month (room temp)	5%	20%	30%	<10%		
Cell Voltage (nominal)	2V	1.2V	1.2V	3.6V	3.8V	3.3V
Charge Cut-off Voltage(V/cell)	2.40 Float 2.25	Full charge detection by voltage signature		4.20		3.60
Discharge Cut-off Voltage(V/cell, 1C)	1.75	1.00		2.50-3.00		2.80
Charge Temperature	-20 to 50°C	0 to 45°C		0 to 45°C		
Discharge Temperature	-20 to 50°C	-20 to 65°C		-20 to 60°C		
Maintenance Requirement	3-6 Months (topping charge)	30-60 days (discharge)	60-90 days (discharge)	Not required		
Safety Requirements	Thermally stable	Thermally stable, fuse protection common		Protection circuit mandatory		
In Use Since	Late 1800s	1950	1990	1991	1996	1999
Toxicity	Very High	Very High	Low	Low		

In Table (1-2), we cite and cover the different types of batteries and their classifications. In more detail we discuss the commonly used accumulators, while trying to

identify its famous terminologies and reactions involved in the evolution of their state [18, 34, 35].

1.12. Batteries comparison

A comparison across battery technologies is possible by comparing their specific power and energy density on the Ragone plot [36]. In a Ragone plot, the y-axis denotes the amount of energy density available, while the x-axis denotes how that energy varies according to their technologies per masse. The Figure (1-13) illustrates how lithium-ion batteries are about a third of the weight and half of the volume when compared to lead-acid and other batteries technologies. Lithium-ion batteries are in a league of their own when compared to all other battery types since they are significantly more energy dense. Furthermore, it can be seen that Li-Ion have high specific energy but high power density, which is showing smaller sizes and lighter weight cells [36].

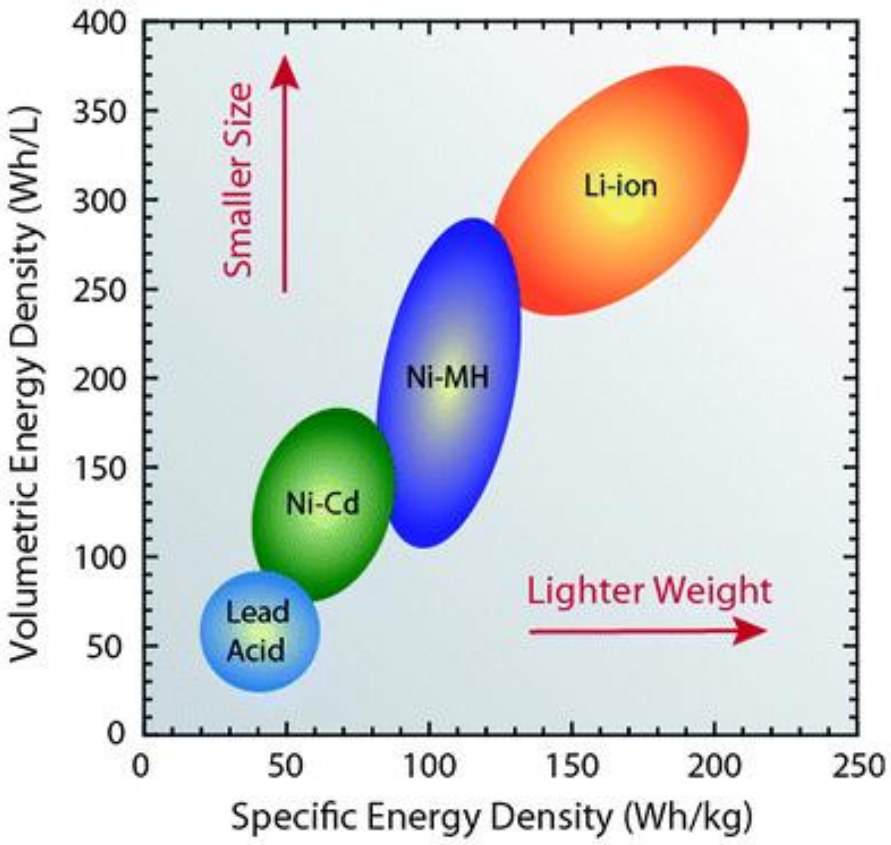

Figure (1-13): Ragone plot of various energy storage technologies [36]

Energy density: is a measure of how much energy the battery can store, in a given size

or mass. So a battery with a higher energy density can power a load for longer than one with a low energy density and the same physical size or mass. Its units are in Wh/kg or Wh/m^3. Note the use of hours in the unit- power x time = energy.

Power density: measures how quickly the battery can deliver energy. In other words, it's equivalent to the maximum current you can draw from a battery of a given size. Units are W/kg or W/m^3.

1.13. Battery terminology

Each battery is characterized by the following parameters:

1.13.1. Terminal voltage

Terminal voltage refers to the voltage across the battery terminal when a load is applied to the battery. This voltage often varies with respect to SOC and discharge/charge currents.

1.13.2. Open circuit voltage

This voltage refers to the voltage across the battery's terminals with no load applied. There is a direct relationship between this voltage and SOC.

1.13.3. Capacity

The coulomb metric capacity is defined as the total Amp-hours available when the battery is discharged at a given C-rate from 100% SOC to cut-off voltage. Capacity decreases with increasing C-rate [37].

1.13.4. Internal resistance

The internal resistance of a battery limits the amount of power that is delivered from the battery. Often internal resistance is designed to be small to allow for more power to be delivered; however, the internal resistance increases over time due to sulfation and grid corrosion of the battery [20]. Furthermore, the amount of energy available in the battery or state of charge (SOC), affects the apparent internal resistance of the battery. Li-ion has higher resistance at a full charge stage and at the end of discharge but little resistance in between [38].

1.13.5. Usable power

It is obtained from the product of battery voltage (V_L) and the maximum current that it can tolerate (I_L). This usable power must be at least equal to the peak power so as to provide the electricity throughout all the operating range.

1.13.6. Cut off voltage

Cut off voltage refers to the minimum allowable voltage at which the battery is referred as "empty".

1.13.7. Full voltage

Called also overcharge voltage, it refers to the maximum voltage, which allows the battery consider fully charged such as Li-ion and Lead-Acid fully charged at **4.2V** and **2.03V**, respectively.

1.13.8. Stored Energy

This parameter is going to determine the autonomy of the electric vehicle (EV) and the possibilities of recovering for a hybrid electric vehicle (HEV). The energy of the battery is expressed as a function of its capacity in Ampere-Hour (Ah) and its voltage, while the storage energy is expressed by Watt-hour.

1.13.9. Self-discharge phenomenon

It is the spontaneous decomposition (without external intervention) of the active ingredients of the cell, from a charged state to a discharge state [20]. It is interpreted as a loss of EMF due to internal leakage current. According to different readings, primary batteries are the least affected by the effect self-discharge, subsequently come the secondary (rechargeable batteries), see Table (1-2).

1.13.10. Life cycle

This number refers to the amount of times the battery may be charge and discharged before its retired, see Table (1-2).

1.13.11. Charge rate

Charge rates are used to describe and compare different batteries' discharge currents. The C-rate is a normalized value against the battery capacity, which differs across batteries.

1.13.12. Notion cell, module and packs

Often HEV or stand-alone systems contain high power battery packs. The smallest battery unit inside a Lead-acid or Li-Ion battery pack is the cell. These cells are arranged in series and parallel to achieve a required voltage and capacity. Often the first arrangement of cells is called module, which are arranged as well in series and parallel to create the battery pack. It is important to mention that each cell has its own SOC, capacity and internal resistance [39]. Figure (1-14) depicted the all possible combinations for battery pack.

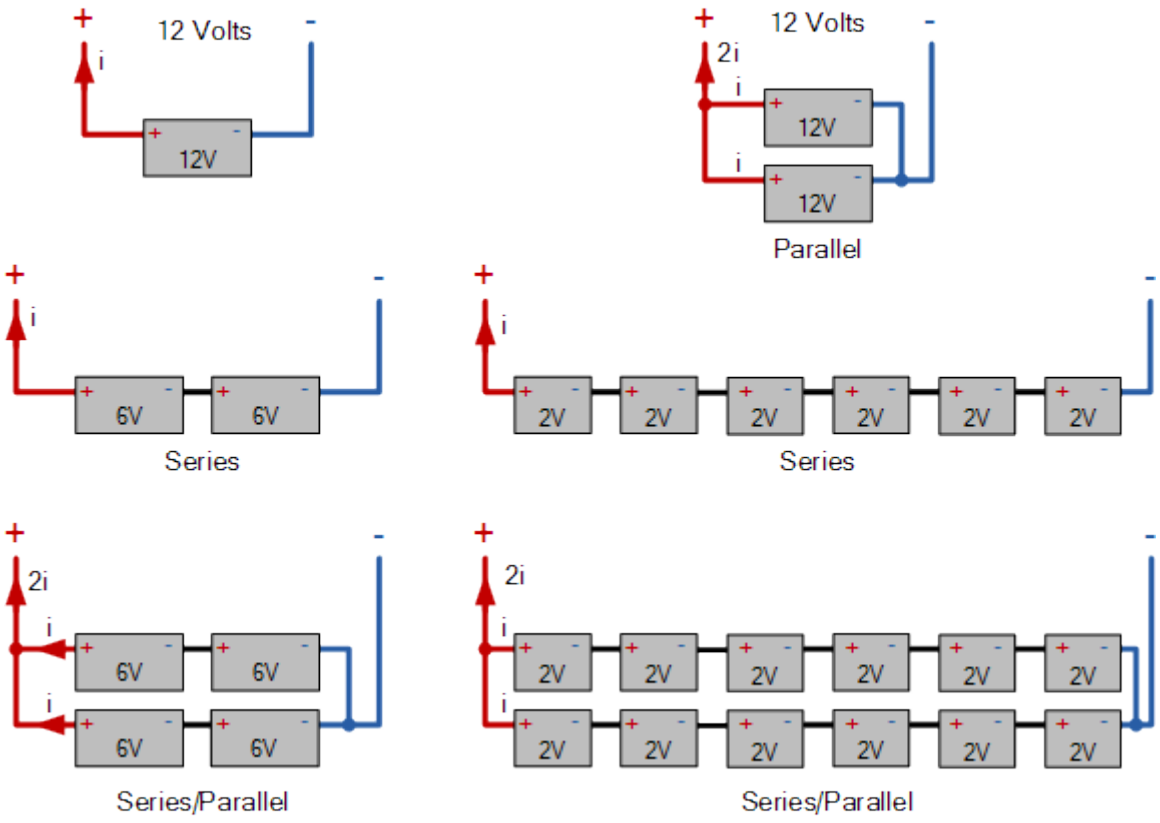

Figure (1-14): Battery packs connections.

1.14. State of charge (SOC)

There exists one possible definition of the state of charge (SOC) could be express its whole meaning, which is defined as the ratio of the remaining charge of the battery and the total charge while the battery is fully charged at the same specific standard condition.

The SOC is often expressed in percentage, where 1 or 100% means fully charged and 0% means fully discharged. This parameter can be compared to the fuel tank gauge of a vehicle [40, 41].

However, the whole meaning of the SOC is illustrated in Figure (1-15) below.

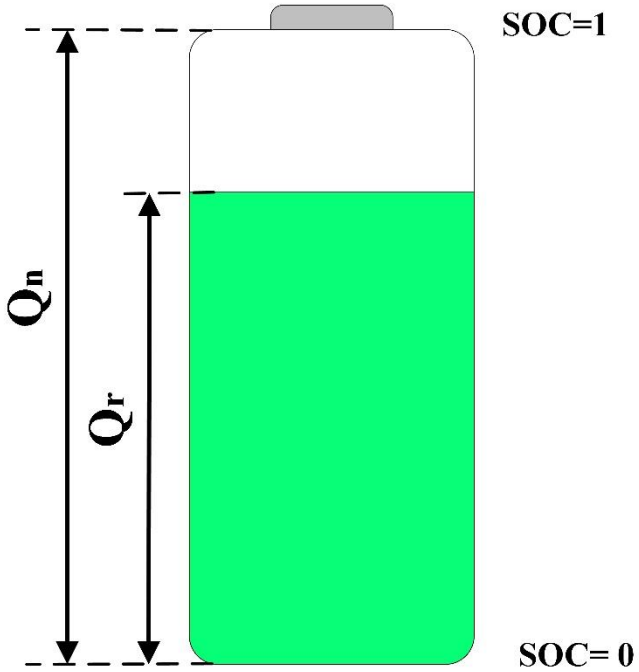

Figure (1-15): State of charge.

$$SOC = \frac{Q_r}{Q_n} * 100 \tag{1.10}$$

Where Q_r represents the capacity remaining and Q_n represents the total capacity available of the battery. Therefore, as a simple solution, SOC evolution can be tracked according to the equation (1.11):

$$SOC(t) = (SOC_0 - \frac{1}{Q_n}\int_0^t I_L(t)dt) * 100 \tag{1.11}$$

Where SOC_0 referes to initial state of charge, I_L is the current applied of load and $SOC(t)$ represents the actual state of charge.

1.15. Depth of discharge

The Depth of discharge (DOD) is a measurement of the percentage of battery capacity that has been used. In others, is represented as the opposite of SOC and may be calculate as [42]:

$$DOD = (1 - SOC) * 100 \quad (1.12)$$

1.16. State of health (SOH)

The SOH measures the irreversible degradation that occurs in the battery performance due to cycling and aging. SOH allows for an easy comparison with a healthy battery. The best way to evaluate the health of a battery is by testing its capacity [40]. Some factors that affect the battery's capacity are the temperature at different SOC, the level of SOC it is charged every time, cycling, and depth of discharge (DOD) [43]. Furthermore, The SOH of a battery serves as an indicator of the battery life conditions between its beginnings of life to retirement. Often SOH is a unit less value similar to the SOC that indicates the available remaining use.

Often, batteries are retired when their overall capacity or maximum power drops to 80%, which is referred as capacity fading and power fading [44].

1.17. Conclusion

In this chapter, we gave some general information about the photovoltaic systems, their usage and how they work, besides a detailed descriptive on the batteries, their history, their operating principle as well as their main characteristics. Then, we presented the lithium-ion technology, its different technologies, and their characteristics. We conclude at this level that lithium-ion technology and Lead-acid battery technology come to maturity and is used in different fields such as transport, satellites, projects space and photovoltaic.

For Lithium-Ion batteries, progress still needs to be made to ensure their safety operating. Two axes are favoured: the choice of materials not very inclined to thermal runaway and control electronics to ensure the use of the cell within its limits.

The identification of the state of the battery and more particularly the state of charge is critical for applications such as space, HEV and EV, the risks and the expectations impose to maintain the SOC at a certain level (in an interval) for delivering the power required during the mission. With a DOD limit so as not to over discharge or shorten battery life. Also, a capped SOC threshold that allows regeneration of stored energy and an optimized charge profile that minimizes the risk of overcharging.

The requirements (protection and performance) of the mission for its storage unit are translated into the appropriate BMS system. Therefore, the expected accuracies are dependent on the adapted approach in BMS, which is adopted in the model and method of identifying the parameters.

Despite the history of research and development in the different fields of application of batteries, there is currently no chemical, mathematical or electrical model to reproduce accurately and in various cases its operation. The only models available do not offer enough precision or only can be used under certain narrowly defined conditions.

On the basis of the knowledge and evolution of the battery in operation storage, a solution which combines the use of modelling with evolutionary parameters to identify the SOC in continuous way is required.

Chapter 2
SOC estimation review

2.1. Introduction

The reliability, safety, and longevity of any battery operations necessitate an efficient battery management system (BMS), which is involved of advanced techniques. Therefore, the number of research articles of BMS strategies published in journals and conferences have been increasing rapidly in lasts years [17, 45], especially on battery states estimation focus.

Generally, it is worthwhile to summarize systemically the states estimation methods for BMS practitioners, in the hope of providing some inspiration and review in this subject.

In this chapter, conducted by an up-to-date literature survey in combination with practical applications, a technical review on the development of BMS and key states estimation methods for batteries have been given.

2.2. Battery management system

In the 1990s, the BMS was developed for monitoring the operation status of lead-acid batteries [46]. At this stage, the acquisition of battery parameters, including the voltage, current and temperature, and battery charge/discharge control were the main functions of BMSs, and the SOC was mainly indicated by the cell terminal voltage and open circuit voltage [2].

From the 2000s, combined with battery models, state observers were developed for battery SOC estimation [47, 48]. In the early years, multiple sampling channels for cell voltage and temperature measurement were commercially integrated as a single chip, which significantly reduces the size and cost of BMSs.

Until now, the functional requirement of BMS appears to be a more sophisticated and complex trend [49], and the core functions of BMS mainly include cell and pack monitoring and protection, states estimation, cell balancing, thermal management, charge/discharge control, and data communication and record, as shown in Figure (2-1).

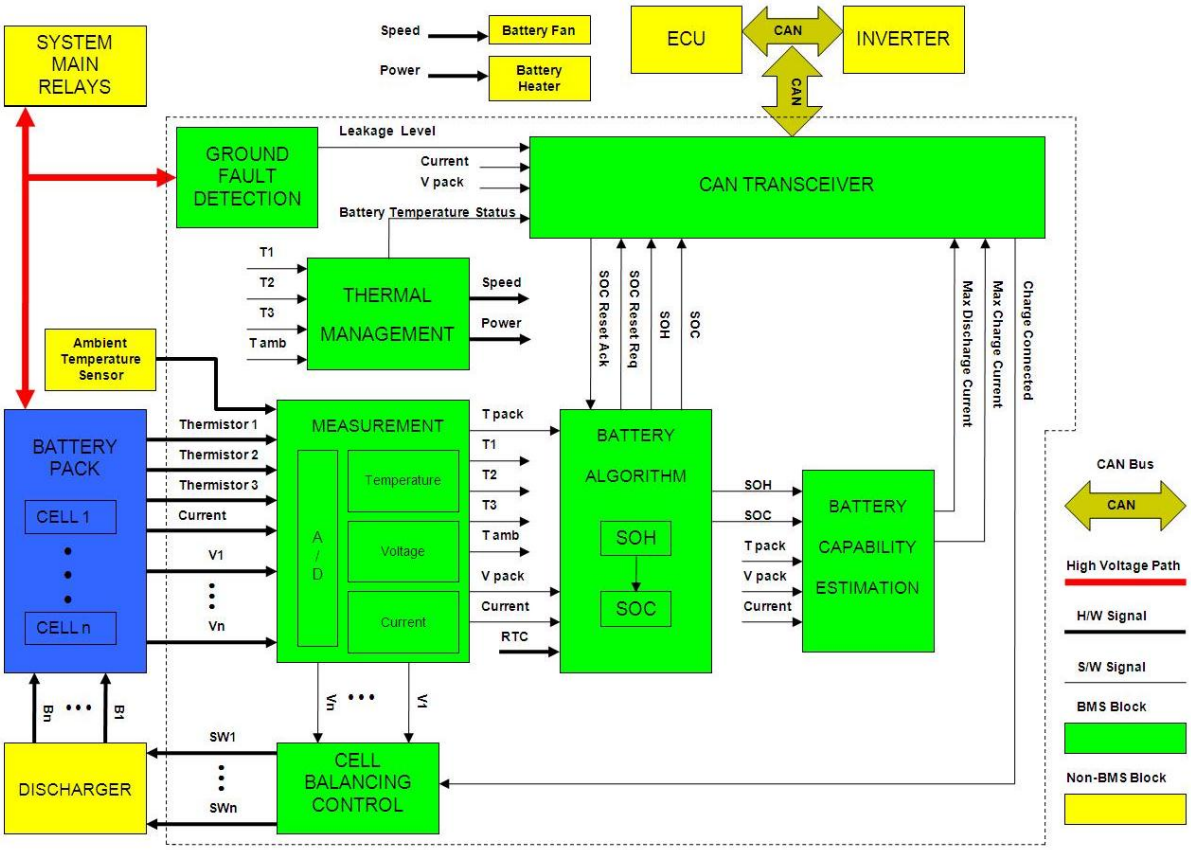

Figure (2-1): Block diagram of battery management system.

So, the role of BMS is to ensure the following tasks:

- Monitor the voltage and current during charge and discharge
- Ensure proper charge/ discharge current.
- Estimate the SOC and SOH of the cells using implemented algorithm.
- The Thermal Control of the battery is intended to keep the batteries within a safe operating range. This control can go from a simple measurement of the temperature in order to review the strategy of the auxiliary equipment to put in service as it is the case for VRLA batteries, until reheating or the cooling of the battery through a thermal control active (active radiator, heater, thermostat ... etc.) in the case of Ni-MH and / or Li-Ion batteries. Ventilation system can be envisaged to release the hazardous gases generated by the battery.
- Balance of the cells, in order to achieve optimal performance of the battery module while this rebalancing is necessary for multi-cell batteries (serial/parallel). The BMS

controls this rebalancing of the cells through a strategy predefined into algorithm.

- The protection of the battery from risks by avoiding overload or over discharge or other major anomalies (temperature increase for Li-Ion) that can occur in case of battery failure or equipment in the surrounding environment. This protection can be physical, relay for emergency stop or sending alarm (report to the user).
- Monitoring the state of the battery and information communication (SOC, DOD, temperature, alarms, gauge ... etc.).

The main functions of the BMS are depicted in Figure (2-2).

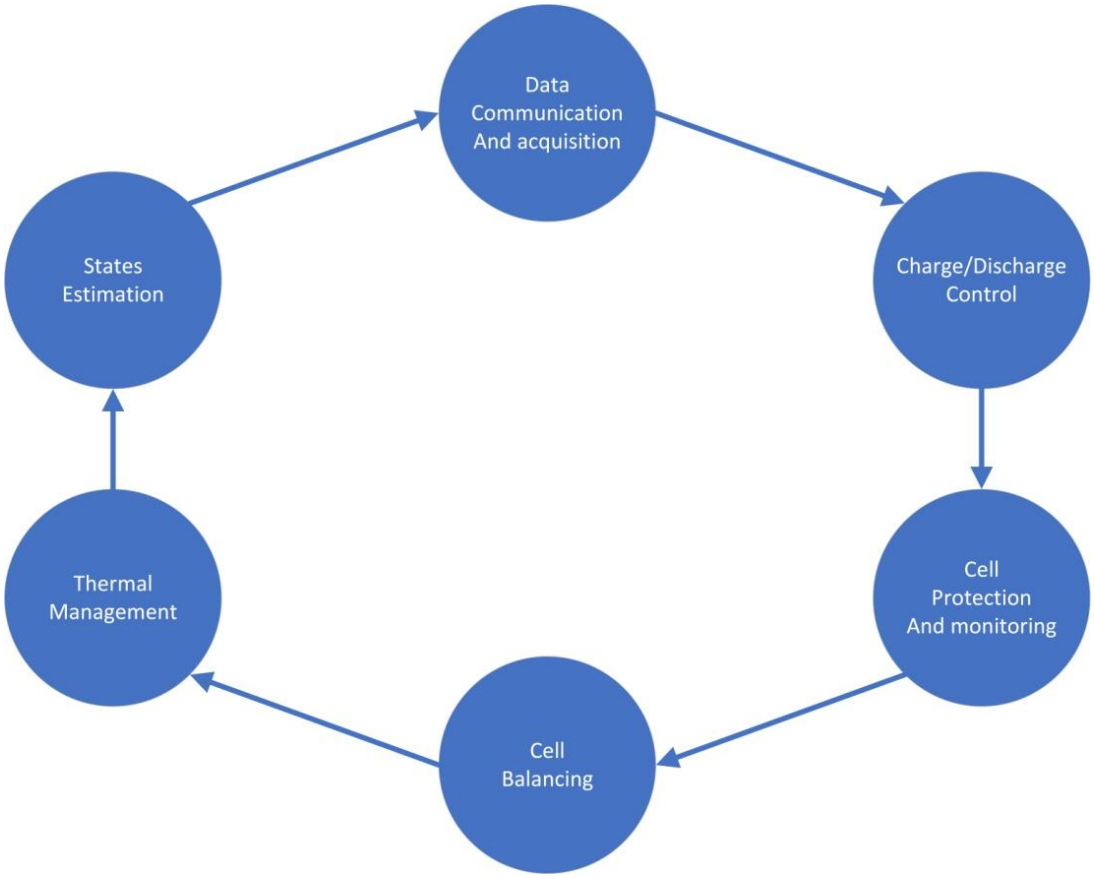

Figure (2-2): BMS main functions.

2.3. Profile of charge and discharge batteries

The safety, durability, and performance of a battery is highly dependent on how it is charged or discharged [50]. An abuse can significantly reduce its life and can be dangerous. Therefore, a BMS includes, on board, both a load control protocol and an implemented discharge strategy.

Figure (2-3) shows the typical profiles of the load protocol used for almost all batteries [51].

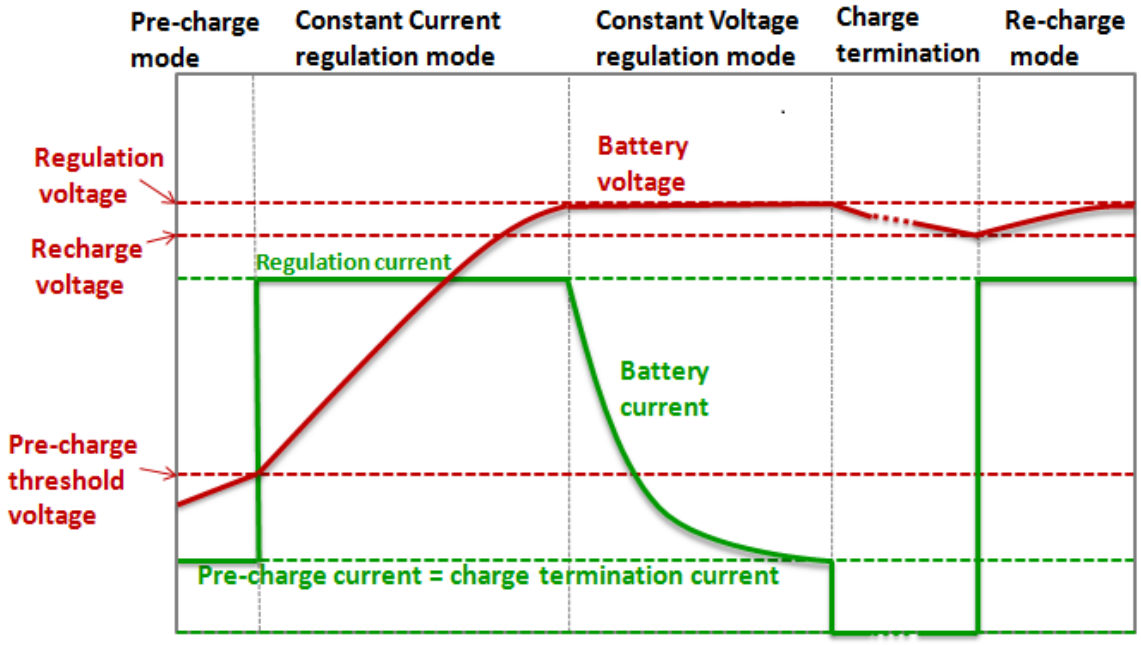

Figure (2-3): Charge profile constant current (CC), constant voltage (CV).

2.3.1. Constant Voltage Charge (CV)

This charging regime that maintains the voltage at a constant value (V_{full}) is suitable for all types of battery; it is probably the most famous profile given the simplicity of its implementation. The charging current (I_b) of the battery varies throughout the charging process. Therefore, I_b can be important at the initial stage of charging and gradually decreases to zero when the battery is fully charged.

The disadvantages of this method are: the requirement of a very high power at the beginning of the load, the need for control of the overload and also the control of the temperature of the battery. In general, the life of the battery is reduced compared to other protocols [52].

2.3.2. Constant current (CC) charge

In this charging regime, the charging voltage applied to the battery is controlled to maintain a constant current ($I_b = I_{cc}$). The SOC will increase linearly as a function of time during this constant current regime. The challenge of this method is to determine the full state of charge SOC = 1 or 100%.

The cut-full threshold can be determined by the monitoring of the parameters (T°, V, t), the increase of temperature, the gradient of increase of the temperature, increase of the tension, the change negative voltage and the elapsed charging time [53].

2.3.3. Combined charge Protocol CC-CV

This method is based on the combination of constant voltage and constant current during the charging process of a battery. Figure (2-3) shows a charge profile of a Li-ion cell (18650HC). At the initial stage, the battery can be pre-charged to a constant low value current if the cell is not pre-charged before ($V_L = V_{pr}$), the factory protection threshold).

Then, it is activated to charge it with a constant current at a higher value (fast charging phase). Thereby, when the battery voltage (or SOC) reaches a certain threshold point (V_L= 4.2 or SOC = 80%), the load is changed to charge at constant voltage (healthy charge phase). Constant voltage charge can be used to maintain battery voltage if the DC charge supply is still available (charge hold phase). As a complementary phase, a constant voltage profile can be added for maintenance at low load currents; an external self-discharge circuit is used to prevent any degradation of the battery.

Also, other proposed load protocols can be used to reduce load time by a linear current decay load (LCD) protocol and to limit overload capacity losses, a modified LCD protocol called MLCD; Their combination is also appreciated [54].

2.3.4. Discharge regime

It should be noted that the discharge regime of a battery depends on the power demand imposed by the application; it can vary from a simple constant current discharge to a random profile. However, the discharge control protocol implemented in the BMS, when sizing the power system, must limit the degradation of the battery while ensuring the safety of battery operations and avoid the deep discharge.

2.4. Internal states relationships

Overly estimates of battery states would result in waste or abuse of battery available capabilities, which could even lead to fire and explosion risks. So, the last researches on BMS focuses on the development of battery states estimation methods that are capable of determining internal battery status robustly for the safe, reliable and efficient battery usage.

Therefore, the battery states of interest include:

- State of charge (SOC), which is a quantity representing the stored charge capability of the battery.
- State of health (SOH), which is a quantity representing the aging level of the battery.
- State of energy (SOE), which is a quantity representing the stored energy capability of the battery.
- State of power (SOP), which is a quantity representing the delivered or absorbed power capability of the battery.

The SOC usually is defined as the level of the remaining charge stored in a battery to its full capacity. Effectively, it is reviewed as fuel gauge of battery available energy, which is determined according to terminal voltage, current of load, cell temperature and battery aging. Likewise, the SOE is also calculating by these factors, which is required for indicating the state of available energy of the battery. While, the SOH is governed by the aging path of the battery, as well as, it is slow varying-time and affected by ambient temperature.

Moreover, The SOP is dependent on SOC/SOE and SOH. In specific, the SOP has a short prediction time which is typically lower than 20 second [55]. The reported relationships between these different states are depicted in Figure (2-4).

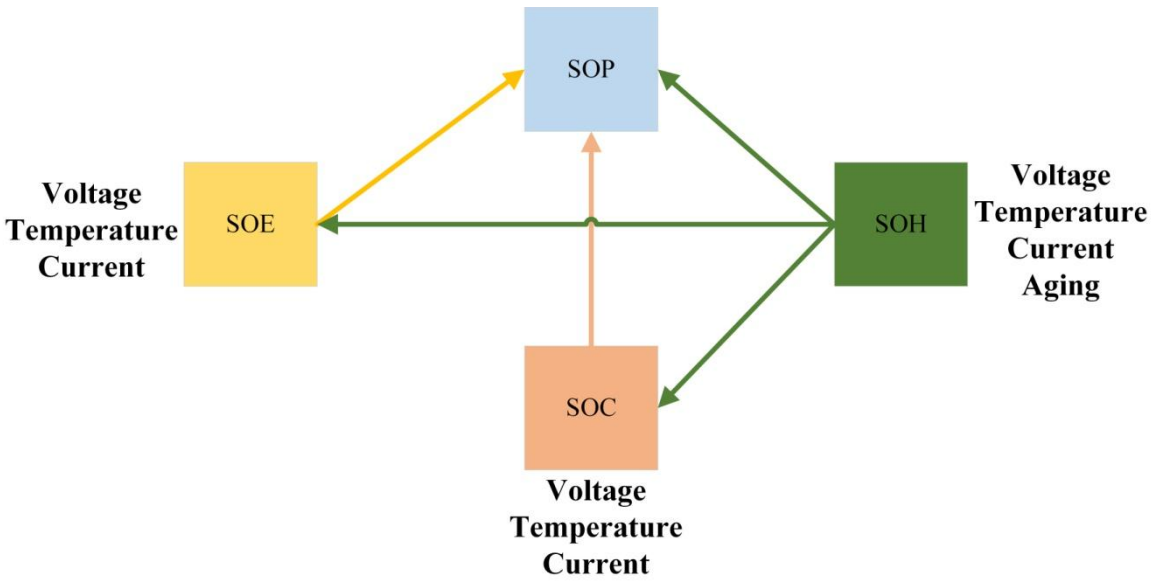

Figure (2-4): Relationships of battery states.

2.5. State of charge estimation methods

The SOC defined as the ratio of the remaining charge to the full charge stored in a battery. It represents a "fuel gauge" where it is an indispensable indicator for the safe operation of batteries.

2.5.1. Coulomb-counting method

Coulomb-counting, also called ampere-hour (Ah) integral, is the most basic and simplest method to estimate battery SOC [40], as expressed as:

$$SOC(t) = (SOC_0 - \int_0^t \frac{\eta I_L(t)}{Q_n} dt) * 100 \quad (2.1)$$

where $SOC(t)$ and SOC_0 denote the SOC values at time t and the initial time, respectively, I_L is the loading current at time t (positive for charging and negative for discharging), and η the coulomb efficiency that can be considered as 1.

Due to the primary advantage achieved by its ease of use and implementation with few computation efforts, the Coulomb-counting method has been widely used in real applications, especially during the early stages of the development of BMSs.

The effectiveness of this method is basically dependent on the accuracy of current measurement and initial SOC value. Because of the inevitable cumulative error of current detection, the SOC estimation results suffer from significant divergence problems, especially after performing over a long period. Therefore, it needs a periodic calibration procedure for correcting the initial accumulated charge value, which is the disadvantage of limits its direct applications in practices. Hence, the Coulomb-counting method is often used in combination with other techniques, such as the following open circuit voltage (OCV) and model-based methods [56-58].

2.5.2. Open circuit voltage method

The OCV method is typically applied to recalibrate the SOC value. An OCV-SOC curve of Lead-acid (LA) battery is depicted in Figure (2-5), where the SOC interval is 5%. However, at each SOC interval the relationship between the OCV and SOC can be fitted as a segmented function, as given in the following equation:

$$OCV = (\alpha_i * SOC) + \beta_i \quad (2.2)$$

where a_i and b_i are the parameters of the ith segmented function.

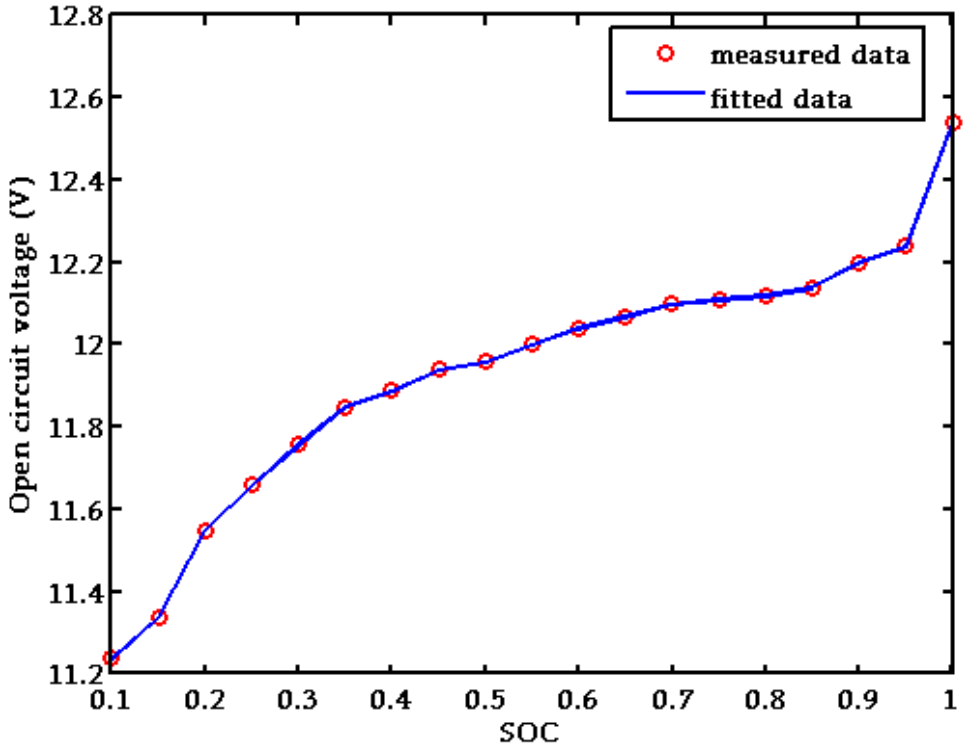

Figure (2-5): The OCV-SOC curve of a Lead-acid battery cell.

If the OCV is obtained in advance, then it is easy to compute the SOC by using equation (2.2). However, there are several existing points that should be taken into account when applying the OCV method for SOC estimation [59].

Accurate SOC estimation requires precise battery OCVs. However, it typically takes a long rest time for batteries to recovery their fundamental terminal voltage, which refers at that point to OCV. Therefore, it limits its feasibility in applications. Thus, the strategy for how to obtain the OCV in a short period of time needs to be further developed.

The OCV strategy is an open-loop estimator that doesn't have the capability to eliminate voltage detection errors and uncertain disturbances [60]. The cell terminal voltage detection sensor with high accuracy and low disturbances noises is therefore needed in this method. Some types of batteries have a relatively flat OCV-SOC curve, especially for LiFePO4 cells. This means that a small OCV measurement error may lead to a larger SOC

divergence. In this case, it requires cell terminal voltage detection sensors with extremely high accuracy, which increases the cost of BMSs.

In [61] addressed that the OCV-SOC curve of LiFePO4 cells of the 18650-cylindrical type is related to the ambient temperature, and a single OCV-SOC table used in the estimation algorithm would cause erroneous results. To address this problem, an offline OCV-SOC-temperature table was established to estimate the SOC in the paper, where the verification indicated that it can provide better results than that without considering ambient temperature.

In [62], it can be observed that OCV-SOC values of a Li-NMC cell differ from different aging levels. For robust and accurate battery SOC estimation at various ambient temperatures and cell aging levels, it is suggested to establish a multi-dimension OCV table including various influenced factors, such as an OCV-SOC-temperature-aging table in advance.

2.5.3. Model-based methods

The schematic of battery model-based method shown in Figure (2-6) mainly consists of a battery cell, a state observer or filter, and a battery electrical circuit model (ECM) or electrochemical model (EM).

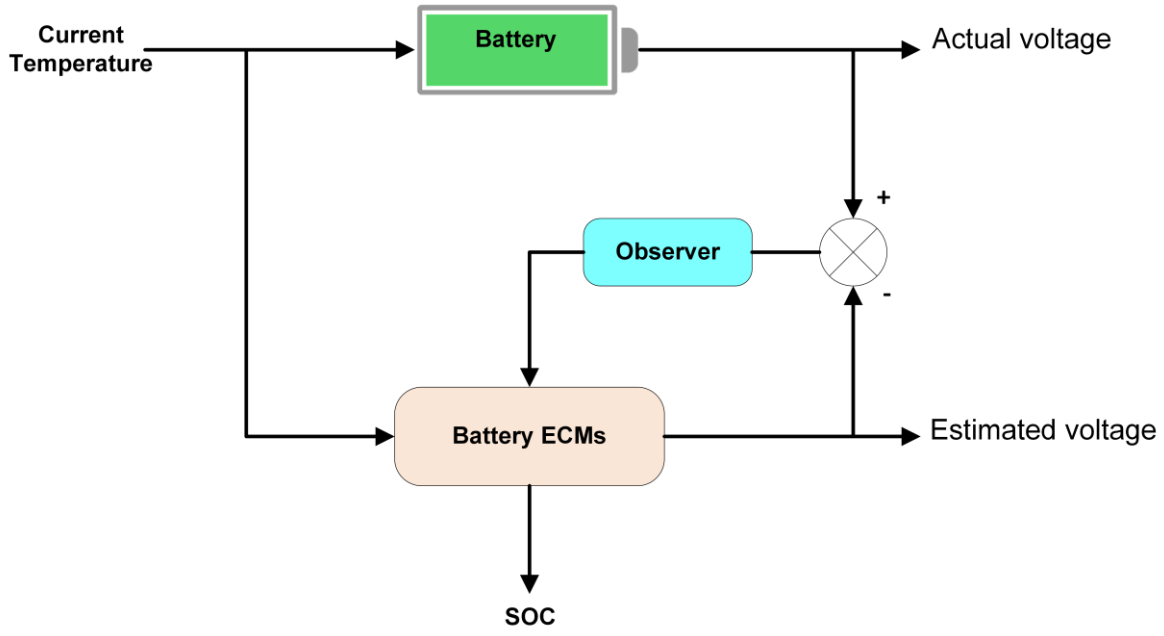

Figure (2-6): Schematic of battery model-based SOC estimation methods.

The input for both the real battery and battery model can be the loading current and ambient temperature. Therefore, the principle of SOC estimation is to compare the cell terminal voltage with the output voltage of the battery model for generating a residual voltage, and then to feed it back to the model through an observer or a filter for revising the model parameters and states. Hence, the residual voltage is gradually eliminated, while the SOC of the battery model is gradually closed to the actual value.

Battery model-based SOC estimation methods always exhibit desirable merits, such as closed-loop, insensitive to the initial SOC value and uncertain disturbances, and availability of estimated error bounds, which have attracted enormous attention. Various techniques of observers and filters including sliding-mode observer (SMO), particle filter (PF), proportional-integral (PI) observer, H-infinity (H∞) observer, different versions of Kalman filter (KF), and so forth, are extensively applied in model-based SOC estimation methods.

2.5.3.1. Kalman filter based methods

The KF is an optimal recursive solution for linear systems, which assume that the noise in both the transition and measurement processes is an independent Gaussian type. However, KF tends to diverge in nonlinear systems. Different extensions of KF, such as extended KF (EKF), sigma-point KF (SPKF), unscented KF (UKF), central difference KF (CDKF), and fading KF (FKF) have been proposed to address this issue, and therefore were widely employed for estimating the SOC of batteries with non-linear characteristics. The key idea and steps of the EKF algorithm for battery SOC estimation including prediction update and measurement update were first elaborated in Plett's series of papers [47, 49].

In the following research, Lee et al. [59] employed a modified OCV-SOC relationship and measurement noise models with EKF to achieve more robust estimates for all cells. Since EKF can equilibrate the algorithm complexity and estimation accuracy well, it is regarded as being capable of implementation into a microprocessor for efficient operations in BMSs.

However, an argument against using EKF is that it linearizes battery model nonlinearities, thus leading to linearization errors. To tackle this problem, Plett [49] proposed the SPKF method for estimating the SOC of LiPB high-power cells, which highlighted its superiority in terms of estimation accuracy compared with the EKF. It is noted that there is little or no additional cost at the gains of SPKF compared with that of EKF, and the

implementation of SPKF requires no analytic derivation or Jacobians as in EKF [49, 63]. Moreover, the performances of EKF and SPKF for SOC estimation were comparatively studied in [64], where both estimated robustness against uncertainties and convergence behaviour with an erroneous initial value were improved in the SPKF method. Meanwhile, CDKF and UKF are the two most common used variants of SPKF, which are also applied for SOC estimation.

A nonlinear enhanced self-correcting battery model was employed with the CDKF estimator to achieve more accurate SOC estimation results in [49]. With a UKF algorithm, obtained accurate estimates while greatly reducing the computational time in inferring SOC from a rigorous battery EM [65].

It is noted that accurate knowledge of process and measurement noises covariance is highly required in all variants of KF for precise SOC estimation. Erroneous knowledge of noises covariance may result in considerable errors in estimated results. In this aim of adaptively matching the process and measurement noises covariance in real-time, adaptive KF based estimators, such as adaptive EKF (AEKF) and adaptive UKF (AUKF) were applied for battery SOC estimation. In [66], an AUKF estimator was investigated with an improved battery Thevenin model achieved by adding an extra RC branch to a conventional Thevenin model for the estimation. Both the maximum SOC estimation error and mean SOC estimation error can be reduced to low levels in comparison to using EKF.

In [67] further developed AEKF for estimating the SOC of a series-connected lithium-ion battery pack, in which a battery pack model was established as a cell unit model for avoiding cell-to-cell variations in the battery pack. Besides, AUKF for SOC estimation was presented in [66], where the comparative study results indicated that AUKF has a better accuracy than AEKF and EKF. The other problem is that the model and measurement noises of varied extensions of KF are restricted by the Gaussian distribution. However, it does not relate well to practices, which may have an adverse effect on the convergence behaviour and estimated accuracy.

2.5.3.2. Sliding-mode observer

The SMO is another effective technique for state estimation in nonlinear systems subject to uncertainties and disturbances [68]. It is designed to force and confine the system state to stay in a pre-constructed surface, known as the sliding (hyper) surface, which

exhibits desired dynamics. The SMO design for SOC estimation was described in [69, 70], where the systematic design approach for SMO in combination with state equations of battery ECMs with was present, and the convergence of SMO was proved by Lyapunov functions.

The modelling errors caused by simple ECMs were effectively compensated by the SMO, and therefore, under the real driving environments, the proposed method showed robust tracking performance against modelling errors and uncertainties. Due to its simple calculation and robust estimation characteristic, the SMO was suggested to be directly applied in hybrid EVs. However, an inevitable issue of the conventional SMO is the chartering phenomenon, which is caused by the discontinuous switching control. To tackle the above problem, in [71] proposed adaptive switching gain SMO approaches for minimizing chattering levels. In the meantime, the accuracy of SOC estimation was improved by adaptively adjusting switching gains for compensating modelling errors. With the same aim, in [70] employed an adaptive discrete-time SMO for estimating the OCV of a battery cell and then predicting the SOC with an enhanced Coulomb-counting algorithm.

In [72], the elimination of chattering in both the output voltage and SOC estimates was achieved by the application of a second order discrete time SMO that can drive not only the sliding variable but also its derivative to zero. Compared with the conventional first-order SMO approach, the proposed method showed a drastic reduction in both the estimation error and chattering phenomenon while maintain the robustness of the SMO approach. Although the effectiveness of adaptive SMO approaches and the second-order SMO method for attenuating chattering levels was validated, this benefits from the additional complexity and computation cost of the algorithms.

2.5.3.3. Particle filter

The particle filter (PF) is a sequential Monte Carlo approach, which aims to obtain a set of particles (also called samples or individuals) as well as importance weights assigned to the particles for representing the posterior probability density of the system [73]. The main operations of PF include particle propagation, importance weight computation, and resampling [74].

In [75], a PF based battery SOC estimation algorithm was proposed, where the experimental results showed that PF and EKF have similar performance in estimation

accuracy, but the execution time of PF is six times faster than that of EKF. Since LFP batteries have very flat OCVs with hysteresis between charging and discharging which bring challenges for estimating the SOC.

For improving the estimation robustness, in [76] presented a PF based multi-model data fusion technique for battery SOC estimation. In this approach, a battery ECM and EM with PF were employed to infer SOC values, separately, and then the SOC values and their weights were adjusted by using PF and weighted average methodology. Although the validations indicated that this method can achieve better accuracy compared with conventional approaches of the single battery model, it was at the expense of additional computational efforts. It was reported that the calculation process of conventional PF requires a massive number of particles for accurate SOC estimation.

Accordingly, the proposal distribution of PF included the new observation information, and the number of particles can be significantly reduced. Moreover, with the consideration of the cells' inconsistencies in a battery pack, in [77] developed a UPF based approach for the estimation of the battery pack SOC.

2.5.3.4. H-infinity observer

H-infinity (H∞) observer has been effectively applied to handle state estimation problems involving multivariate systems with cross-coupling since the late 1990s [78, 79]. It is a worst-case robust design approach, which means that it is less sensitive to model uncertainties and disturbances. The satisfactory battery SOC estimates can be obtained by the application of H-infinity in model-based estimation blocks.

Yan et al. [79] designed a H infinity observer for addressing SOC estimation problems of nickel metal hydride (Ni-MH) batteries in noised and uncertain environments. The verification indicated that the proposed approach has the stronger robustness than current integral and KF methods. When unknown or erroneous statistical properties of errors were provided, the H-infinity observer based method still offered good SOC estimation accuracy for a battery-powered robot that is used for inspecting power transmission lines.

Likewise, for accurately estimating battery SOC and terminal voltage without a prior knowledge of process and measurement noises, H-infinity observer with a battery ECM whose parameters were extracted by a genetic algorithm was used in [80], where the SOC

and voltage estimation error bounds are invariant with different measurement noise levels.

Furthermore, to weaken the errors caused by a single battery model, Lin et al. [81] focused on a multiple battery ECMs fusion approach using the H-infinity algorithm for SOC estimation. In the proposed method, three H-infinity observers were applied with three different kinds of ECMs to predict their respective SOCs. Then, the SOCs were synthesized with optimal weights to determine the battery SOC by the Bayes theorem.

It was stated that the proposed approach highlighted its superiority in terms of robustness and estimation accuracy for both LMO and LFP batteries operated under dynamic conditions in comparison with the methods using sole battery ECM. However, the proposed distributed architecture with three observers, three models, and a fusion technique inevitably increases the computational burden, and the computational efficiency has not been evaluated in the article.

For increasing the robustness and accuracy of the conventional H-infinity algorithm, the adaptive H-infinity estimator was designed for both SOC and SOE estimation in [82], where a moving estimation window of samples was employed to develop the covariance of the error innovation for adaptively updating the observation and system noise covariance. Compared with the conventional H-infinity and EKF methods, the adaptive H infinity estimator can reduce the maximum SOC estimation error and the mean SOC estimation error as well as the convergence time.

According to the authors, the estimation results kept extremely high accuracy within 0.1% when an erroneous initial SOC value was provided. However, the robustness of the proposed method against various ambient temperature and cell aging levels is suggested for further evaluation.

2.5.3.5. Proportional-Integral observer

The proportional integrator (PI) observer inherits the advantages of the proportional controller and integral controller and exhibits strong robustness against system uncertainties, which is the most usually used control approach in engineering applications.

The PI observer has the advantage over other observer and filter techniques in that it is computationally efficient, and therefore, it is well tracking to be embedded in low-cost target BMSs [83, 84]. Since it is hard to establish an accurate battery model for exactly

matching a battery's dynamic behaviours, the PI observer was employed to improve the robustness against modelling uncertainties for SOC estimation in [85], where the structure of the proposed method with a battery ECM was presented, and its convergence with model errors was validated.

Moreover, in [86] quantitatively analysed the error sensitivity of battery ECM parameters including OCV, Ohmic resistance, polarization resistance, and capacity for the PI observer based SOC estimation method. It was stated that the OCV has a more significant influence on the estimation accuracy than other parameters.

2.5.4. Machine learning methods

Without the physical knowledge of a system, machine learning methods such as neural network (NN), support vector machine (SVM), and fuzzy logic (FL) have the ability to learn and approximate the relationship between the input and the output of the system, which have been widely applied to battery systems to estimate SOC.

2.5.4.1. Artificial neural network

Artificial neural network (ANN) is inspired by the way that the human brain processes information and is an intelligent mathematical tool for system modelling [87]. Therefore, an ANN typically consists of an input layer, one or more hidden layers, and an output layer to demonstrate a complex nonlinear system. Different learning algorithms can be employed to train the input data and the target data to acquire the parameters of the network.

However, the most often used learning method, back-propagation, was employed to train the relationship between battery parameters including cell terminal voltage and loading current and targeted SOCs in [88] for estimating battery SOC. The experimental results indicated that the NN method could perform well if the trained data is identical to the real experience.

Considering the effect of battery capacity degradation, a battery capacity aging model that was built according to the test data at various temperatures was introduced as an input parameter of a Radial Basis Function ANN (RBFNN) in response to the varying aging levels and temperatures in [88, 89].

The verification of the proposed method showed a good robustness against varying battery degradation, temperature, and loading profiles. Moreover, a large amount of reliable experiment data is required for accurately deducing the battery aging model and training the network.

2.5.4.2. Support vector machine

Support vector machines (SVMs), originally introduced as support vector networks [90], are supervised learning models that are used for data classification and regression analysis. SVMs can effectively transform a non-linear model using kernel functions and regression algorithms to a linear model in high dimension by using creditable training data [91]. The training process is also likely to be time-consuming. A battery SOC estimator using the SVM technique was proposed in [91].

The battery test data including cell terminal voltage, loading current, temperature, and SOC were used for training the parameters of the SVM model. With the input variables of battery cell voltage, current, and temperature, the SVM model was able to estimate battery SOC accurately with an estimated coefficient of determination of 0.97.

Furthermore, it is addressed that a relatively large estimated error can be observed for some points of discontinuity of the current. This may cause problematic estimates in real applications especially with dramatically changed loading current. With the goal of achieving robust SOC estimation, an iterative weighted least squares SVM (WLS-SVM) algorithm was proposed in [92], where the key idea is similar to that of [91], namely establishing a relationship of SOC to cell voltage, current and temperature. The verified results showed that the proposed estimator can achieve good robustness for SOC estimation.

Moreover, an optimized SVM for regression (SVR) with double search optimization process was employed for SOC estimation in [90]. The main purpose of the double step search was to reduce the time of training processes for selecting the optimal parameters. The proposed SOC estimator outperformed the estimations based on artificial NN in terms of efficiency and accuracy. However, since the results were verified in a vehicle simulator ADVISOR, it is recommended to evaluate the performance of the proposed method in real situations.

2.5.4.3. Fuzzy logic

Fuzzy logic (FL) mimics human control logic and is a way of processing data which incorporates a simple and rule-based approach to solving a control problem. The implementation process of FL includes fuzzifying inputs into membership functions, computing the output based on the rules, and de-fuzzifying the fuzzy output. In [93], they used ac impedance and voltage recovery measurements as the input of an FL model for estimating battery SOC. The proposed method was implemented in a microcontroller for the application of portable defibrillators.

Moreover, in [94] proposed an adaptive neuro fuzzy inference system (ANFIS) for online SOC correction. The average SOC of the battery pack was estimated by the KF method and then was corrected by the ANFIS with the information of cell differences and current. The proposed method has good accuracy and robustness against varying loading current, battery state, and aging, but it needs relatively high computational efforts.

Several numbers of approaches for estimating battery SOC have been proposed in literature, most of them are classified in Figure (2-7).

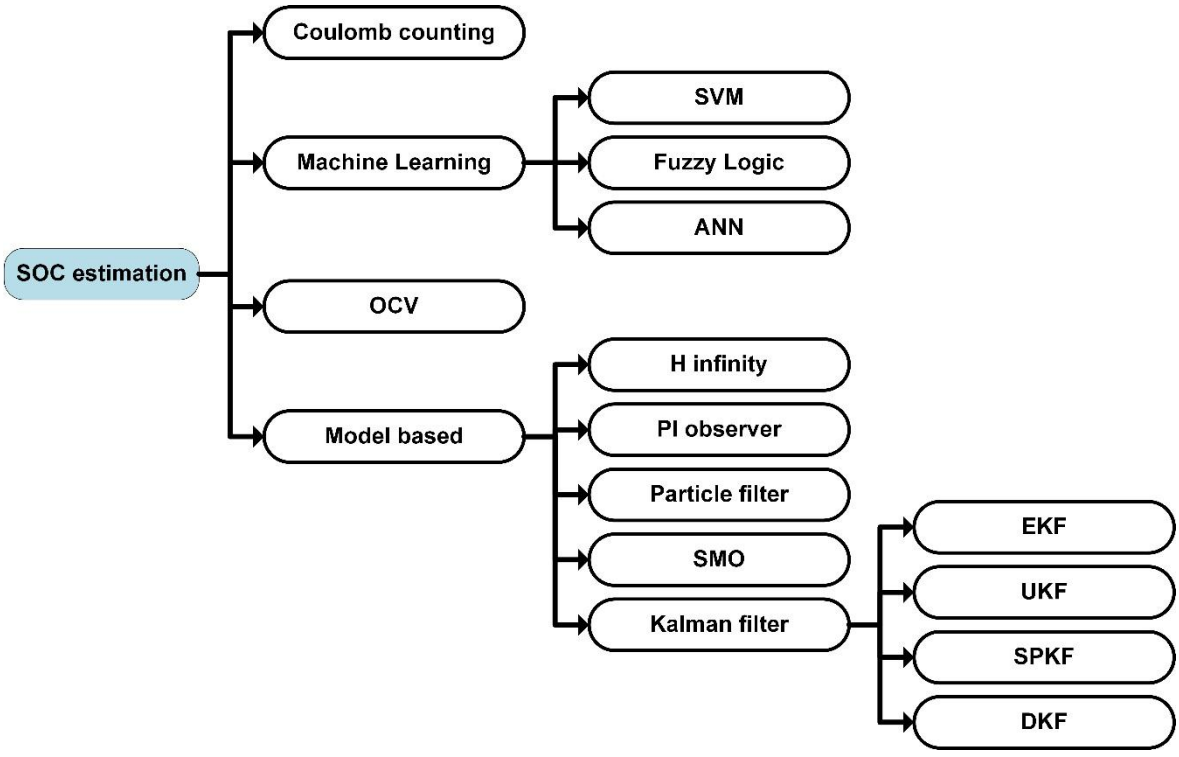

Figure (2-7): Classification the approaches for SOC estimation

2.6. Conclusion

A brief comparison of the aforementioned SOC estimation methods regarding to their complexity and accuracy is summarized in Table (2-1).

Table (2-1): The comparison of different SOC estimation methods regarding to their complexity and accuracy [1].

	Methods	Complexity	Accuracy
SOC estimation	**Coulomb counting method**	**low**	**Low (especially after performing over a long period)**
	OCV method	**low**	**Low (especially for batteries with flat voltage plateau)**
	Model based methods	**High (especially with a battery electrochemical model)**	**High**
	Machine learning methods	**medium**	**Depending on training data sets**

The functional requirement of the lithium-ion battery management system (BMS) has appeared as a more sophisticated and complex trend, especially in estimating battery states. Overly pessimistic or optimistic estimates of battery states would lead to waste or abuse of battery available capabilities, and the states estimation is therefore one of the major challenges of BMSs.

This chapter mainly presents a technical review on key states estimation methods for lithium-ion batteries. It is noted that the machine learning methods can be applied for modelling the relationship of target state to input variables, but the estimated error is highly dependent on the training data. Among the reported techniques, model-based methods are the most popular ones for different states estimation, which is primarily attributed to their inherent traits such as closed-loop and insensitive to the initial value and uncertain

disturbances. However, in order to achieve more reliable and robust states estimation; the exiting issues of different techniques need to be further addressed.

Chapter 3
Battery modelling

3.1. Introduction

Researches in the field of stand-alone systems, electric vehicle, energy distribution, and power control strategy, as well as the estimation of batteries state of charge (SOC) and state of health (SOH), are experiencing an important increase, due to the growing interest in this field. Therefore, a lot of Researches are settled to improve battery models accuracy, especially those concerning lead-acid and Lithium-ion batteries, where has become a crucial objective. Therefore, for that reason, in literature, a wide range of different approaches are representing battery behaviour. They are varying from simple to complex degrees while the battery is treated as a nonlinear system.

A battery pack is composed of smaller batteries called cells. They are arranged in series and parallel to achieve the desired voltage and capacity. Each cell has its own SOC, capacity and internal resistance, which makes it instinctively to represent a battery pack as an electric circuit. The representation of this circuit of the battery circuit is known as the equivalent circuit model (ECM).

This model is popular due to its simplicity and fast computing time, which making it a good candidate for control-oriented applications [95, 96].Thus, making them perfect to be used and implemented in a BMS.

ECMs are models based on electrical components such as ideal voltage sources, resistors, and capacitors to simulate the behaviour of the battery [97]. The vast majority of ECM models are semi-empirical models where the process of calculating the final outputs is based on two distinctive activities. First, the OCV with respect to SOC must be known as prior by performing laboratory experiments where the battery is put through sequences of discharge and resting periods [98]. Second, ECM parameters such as resistors and capacitors must be calibrated through input/output data using mathematic parameter identification techniques such as least square methods [97].

A drawback of this kind of ECM is that these models do not rely on the physical behaviour of the battery, therefore calculating the power fading and aging effect of the battery becoming impossible. In this thesis, different ECMs models were identified and selected for analysis, which will be detailed in the following subsections.

3.2. What's the importance of modelling a battery?

For most applications using battery models, it is generally important to accurately predict the electrical characteristics of the battery, including the voltage across it, and the current flowing through it. Additionally, an estimation of State of Charge (SOC, a normalized estimation of how much chemical energy is stored in a cell) is required. If battery models are linked to thermal management simulations, accurate heat dissipation from the battery must be captured [99].

Batteries are used in our life with several applications, so anyone has a portable device can tell you batteries degrade over time. There are many electrochemical factors that lead to the degradation of a Li-ion battery. For instance, the active materials in the cathode and anode tend to crack over time and there are undesirable side reactions that lead to growth of films on active material particles in both the cathode and anode in case of Lithium-Ion battery.

Furthermore, under extreme conditions, such as lead-acid battery suffers from sulfation phenomena, which shorten the battery life whereas Lithium-ion battery suffers from Lithium plating process.

Security simulation and testing is a significant theme. Extreme conditions, for example; hot, cold environment or deep discharge could be disastrous for the battery. This is the main reason to use cell models while efforts trying to enhance them in order to capture electrochemical behaviour and prediction of the internal state.

3.3. Battery models

The use of mobile devices is often limited by the capacity of the employed batteries. Therefore, the battery lifetime determines how long one can use a device. Thereby, battery modelling can help to predict, and possibly extend its lifetime. For this reason, many different battery models have been developed over the past years [97, 99].

However, we will give an overview of the different battery models are available, and evaluate their suitability to track the battery state.

3.3.1. Electrochemical models

It is possible to achieve a high accuracy by using electrochemical models that aim to capture all the behaviours' of the battery. They are suitable for understanding the distributed electrochemistry reactions in the electrodes (such as, the reactions from Figure (3-1), assuming LixC6 anode and LixCoO2 cathode) and electrolyte.

However, in order to describe the battery chemistry charge/discharge carrier mechanisms, they deploy a high number of partial differential equations (PDEs) with a large number of unknown parameters, which must be solved simultaneously with a high computational expense and a significant requirement of memory. It is not allowed to use for online estimation due to their poor fitting extrapolation problem [100].

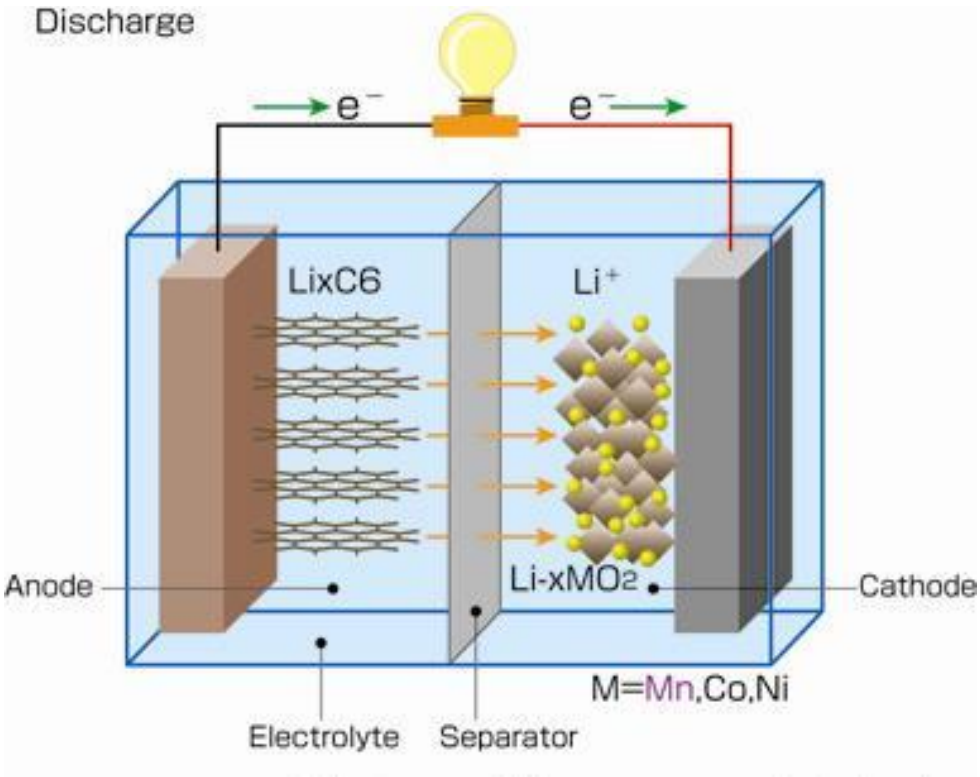

Figure (3-1): Basic reactions diagram of a Lithium-ion cell.

This kind of battery modelling tries to describe all the details of physics phenomenon that occurs inside the battery. Figure (3-1) shows the anatomy of a Lithium-ion cell battery, which has four main components:

- The negative composite electrode connected to the negative terminal of the cell.
- The positive electrode connected to the positive terminal of the cell.
- The separator.
- The electrolyte.

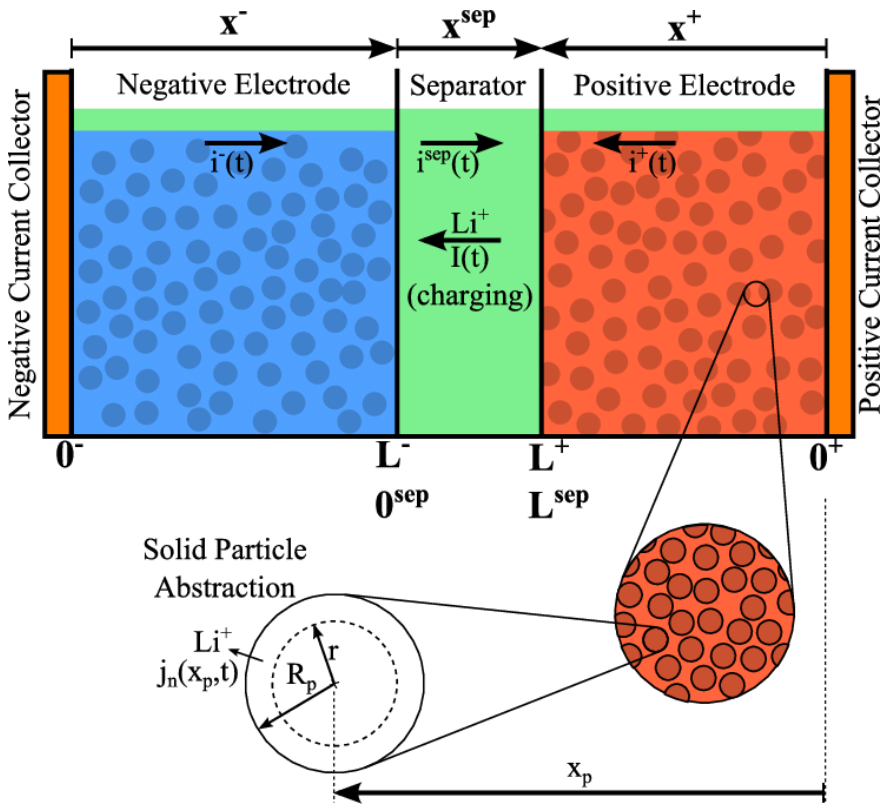

Figure (3-2): Schematic of a lithium-ion battery electrochemical model.

Based on the electrochemical principles shown in Figure (3-2), it is assumed that the solid spherical particles uniformly disperse along X-axis, and the intercalation and de-intercalation process of lithium-ion in and out of these solid spherical particles, which are presented by the complex governing equation of the cell terminal voltage as follow [101]:

$$V_L(t) = \Phi_s(O^+, t) - \Phi_e(O^-, t) - I_L(t)R_{em} \tag{3.1}$$

where $\Phi_s(O^+, t)$ and $\Phi_e(O^-, t)$ represent the electric potential at the ends of two solid electrodes, respectively. R_{em} represents an empirical resistance though $I_L(t)$ and $V_L(t)$ are the loading current and terminal voltage, which play the role of input and output respectively.

Furthermore, this section will explain briefly the complex governing equations of the electrochemical model:

- Transport in solid phase:

The diffusion of solid in the electrolyte phase as shown in Figure (3-2) may be described the amount of concentration of lithium inside the electrode by spherical shape using the following equation:

$$\frac{\partial C_s(x,r,t)}{\partial t} = \frac{D_s}{r^2}\frac{\partial}{\partial r}\left(r^2 \frac{\partial C_s(x,r,t)}{\partial r}\right) \tag{3.2}$$

where this equation refers to both electrodes and D_s is the Li^+ coefficient of diffusion in the intercalation of the electrodes. C_s refers to concentration of solid phase lithium and r is the radius of sphere (see Figure (3-2)).

- Transportation in electrolyte:

The concentration of Li+ in the electrolyte phase is governed by deriving the changes in gradient diffusive flow of ions. The following PDE describes the dynamics [100]:

$$\epsilon \frac{\partial C_e(x,t)}{\partial t} = \frac{\partial}{\partial x}\left(D_{eff}\frac{\partial C_e(x,t)}{\partial x}\right) + \delta(1+t^+)j(x,t) \tag{3.3}$$

where ϵ is the volume fraction, D_{eff} is the Li+ diffusion coefficient in the electrolyte which can be calculated based on Bruggman relation [102]. t^+ is the Li+ transference in the electrolyte and j is the wall-flux of Li+ on the intercalation particle of electrode. C_e refers to electrolyte concentration.

Furthermore, δ denote the specific electrode surface area and it can be defined as the porosity equation of the electrode expressed as:

$$\delta = \frac{3}{R_s}(1-\epsilon-\epsilon_f) \tag{3.4}$$

R_s is the radius of intercalation of electrode, ϵ_f is the volume fraction of fillers and ϵ refers to volume fraction of the electrode.

- Electrical potentials:

The relationship between the current inside the electrode and the electrode potential is described by Ohm's law.

$$\sigma_{eff}\left(\frac{\partial^2}{\partial x}\Phi_{\mathrm{s}}\right) = \delta \mathrm{F} j \tag{3.5}$$

In the electrolyte phase, the σ_{eff} effective electronic conductivity may be expressed as: $\sigma(1-\epsilon-\epsilon_{\mathrm{f}})$ and σ refers the electronic conductivity in solid phase. F refers to Faraday's constant. j is the applied current density. Furthermore, by combining Kirchhoff's law with Ohm's law the electrolyte phase yields:

$$-\sigma_{eff}\left(\frac{\partial \Phi_s}{\partial x}\right) - k_{eff}\left(\frac{\partial \Phi_{\mathrm{e}}}{\partial x}\right) + \frac{2k_{eff}RT}{\mathrm{F}}(1-t^{+})\frac{\partial \ln(C_e)}{\partial x} = j \tag{3.6}$$

Where k_{eff} is the effective ionic conductivity of the electrolyte, and Φ_s and Φ_e represent potential reaction for each electrode. F refers to Faraday's constant and T is the ambient temperature.

- Butler-Volmer kinetics

The equation that describes the relationship between the current density, concentrations and over-potential:

$$j = k(C_{s,max} - C_{s,surf})^{0.5}(C_{s,surf})^{0.5}(C_e)^{0.5}\left(\exp\left(0.5\frac{F\mu}{RT}\right)\right) - \exp\left(0.5\frac{F\mu}{RT}\right) \tag{3.7}$$

Where $C_{s,max}$ is the maximum concentration of Li+ ions in the intercalation particles of the electrode and $C_{s,surf}$ the concentration of Li+ ions on the surface of the intercalation particles of the electrode [100, 103]. k refers to the reaction rate constant.

Furthermore, $\mu = \Phi_s - \Phi_e - U_0$ is the over-potential of intercalation reaction, U_0 refers to the open circuit potential for the electrode material (generally determined from curve-fitting on experimental measurement terminal voltage).

3.3.2. Thermal model

Most of battery types have good performance at room temperature. If the temperature of the battery is too high or too low its performance is affected significantly. Lithium-Ion battery have need a special care in case of high temperature, thermal management systems ensure that the battery remains within the range of safe temperature preventing it from bursting into flames or significantly reducing its life expectancy [104, 105]. Temperature models have been developed for thermal control purposes. It used for determining the core and surface temperature of the cell as depicted in Figure (3-3).

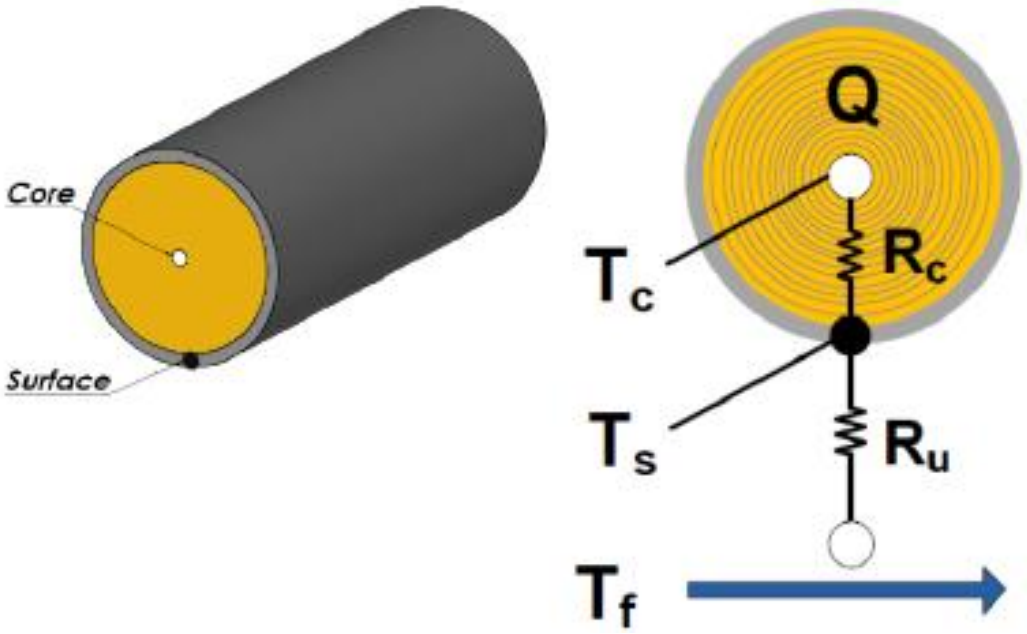

Figure (3-3): Schematic of Thermal model [105].

It is based on cylindrical battery cell using classical heat transfer theory, while the heat transfer can be expressed by these equations [105]:

$$\dot{T}_c = \frac{dT_c}{dt} = \frac{I_L^2 R_e}{C_c} + \frac{T_s - T_c}{C_c R_c} \tag{3.8}$$

$$\dot{T}_s = \frac{dT_s}{dt} = \frac{T_f - T_s}{C_s R_u} + \frac{T_s - T_c}{C_s R_c} \tag{3.9}$$

where T_s and T_c are the surface and core temperature, respectively measured. T_f is the input ambient or coolant temperature of the system. The parameter C_c is the heat capacity of the battery core , C_s is related to the heat capacity of the battery surface. R_e represent the internal resistance where it is considered as an unknown parameter to be identified. A convection resistance R_u is modelled between the surface T_s and the surrounding coolant T_f to account for convective cooling. R_c denotes a conduction resistance between T_c and T_s. I_L represents the load or charge current to the model.

The complete parameter set for this model includes C_c, C_s , R_e, R_c, and R_u, of which the values cannot be easily calculated. Furthermore, the core's resistance and surface's resistance are formulated to store the entering or leaving amount of heating flux similarly. This is yielding four parameters as summarized in Table (3-1).

Table (3-1): Thermal model parameters.

Thermal Model		
Core	C_c	R_c
Surface	C_s	R_s
States	T_c	T_s
Inputs	I_L	T_f

3.3.3. Mathematical models

In general, these models are so abstract that they cannot be used to develop a specific model, but they are still considered as a useful resource for system designers. They use empirical equations or mathematical methods to predict the system state behaviour and evolution, as well as its properties, such as the autonomy of a battery or its capacity [106].

3.3.3.1. Behavioural model

Behavioural models use empirical data and often neglect the underlying physical or electrochemical behaviour of the battery. Based on the experimental data, their model was therefore labelled by collecting the data in a one-dimensional array up to an n-dimensional array, which is known as a look-up table. One of the most established patterns of behaviour is Peukert's Law [65] :

$$Q_{th} = I_{dis}^{pk} * t_{dis} \tag{3.10}$$

Where Q_{th} denotes the theoretical capacity of the battery expressed in Ah. I_{dis} represents the discharge current, t_{dis} is the maximum discharge time expressed in hour (h) while pk is known as the Peukert coefficient or Peukert constant, which varies from 1 to 2. This parameter is strongly depending on the battery technology. The battery capacity in equation (3.9) is then can be expressed as follow [65, 107, 108]:

$$Q_{th} = \frac{K_1}{(I_{dis})^{pk-1}} \tag{3.11}$$

where Q_{th} represents the theoretical capacity remaining at the given discharge current I_{dis}. And the values of parameters K_1, pk depend on temperature, concentration of electrolyte and type of battery technology. Therefore, it can be determined by identification with experimental data curve. For example, Figure (3-4) shows the remaining capacity for a Lead-acid battery of 120 Ah at different C-rate.

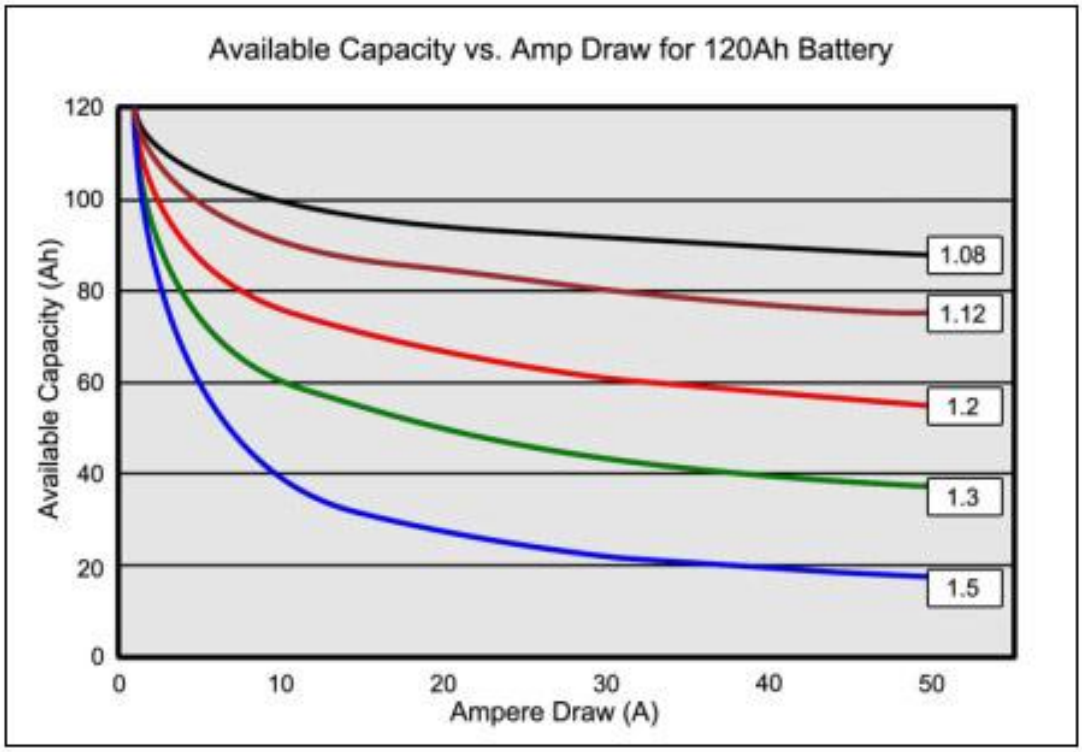

Figure (3-4): Available capacity at Peukert's coefficient 1.08-1.5 [107].

3.3.3.2. Shepherd model

Another well-established Behavioural model is the Shepherd model [38]. It uses the following equation to predict the terminal voltage during charging/discharging conditions:

$$V_{L,k} = V_{oc} + R_s I_{L,k} + \frac{\mu}{q_s(t)} \tag{3.12}$$

where, k is time index. V_L represents the model terminal voltage, V_{oc} refers to the initial cell voltage (E_o), R_s is the cell's internal resistance, μ is a constant number and q_s is the instantaneous stored charge of battery and I_L denotes cell current (positive for discharge and negative for charge).

Since its introduction, further modification has been done to this equation which introduced more μ to μ_n constants to capture higher nonlinearities resulting in following models such as: Unnewehr model, Nernst model and Plett who combined several of the previously mentioned models to derive a self-correcting model which accounted for hysteresis effects of the battery [38, 47].

It is one of the most widely used electrochemical models, for instance it is commonly employed for the hybrid electric vehicle (HEV) description. This model describes directly the electrochemical behaviour of the battery in terms of voltage and current [106].

$$V_{L,k} = V_{oc} - R_s I_{L,k} + \frac{\mu}{SOC_k} \tag{3.13}$$

where k is a time step, $V_{L,k}$ is the terminal voltage of the model, V_{oc} is the open circuit voltage (V_{oc}), R_s is the internal Ohmic resistance of the battery, μ is the polarization resistance (expressed in ohms), $I_{L,k}$ is the instantaneous current (amps), and SOC_k is the cell SOC.

3.3.3.3. Electrical equivalent circuit models

Electrical equivalent circuit (EEC) models consist of a combination of voltage sources, resistors and capacitors. Unlike the other models in constructive components but they try to model the battery behaviour.

They are based on the reproduction of the dynamic characteristics and working principles of the battery using circuit theory. Their accuracy lies within 1-5% and their low computational intensity makes them really accurate for real-time simulation use [106].

In literature, there exist several models based on simple electrical components. They collect together to form a complex circuit with different degree of complexity and numerous parameters.

3.3.3.3.1. Simple battery model

The most commonly used model and the simplest ECM, which it is used to approximate the output voltage of the battery. It consist of two most critical parameters: Open Circuit Voltage (OCV) based on the SOC of the battery, and equivalent Internal Resistance R_{int} of the battery [109].

In simple terms, the battery is modelled as an ideal voltage source (OCV) and the resistor represents the energy loss when releasing that energy. Figure (3-5), depicts the R_{int} Model circuit.

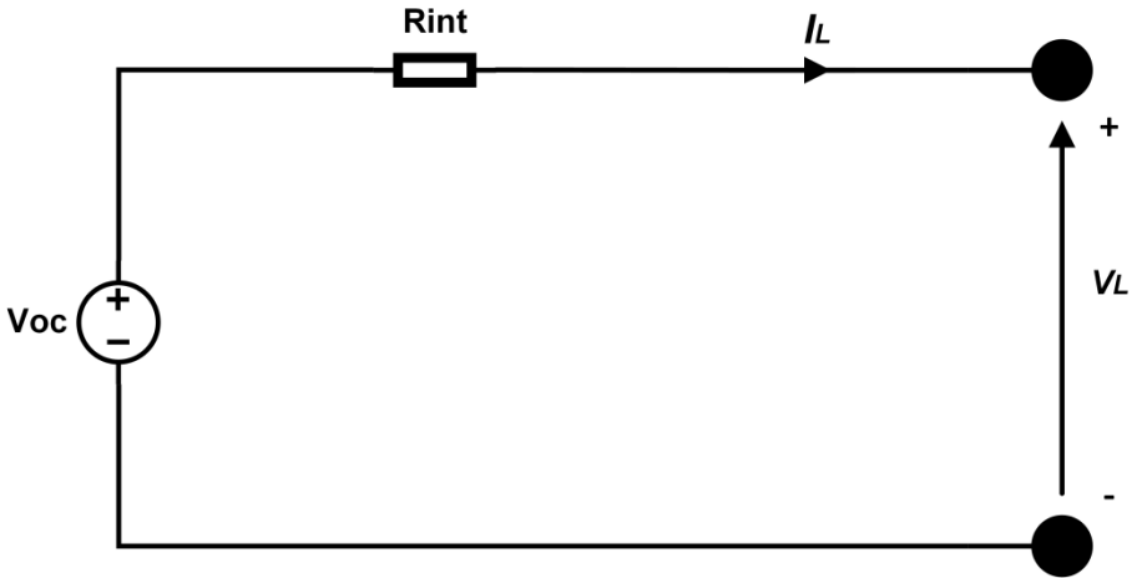

Figure (3-5): Schematic of simple battery model.

The output voltage of the ECM $\boldsymbol{V_L}$, or also called terminal voltage, is calculated as follows:

$$\boldsymbol{V_L = Voc(SOC) - R_{int}\, I_L} \qquad (3.14)$$

A disadvantage of this model is the parameter dependence on SOC levels, and temperature. Parameter curves have to be derived offline experimentally using constant current (CC) and constant voltage (CV) charge and discharge cycles while subject to a constant temperature [110]. The experimental setup is often composed of a battery test system, a thermal chamber for environment control, and a host computer.

Similar experiments are performed at different temperatures and look-up tables are created for the models. Afterwards, the data is processed using software such as MATLAB for parameter identification. Other parameter identification techniques include genetic algorithms, and least square method [111].

Lastly, the battery output voltage suffers from hysteresis making the R_{int} vary when charging/discharging. Figure (3-6), illustrates a model of the hysteresis effect in Lead-acid battery.

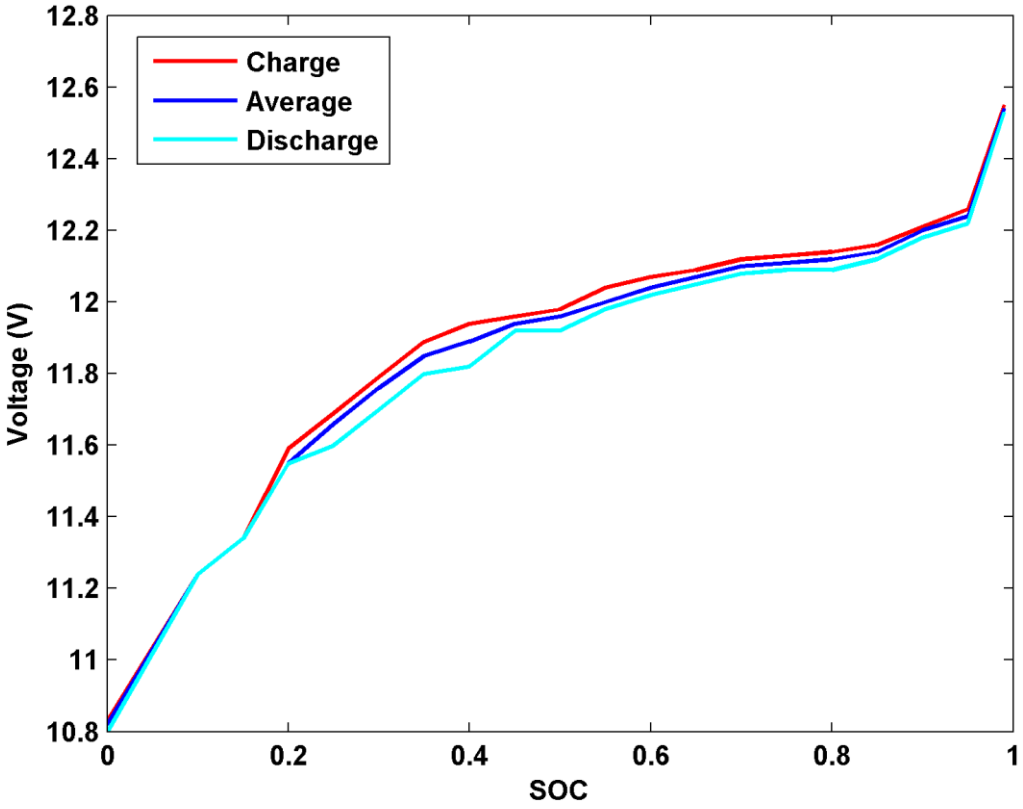

Figure (3-6): The average hysteresis between charge and discharge.

In this purpose, a modified R_{int} model includes the effects of hysteresis is proposed in Figure (3-7), which consists of charge and discharge resistors [112].

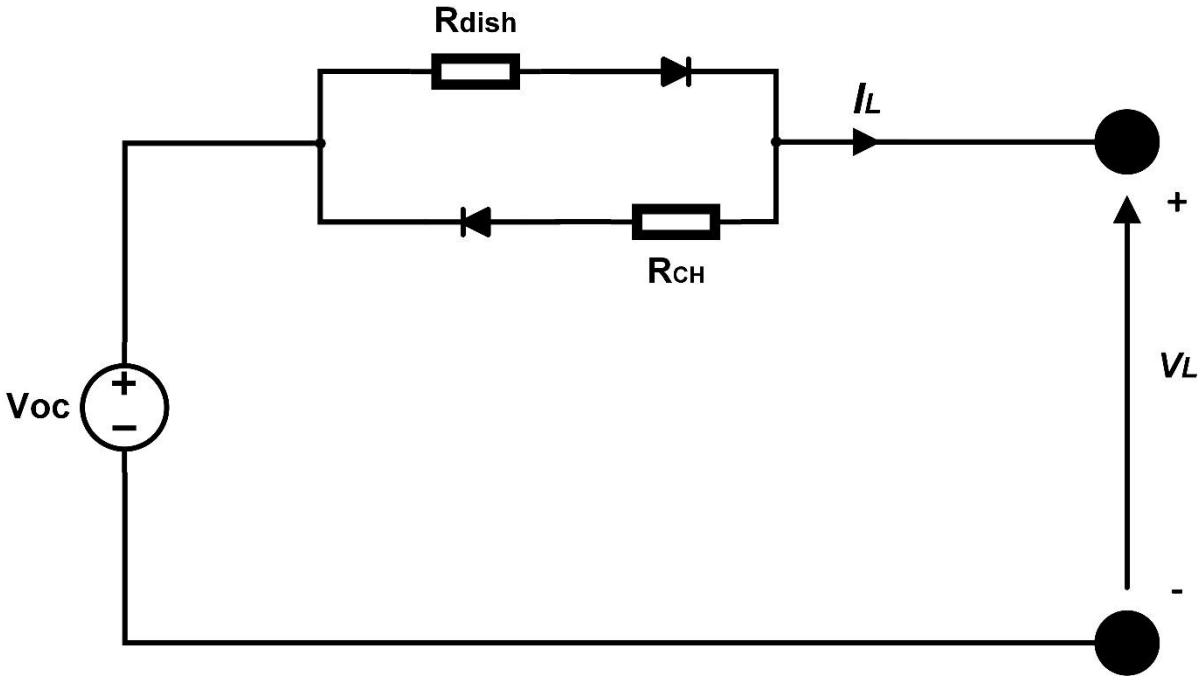

Figure (3-7): Schematic of hysteresis model.

$$V_L = Voc(SOC) - R_{dish/ch}\, I_L \qquad (3.15)$$

3.3.3.3.2. Partnership for a new generation of vehicle (PNGV) model

The US government and the US council for automotive research (USCAR) established the Partnership for a New Generation of Vehicles (PNGV) model in 1993 based mainly on the polarization characteristics of the battery [113].

Moreover, this model has been adopted in the "PNGV battery test Manual", which details test to be performed to batteries. The program addresses improvements in national competitiveness in manufacturing and in the implementation of energy saving innovations in passenger vehicles [114].

The PNGV model is illustrated in Figure (3-8). The model consists of 5 parameters:V_{oc}, C_0, R_0, R_1 and C_1 which correspond to physical traits of the battery. V_{oc} represents the OCV of the battery. C_1 represents the capacitance of the parallel plates and the diffusion effects of the battery. R_1 represents the non-linear resistance of the battery due

to the contact resistance between the plates and the electrolyte. Lastly, C_0 depicts the V_{oc} variation generated by the accumulation of the load current and scales the battery storage capacity [113].

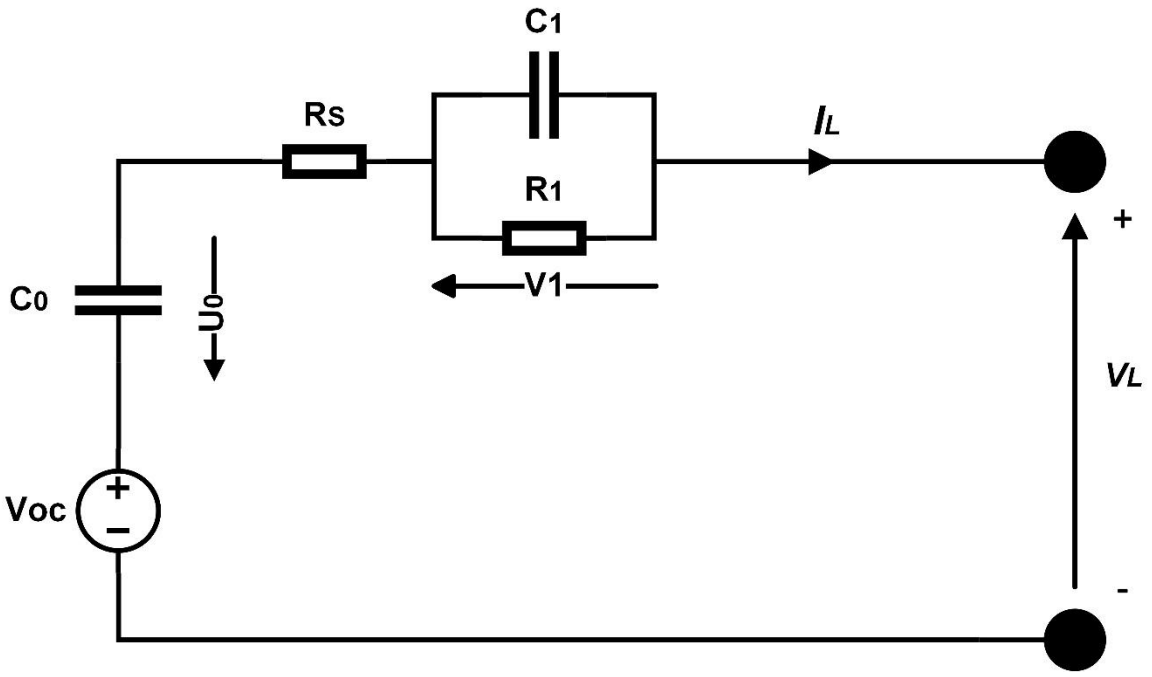

Figure (3-8): Schematic of Partnership for a new generation of vehicle model [113].

Therefore, the PGNV model can be represented by the following equations:

$$\dot{U}_0 = \frac{1}{C_0} \tag{3.16}$$

$$\dot{V}_1 = -\frac{1}{R_1 C_1} V_1 + \frac{1}{C_1} I_L \tag{3.17}$$

$$V_L = Voc(SOC) - U_0 - V_1 - R_s I_L \tag{3.18}$$

3.3.3.3.3. Thevenin Model

The Thevenin model is often called the first-order RC model, because it consists of a parallel resistor-capacitor (RC) circuit in series with a resistance R_s . This model is similar to the Rint model with the addition of a RC branch. Figure (3-9), depicts the Thevenin ECM.

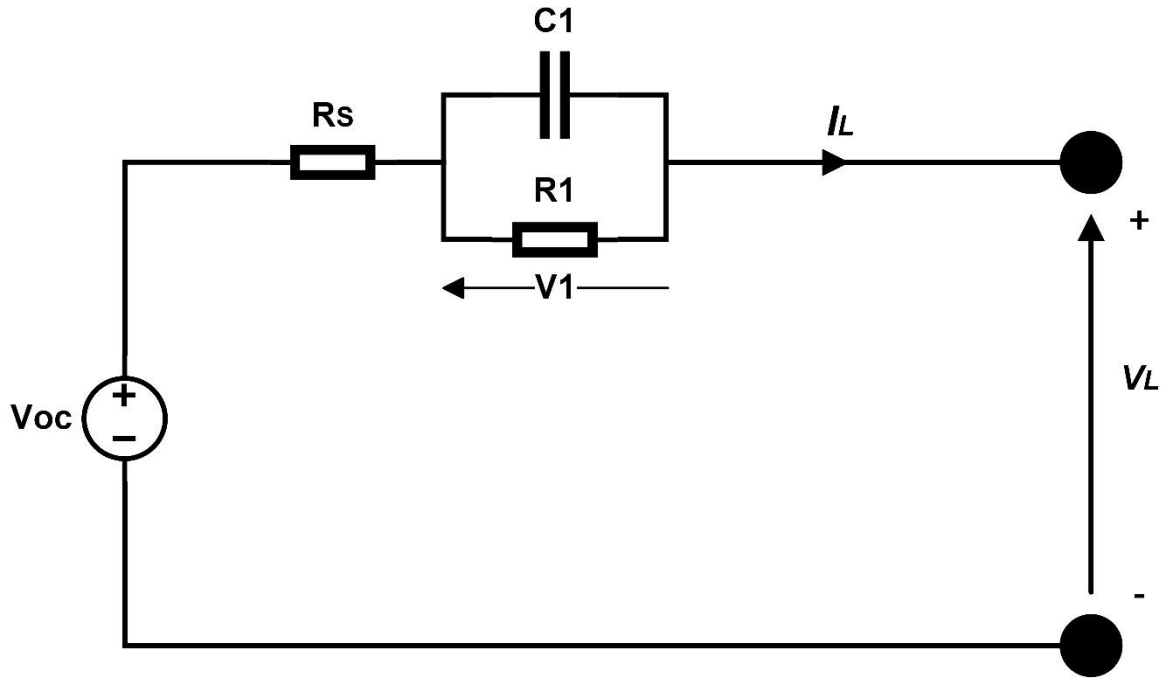

Figure (3-9): Schematic of the First-order Thevenin model.

The RC branch is composed of $\boldsymbol{R_1}$ and $\boldsymbol{C_1}$ elements which represent the polarization resistance and the transient response during charging and discharging of the battery. The polarization resistance is used so that the battery does not provide energy right away to the system. In simple words, the RC circuit represents the time for the battery takes to release the total amount of power [47].

Furthermore, $\boldsymbol{V_1}$ represents the voltage across the RC branch, $\boldsymbol{I_L}$ represents the current passing through the $\boldsymbol{R_s}$, and $\boldsymbol{V_L}$ represents the terminal voltage, $\boldsymbol{V_{OC}}$, of the ECM.

Lastly, the Thevenin model may be represented by the following ODE and corresponding terminal voltage equation [99]:

$$\dot{\boldsymbol{V}}_{\boldsymbol{1}} = -\frac{\boldsymbol{1}}{\boldsymbol{R_1 C_1}}\boldsymbol{V_1} + \frac{\boldsymbol{1}}{\boldsymbol{C_1}}\boldsymbol{I_L} \tag{3.19}$$

$$\boldsymbol{V_L} = \boldsymbol{Voc(SOC)} - \boldsymbol{V_1} - \boldsymbol{R_s I_L} \tag{3.20}$$

3.3.3.3.4. Dynamic model

To include in the model the phenomenon of diffusion at the electrode-electrolyte effect, based on the R_{int} model a series resistance R_s is included to capture the internal resistance and a polarized capacitor (C_p) is integrated as well as shown in Figure (3-10).

Therefore in this model [112], the effect of the transient currents seen on various applications (e.g. EV and/or HEV in urban traffic) during the change of regime (C-rate) or the phase (charge/discharge) is taken into consideration.

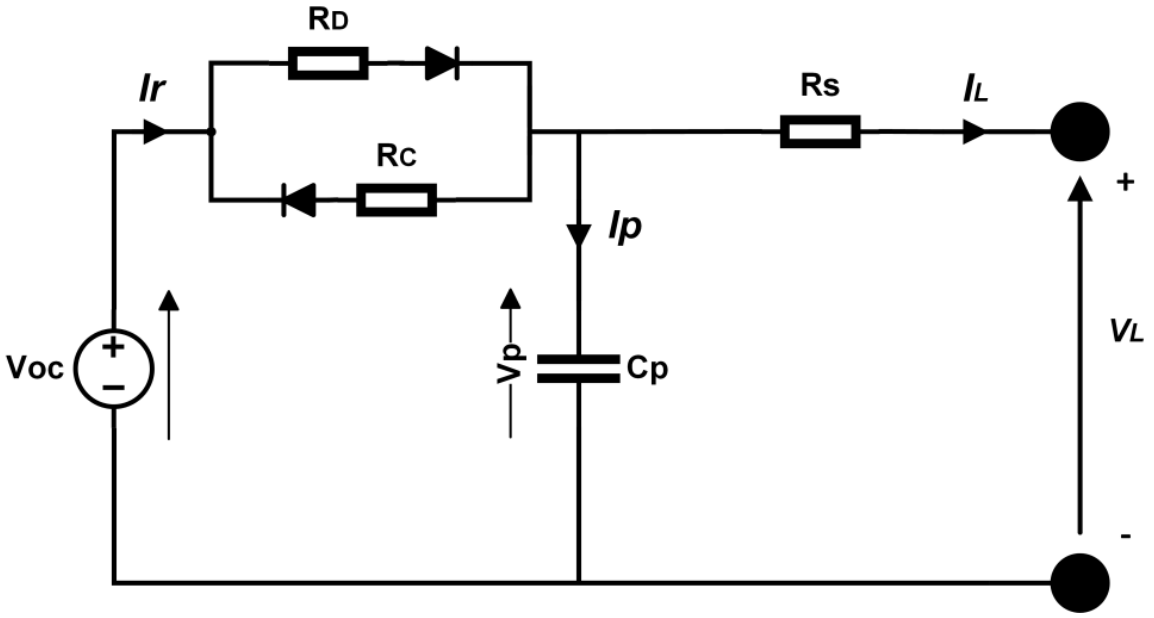

Figure (3-10): Schematic of the dynamic model.

Since this model adopted to develop a state of charge estimation, its dynamic equations for charge and discharge are given by:

$$I_L = \frac{V_P - V_{oc}}{R_s} \tag{3.21}$$

$$\dot{V}_p = -\frac{1}{R_C C_p} V_p + \frac{1}{R_C C_p} V_{oc} - \frac{1}{C_p} I_L, \quad V_p > V_{oc}$$
$$\dot{V}_p = -\frac{1}{R_D C_p} V_p + \frac{1}{R_D C_p} V_{oc} - \frac{1}{C_p} I_L, \quad V_p < V_{oc} \tag{3.22}$$

$$V_L = V_p - R_s I_L \tag{3.23}$$

The current I_L is considered to have positive sign when the battery is charging. This circuit model is formed to model the internal working of the battery to count the losses energy [112].

3.3.3.3.5. Second-order Thevenin model

In document [113, 115], they carried out a Dual Polarity (DP), which is an enhancement to the first-order Thevenin model. Since the first-order Thevenin model cannot accurately capture both of the polarization characteristics of the battery by using one RC branch, the DP model attempts to capture the concentration polarization and the electrochemical polarization separately by using two different RC branches, hence its name dual polarity [98]. Figure (3-11), shows the DP model circuit schematic.

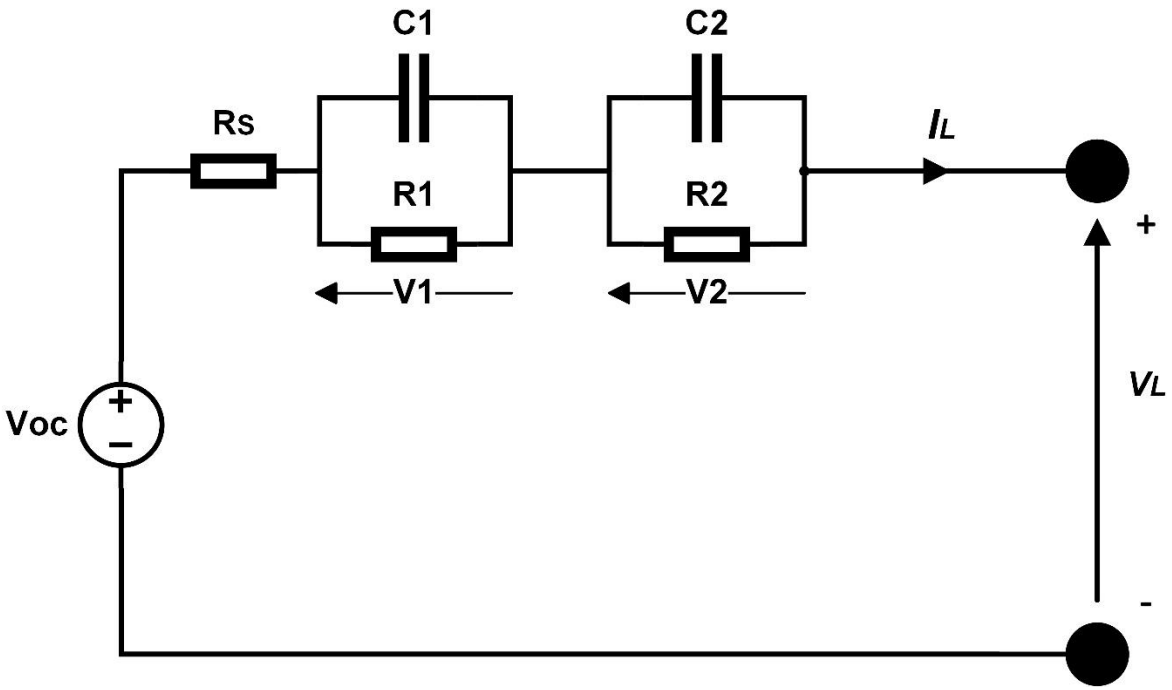

Figure (3-11): Schematic of the second-order Thevenin model (DP).

This model allows refining the description of polarization characteristics of the battery and simulating the concentration polarization and the electrochemical polarization separately, which leads to an improved simulation at the moments of end of charge or discharge compared to the first-order Thevenin model.

The DP model may be studied by breaking it into three pieces: The open-circuit voltage $\boldsymbol{Voc}$, which is reproduced by a voltage source. resistances R_s , R_1, R_2 which describe the battery's internal resistance, electrochemical polarization, and polarization resistance, respectively. Besides, the capacitances C_1, and C_2 implemented to characterize the transient response during the transfer of power to/from the battery and the

electrochemical and concentration polarization separately. Finally, the circuit behavior may be described by the following set of equations:

$$\dot{V}_1 = -\frac{1}{R_1 C_1} V_1 + \frac{1}{C_1} I_L \quad (3.24)$$

$$\dot{V}_2 = -\frac{1}{R_2 C_2} V_2 + \frac{1}{C_2} I_L \quad (3.25)$$

$$V_L = Voc(SOC) - V_1 - V_2 - R_s I_L \quad (3.26)$$

3.3.3.3.6. Third-order Thevenin model

The DP model may modify by adding another RC branch due to more accuracy and efficiency as denoted in [116, 117]. It contains three pieces: The open-circuit voltage $\boldsymbol{Voc}$, series resistances R_s , and three parallel branches formed by R_1, R_2, R_3, which represent the battery's internal resistance, electrochemical polarization, and polarization resistance, and the capacitances C_1, C_2 and C_3 implemented to characterize the transient response under different current profiles. The Figure (3-12) depicted the schematic of the third-order Thevenin model.

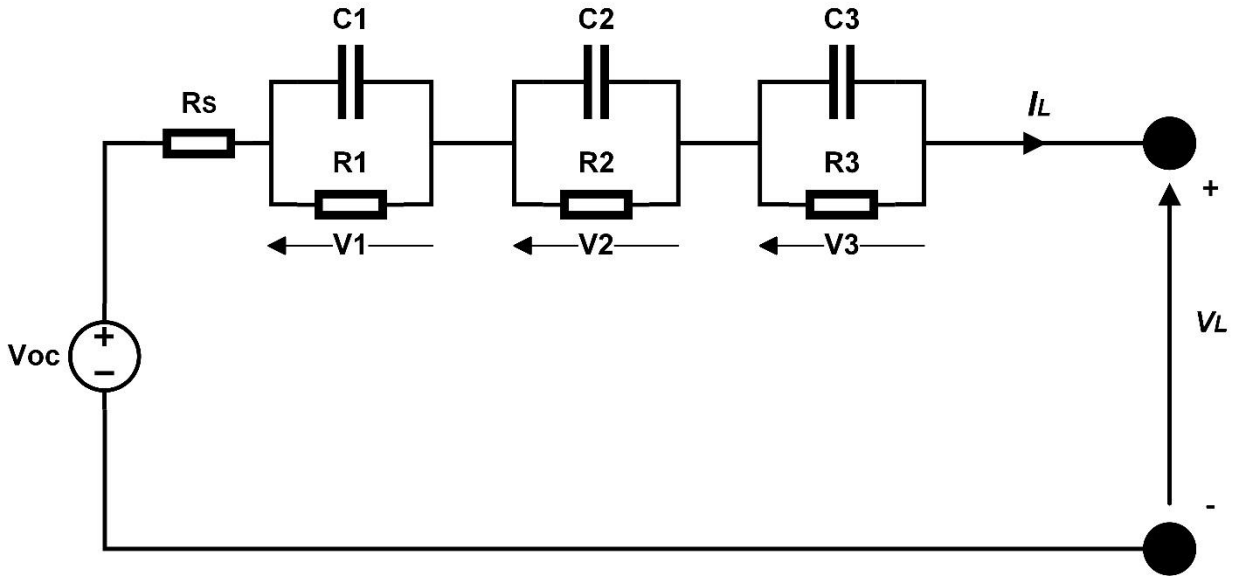

Figure (3-12): The third-order Thevenin model.

Where the governing equations can be expressed as:

$$\dot{V}_1 = -\frac{1}{R_1 C_1} V_1 + \frac{1}{C_1} I_L \quad (3.27)$$

$$\dot{V}_2 = -\frac{1}{R_2C_2}V_2 + \frac{1}{C_2}I_L \quad (3.28)$$

$$\dot{V}_3 = -\frac{1}{R_3C_3}V_3 + \frac{1}{C_3}I_L \quad (3.29)$$

$$V_L = Voc(SOC) - V_1 - V_2 - V_3 - R_sI_L \quad (3.30)$$

3.3.3.3.7. N-order Thevenin model

The n-order model called also Randle model, it consists of n network branches as illustrated in Figure (3-13). It uses multiple RC branches, which is expressed by the N order to get more accuracy and high precision [118, 119].

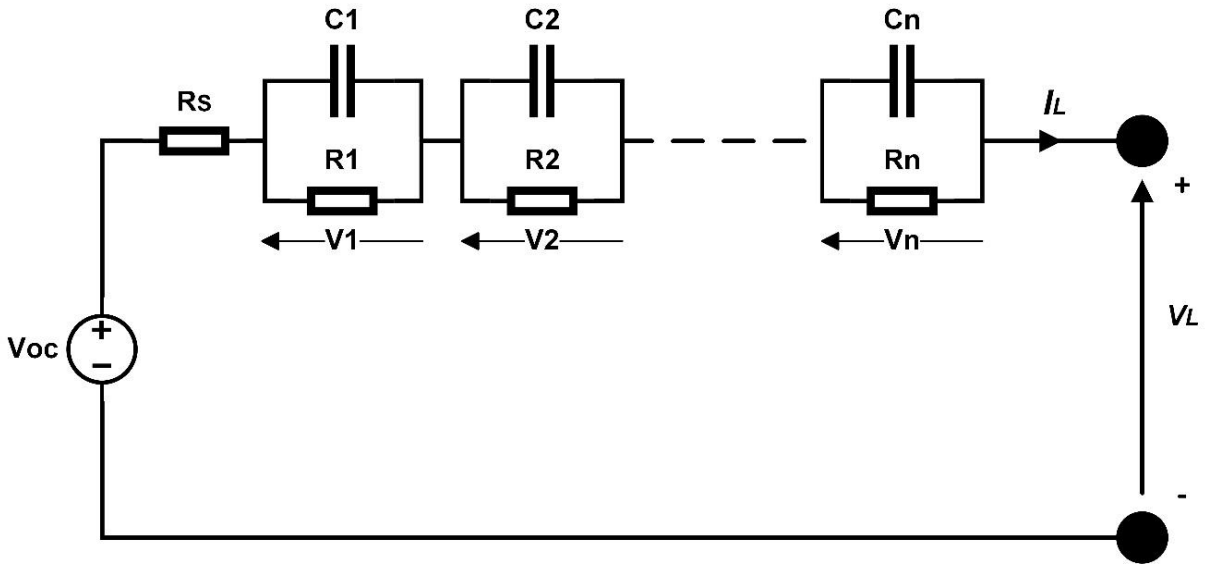

Figure (3-13): The N-order Randle model.

$$\dot{V}_1 = -\frac{1}{R_1C_1}V_1 + \frac{1}{C_1}I_L \quad (3.31)$$

$$\dot{V}_2 = -\frac{1}{R_2C_2}V_2 + \frac{1}{C_2}I_L \quad (3.32)$$

.
.
.

$$\dot{V}_n = -\frac{1}{R_nC_n}V_n + \frac{1}{C_n}I_L \quad (3.33)$$

$$V_L = Voc(SOC) - V_1 - V_2 - \cdots - V_n - R_sI_L \quad (3.34)$$

3.3.3.3.8. Resistor-Capacitor (RC) model

The resistor-capacitor (RC) model is composed of two capacitances and three resistances as shown in Figure (3-14) [120, 121]. The large capacitance C_b describes the ability of the battery to store electric charges, the small capacitance C_s represents the surface capacity and the diffusion effect of the Li-ion battery, R_{int} is the terminal resistance, R_s is the surface resistance, and R_b is the end resistance.

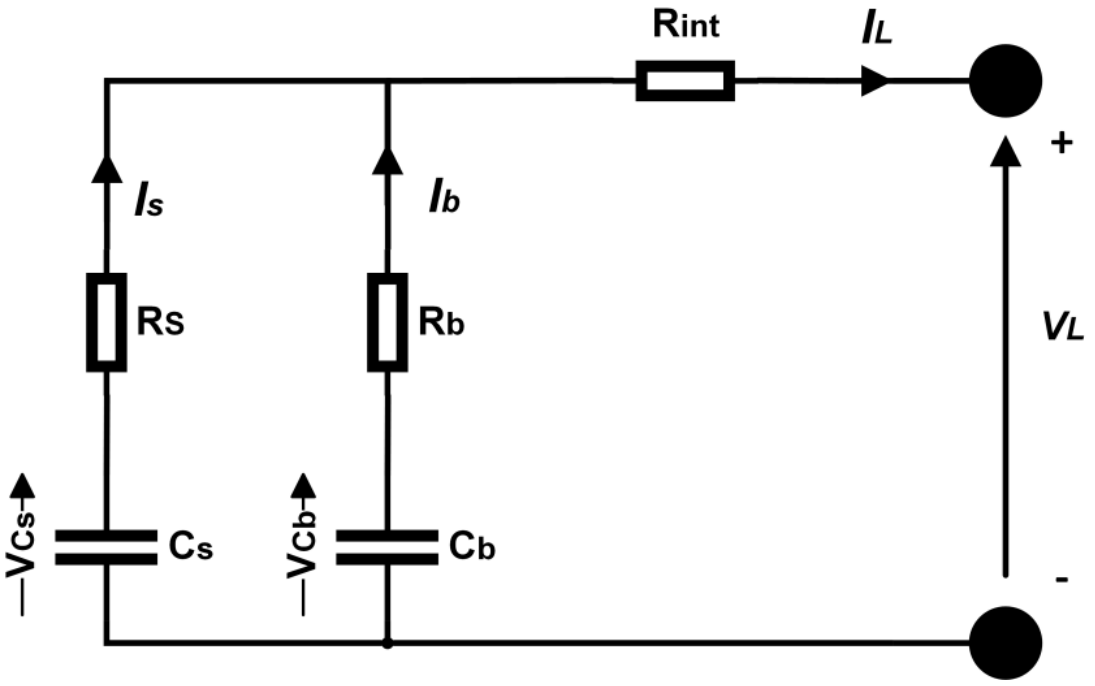

Figure (3-14): Resistor-Capacitor model.

Voltages V_{cb} and V_{cs} at both ends of the two capacitances are the status variables, terminal current I_L is the input variable, and terminal voltage V_L is the output variable. Governing equations are formulated based on Kirchhoff's law from which the RC model equations are deduced.

$$\dot{V}_{cb} = -\frac{1}{(R_s + R_b)C_b}V_{cb} + \frac{1}{(R_s + R_b)C_b}V_{cs} + \frac{R_s}{(R_s + R_b)C_b}I_L \qquad (3.35)$$

$$\dot{V}_{cs} = \frac{1}{(R_s + R_b)C_s}V_{cs} - \frac{1}{(R_s + R_b)C_s}V_{cs} + \frac{R_b}{(R_s + R_b)C_s}I_L \qquad (3.36)$$

$$V_L = \frac{R_s}{R_s + R_b}V_{cb} + \frac{R_b}{R_s + R_b}V_{cs} + (\frac{R_s R_b}{R_s + R_b} + R_{int})I_L \qquad (3.37)$$

3.3.3.3.9. Hybrid model

A hybrid model is composed of two sub-circuits. The first circuit is a first-order Thevenin model, second , third or RC model to capture the dynamics of the battery but the second one is formed by a capacitor C_b to indicate the maximum energy available. Therefore, Figure (3-15) presents an overview of its general structure [122].

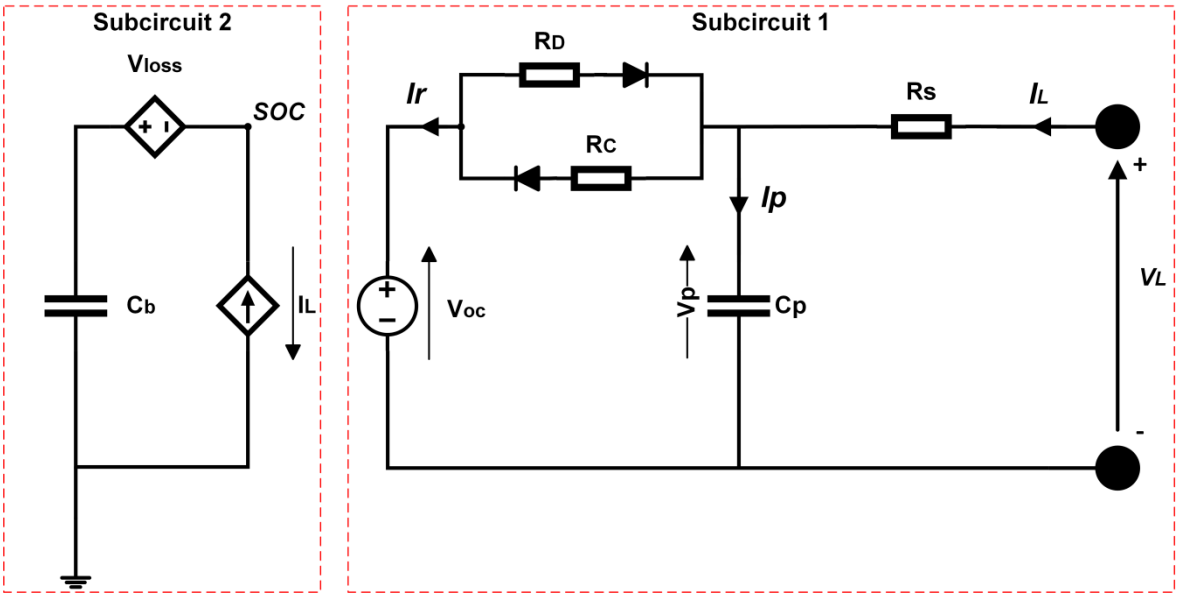

Figure (3-15): Schematic of hybrid model with two stages.

3.4. Conclusion

The aforementioned models are mainly developed and proposed on the basis of equivalent circuit models (ECMs). Therefore, these ECMs are basically derived from empirical knowledge and experimental results, which is used to idealize element of the circuit to represent electrical behaviours of batteries.

In literature, there exist a lot of ECMs models, which are designed in various circuit but they lie in main basis of simplicity. The flexibility of this kind of model is remarkable in representing the behaviour of battery when include network branches.

Chapter 4
Battery SOC estimation based on EKF and SMO observers

4.1. Introduction

In this chapter, estimation strategies for State of Charge (SOC) are discussed. Therefore, a description of the evolution of SOC estimation techniques and strategies is considered. The application of various estimation techniques to estimate SOC in battery systems is presented and It is followed by simulation and experimental procedure used in model fitting and SOC estimation.

Furthermore, this chapter summarized two SOC estimation techniques which are extended Kalman filter (EKF) and sliding mode observer (SMO). At the end, a conclusion is provided.

4.2. Estimation technique

Estimation theory is a branch of statistics science that concentrates on generating estimated values of parameters using measured empirical random data. Therefore, Estimation is used to extract information from measurement signals provided by sensors. It is used in many fields such as target tracking, control, monitoring, filtering, navigation, and communication [52].

Furthermore, some of the estimation algorithms are embedded in most daily used devices in our life and in industry. Extracting information from known signal has received high demand in recent years especially into industry caused by the absence of a real sensor or the high cost of building one to predict invisible internal states.

However, this problem is called parameters estimation, which belongs to probability science that investigates into engineering problems. It is based on optimizing the quality of extracted information and its robustness and reliability.

The state estimation problem consists of three parts: the physical system, the measurement system, and the state estimator. Furthermore, Figure (4-1) shows the general block diagrams of the state estimation process, where both the physical system and the measurement system will add noise to the input and output signals since it will be used by the state estimator to derive an estimate of the true states of the physical system.

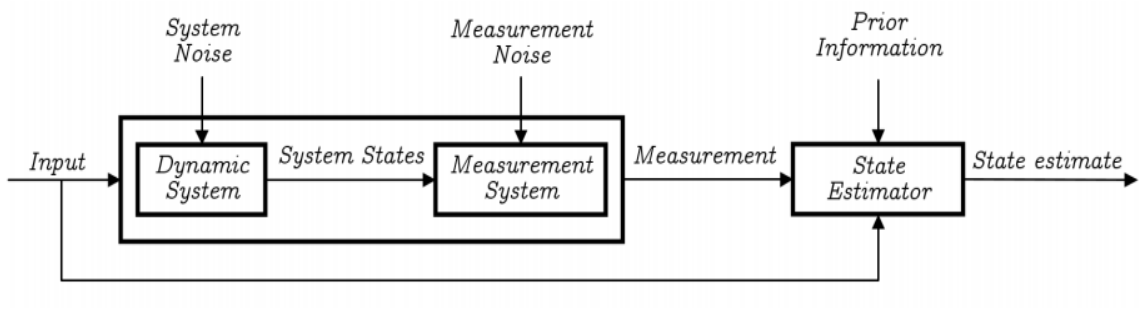

Figure (4-1): General blocks of state estimator.

In this thesis, the physical system to be analysed is the battery and the states will vary depending on the selected ECM but may include SOC and values of the polarization effects (capacitors) as it can be seen in Chapter 3.

Discrete time state-space representation is commonly used in filtering for modelling of a system under consideration as follows [52]:

$$\boldsymbol{x_{k+1}} = \boldsymbol{A_k x_k} + \boldsymbol{B_k u_k} + \boldsymbol{w_k} \tag{4.1}$$

$$\boldsymbol{y_k} = \boldsymbol{C_k x_k} + \boldsymbol{D_k u_k} + \boldsymbol{v_k} \tag{4.2}$$

where $x_k \in \mathbb{R}^{n*1}$ is the state vector, $u_k \in \mathbb{R}^{p*1}$ is the input vector, $y_k \in \mathbb{R}^{m*1}$ is the system output vector, $w_k \in \mathbb{R}^{n*1}$ is the system noise, and $v_k \in \mathbb{R}^{m*1}$ is the measurement noise. $A_k \in \mathbb{R}^{n*n}$,$B_k \in \mathbb{R}^{n*p}$, $C_k \in \mathbb{R}^{m*n}$, and $D_k \in \mathbb{R}^{m*p}$ are the system input, measurement and feed through matrices. Therefore, equation (4.1) and (4.2) are the state and measurement equations.

4.3. Kalman filter observer

The basic Kalman filter is limited to a linear assumption. However, there are more complex systems which they can be nonlinear. Furthermore, there exist different versions of Kalman filter to deal with this problem. In this part we will introduce different Kalman filter versions.

4.3.1. Kalman filter

Kalman filter (KF) is a well-known estimation theory introduced by Rudolf Emil Kalman in 1960 [123]. This filter provides a recursive solution through linear optimal filtering to estimate systems' state variables. The Kalman filter is an optimal state estimation method for discrete linear time-varying (LTV) systems [124].

It uses a set of recursive equations and input measurements containing noises. The Kalman filter estimates unknown variables more precisely by finding the minimum mean squared error estimate of the present state of the system.

Considering the discrete LTV system of Figure (4-2), whereas the state space model of the process has been described in equations (4.1) and (4.2).

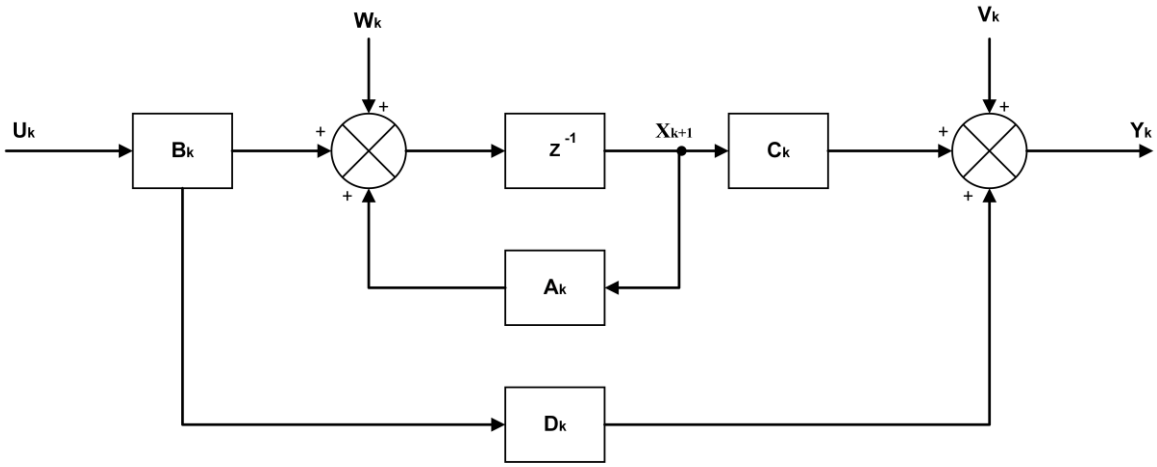

Figure (4-2): Block diagram of discrete Kalman filter system.

Figure (4-3) depicts the Predictor-Corrector algorithm of the KF. The states of the system are estimated using the system model and input, where the estimate is projected forward in time of the current state estimate to obtain the 'a priori' for the next time step.

Therefore, a correction step is then added based on the innovation technique, thus forming the updated or a posterior. The corrector step is responsible for the feedback, which is adding the new measurement into the 'a priori' estimate to generate an improved version of it [124].

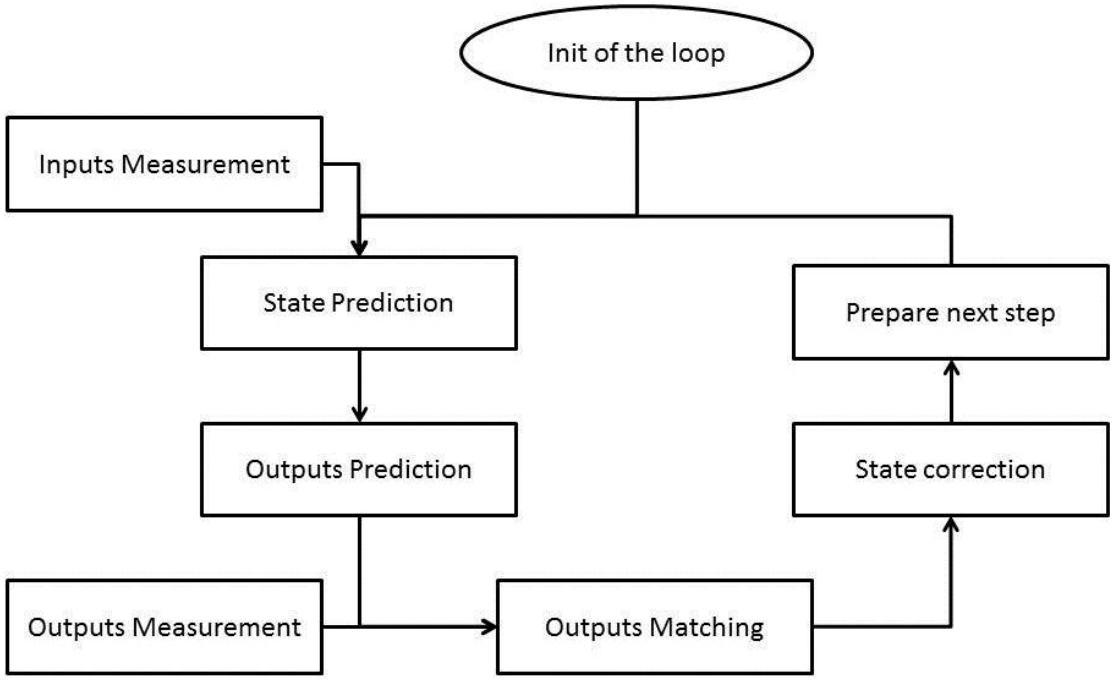

Figure (4-3): Overview of predictor-corrector technique.

Consider the discrete-time system defined by equation (4.1) and (4.2), where the variable w_k is the system noise, and v_k is the measurement noise. The KF assume that both w_k and v_k are independent of each other, and have zeros mean Gaussian distribution as shown below:

$$\boldsymbol{p(w_k) \sim \mathcal{N}(0, Q_k)} \tag{4.3}$$

$$\boldsymbol{p(v_k) \sim \mathcal{N}(0, R_k)} \tag{4.4}$$

Where Q_k and R_k are the system and measurement noise covariance, respectively.

The KF has two stages. The first stage called the prediction, which consists of two main equations form the system states and covariance by using the model and input measurement. The predicted state vector and covariance expressed by:

$$\boldsymbol{\hat{x}_{k+1} = A_k \hat{x}_k + B_k u_k} \tag{4.5}$$

$$\boldsymbol{P_{k+1/k} = A_k P_{k/k} A_k^T + Q_k} \tag{4.6}$$

$\hat{\boldsymbol{x}}_{\boldsymbol{k+1}}$ denotes priori state estimate at step $k+1$, whereas $\hat{x}_k$ is the posterior state estimate at step k. $\boldsymbol{P_{k+1/k}}$ denotes priori error covariance update at step $k+1$, whereas $\boldsymbol{P_{k/k}}$ is the posterior error covariance at step k. Where k denotes the time step and T denotes the transpose matrix of A_k.

The second stage involves three recursive equations. Thereby, a correcting step referred to computing the Kalman gain (L_k), which is denoting the level of uncertainty 'boundary of error'. It will be calculate using the following equation:

$$\boldsymbol{L_k = P_{k+1/k} C_k^T * (C_k P_{k+1/k} C_k^T + R_k)^{-1}} \tag{4.7}$$

Thus, a refined posteriori state estimate $\hat{\boldsymbol{x}}_{\boldsymbol{k+1/k+1}}$ is then calculated based on the output measurement of the system, such that:

$$\hat{\boldsymbol{x}}_{\boldsymbol{k+1/k+1}} = \hat{\boldsymbol{x}}_{\boldsymbol{k+1/k}} + \boldsymbol{L_k(y_k - C_k x_{k+1/k})} \tag{4.8}$$

The associated posterior error updates the covariance $\boldsymbol{P_{k+1/k+1}}$ as:

$$\boldsymbol{P_{k+1/k+1} = (I - L_k C_k) P_{k+1/k}} \tag{4.9}$$

Where I is the identity matrix. Lastly, this process is repeated iteratively throughout the linear state estimation problem until the input/output data reached the end.

In summary, the KF uses the entire observed input data and output measurement data to find the minimum squared error estimate state of the true state x_k. However, the KF yields the optimal solution to the linear estimation problem.

4.3.2. The extended Kalman filter (EKF)

Since the KF has been received the first time in 1960, extensive research has been done after to edit and performs its reliable mathematical with nonlinear systems as a tool that enhances the computational efficiency. Furthermore, its cost for implementation is significantly cheaper than enhancing the system with more accurate sensors if exist or enhance the estimator if there is no sensor able to measure internal states.

In reality, most of the systems are highly nonlinear systems. Therefore, it was natural for the KF to be extended to tackle nonlinear systems.

In the EKF the system model is linearized around the current a priori state estimate. The linearized model is then used for the calculation of the Kalman gain. In this way the nonlinear system can be presented as:

$$x_{k+1} = f(x_k, u_k) + w_k \tag{4.10}$$

$$y_k = g(x_k, u_k) + v_k \tag{4.11}$$

where equation (4.10) represent the state equation at the previous time step k to the future time step $k+1$, and equation (4.11) represents the output equation which relates the state to the output, both w_k and v_k represent the system and measurement noise and are assumed to be white noise with zero mean and known covariance Q and R respectively.

The EKF linearizes the estimation around the current estimate using partial derivatives (First-Order Taylor series expansion) of the system and measurement functions to compute estimates. By linearizing, the EKF may introduce instability as it may overlook system nonlinearities that were not capture with the model [88, 104, 117, 118]. The following equation depicts the first-order Taylor approximation:

$$\boldsymbol{f(x) \approx f(\hat{x}) + \frac{\partial f}{\partial x}\Big|_{x=\hat{x}} (\hat{x} - x)} \tag{4.12}$$

By applying the first order into equations (4.10) and (4.11), yields to:

$$\boldsymbol{F_k = \frac{\partial f(x_k, u_k)}{\partial x_k}} \tag{4.13}$$

$$\boldsymbol{G_k = \frac{\partial g(x_k, u_k)}{\partial x_k}} \tag{4.14}$$

the matrices A_k, B_k, C_k and D_k as follows :

$$\boldsymbol{A_k = \frac{\partial f(x_k, u_k)}{\partial x_k}} \tag{4.15}$$

$$\boldsymbol{B_k = \frac{\partial f(x_k, u_k)}{\partial u_k}} \tag{4.16}$$

$$\boldsymbol{C_k = \frac{\partial g(x_k, u_k)}{\partial x_k}} \tag{4.17}$$

$$\boldsymbol{D_k = \frac{\partial g(x_k, u_k)}{\partial u_k}} \tag{4.18}$$

After update state estimation and error covariance as previous equations (4.5) and (4.6). The Kalman gain is then calculated using the linearized model as:

$$\boldsymbol{L_k = P_{k+1/k} C_k^T * (C_k P_{k+1/k} C_k^T + R_k)^{-1}} \tag{4.19}$$

The posteriori estimates are then obtained as:

$$\boldsymbol{\hat{x}_{k+1/k+1} = \hat{x}_{k+1/k} + L_k(y_k - C_k x_{k+1/k})} \tag{4.20}$$

In this step, posterior state is estimated. $\boldsymbol{y_k}$ is the real measurement output which refers to the real terminal voltage of battery.

The associated posterior error updates the covariance $\boldsymbol{P_{k+1/k+1}}$ as:

$$\boldsymbol{P_{k+1/k+1} = (I - L_k C_k) P_{k+1/k}} \tag{4.21}$$

In this stage, posteriori error covariance is estimated and updated. The Kalman steps repeat again until reaches all time step.

The Extended Kalman Filter algorithm is summarized in Figure (4-4).

Time Update (Predictor)
Predict the state ahead $\hat{x}_{k+1\|k} = f(\hat{x}_{k\|k}, u_k)$
Predict the error covariance ahead $P_{k+1\|k} = F_k P_{k\|k} F_k^T + Q_k$

Measurement Update (Corrector)
Compute Kalman Gain $K_{k+1} = P_{k+1\|k} G_{k+1}^T \left(G_{k+1} P_{k+1\|k} G_{k+1}^T + R_{k+1}\right)^{-1}$
Update estimate with measurement $\hat{x}_{k+1\|k+1} = \hat{x}_{k+1\|k} + K_{k+1}\left(z_{k+1} - g(\hat{x}_{k+1\|k}, u_k)\right)$
Update error covariance $P_{k+1\|k+1} = (I - K_{k+1} G_{k+1}) P_{k+1\|k}$

Figure (4-4): Overview on general extended Kalman filter equations.

The EKF may provide big error since Q_k and R_k are depending on P_k and L_k. If the variance of the measurement noise R_k is small, for P_k constant, the measurement is weakly noisy.

Furthermore, the high value of the gain will give more weight to the measurements, which indicate low confidence in the model. Therefore, an adaptive way is adopted in term of control the covariance Q_k and R_k to provide more confidence to the model since they update iteratively.

4.3.3. The adaptive extended Kalman filter (AEKF)

Based on the previous work on the Kalman filter (KF), it became clear to us that to reach optimal performances, it is necessary to have correct aprioris on matrices *F*, *G*, *H*, *Q*, *R* and initial *P*, while the Kalman filter works on the assumption that state and measurement models as well as the statistical distribution of noise are well known. If any of these conditions are not fulfilled, the KF estimator is degraded. Generally, these parametric knowledge of the parameters are taken through analyses empirical data on previously acquired data or simulator.

The results are considered constant and implemented in the filter. This approach leads to the non-adaptation of the system with evolution to external conditions (sensors) where it does not take into account unknown disturbances during the implementation of the filter and the lack of information on the physical system.

In order to make the Kalman filter more robust, several methods are put forward. There are a lot version focuses on adaptive versions, the famous version is focused on the adaptive law that tries to update the statistical distributions of the noise of the system (state) or /and that of the observation, in the most comprehensive formulation of the Kalman filter, which is the EKF filter.

The adaptive EKF (AEKF) based on the previous equations of the EKF, which is popular in estimation. On the other hand, the AEKF includes an adaptive law, which allows us to estimate the covariance of noises recursively and regressively while they vary with the operating conditions [125, 126].

According to equations (4-5) and (4-6), the computation of EKF requires accurate estimation of Q_k and R_k, which is vary during the operation process. The advantage of

AEKF is that can adaptively update Q_k and R_k, therefore the AEKF is formulated as follows:

1. **Innovation:**

$$e_k = y_k - g(\hat{x}_k^-, u_k) \tag{4.22}$$

e_k is innovation sequence which calculate the error between real output measurement y_k and estimated state.

2. **Adaptive law:**

The covariance has been iteratively calculating $\boldsymbol{H_k}$ and updating $\boldsymbol{R_k}$ respectively

$$H_k = \frac{1}{M} \sum_{k-M+1}^{k} e_i * e_i^T \tag{4.23}$$

$$R_k = H_k - C_k P_k^- C_k^T \tag{4.24}$$

M is the size of moving estimation windows. e_i is defined as the difference between y_k and the predicted observation $g(\hat{x}_k^-, u_k)$ at step k .

3. **State estimation covariance**

$$P_K^- = (I + A_k t) P_{k-1} (I + A_k t)^T + Q_k \tag{4.25}$$

$\boldsymbol{t}$ is the sampling time and T is the transpose matrix.

4. **Kalman gain**

$$L_k = P_k^- C_k^T * (C_k P_k^- C_k^T + R_k)^T \tag{4.26}$$

5. **State estimate update**

$$\hat{x}_k^+ = \hat{x}_k^- + L_k e_k \tag{4.27}$$

6. **Update state covariance**

In this stage the AEKF estimate and update the process noise covariance Q_k and covariance P_k^+, respectively[127].

$$Q_k = L_k H_k L_k \tag{4.28}$$

$$P_k^+ = (I - L_k C_k) P_k^- (I - L_k C_k)^T + L_k R_k L_k^T \tag{4.29}$$

4.3.4. State of Charge Estimation using KF

The fundamental feature that makes the EKF optimum observatory for nonlinear systems is the recursion option, while the linearization process makes it suffer from disturbances. The EKF is designed to deal with noisy measurement data and can be correct wrong initial state value due to its feedback control.

Furthermore, its equations are formed in discrete space to estimate SOC, whereas the state equation for the battery model is obtained through multiple internal or hidden states as: $x_1 = V_1, x_2 = SOC$. As depicted in Figure (4-5)

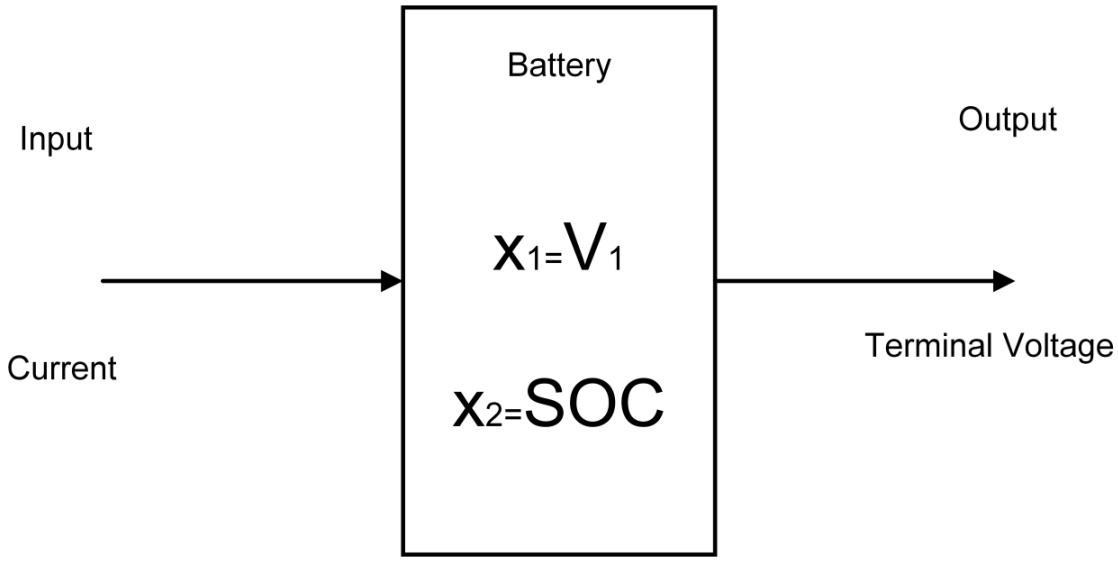

Figure (4-5): Presentation of internal states estimation.

As mentioned before, SOC, in contrast to terminal voltage and current, is an inner state of the battery and should be estimated instead of directly measurement and absence of real sensor. The equations (4.5) and (4.6) linearized and transformed in discrete space as:

$$\boldsymbol{x_{k+1} = A_k x_k + B_k I_{L,k} + w_k} \tag{4.30}$$

$$\boldsymbol{V_{L,k} = C_k x_k + D_k I_{L,k} + v_k} \tag{4.31}$$

where $\boldsymbol{SOC_k}$ is the observation of $\boldsymbol{SOC}$ at time step**,** which is computed by the equation (4.29):

$$\boldsymbol{SOC_k = \left(SOC_0 - \frac{\eta I_{L,k} t}{Q_n}\right) * 100} \tag{4.32}$$

In this equation, $\boldsymbol{t}$ is the sampling time, $\boldsymbol{\eta}$ is the columbic efficiency, in this thesis assumed to equal to one. $\boldsymbol{Q_n}$ denotes the usable capacity of the battery's available capacity.

4.3.4.1. Partnership for a new generation of vehicle (PNGV) model

The PNGV model may be represented by transforming its continuous equations to state space form as:

$$\boldsymbol{\dot{U}_0 = \frac{1}{C_0} I_L} \tag{4.33}$$

$$\boldsymbol{\dot{V}_1 = -\frac{1}{C_1 R_1} V_1 + \frac{1}{C_1} I_L} \tag{4.34}$$

With terminal voltage expressed as:

$$\boldsymbol{V_L = V_{oc} + V_1 + U_0 + R_s I_L} \tag{4.35}$$

The states space forms are:

$$\begin{bmatrix} \boldsymbol{U_{0,k+1}} \\ \boldsymbol{V_{1,k+1}} \end{bmatrix} = \begin{bmatrix} \boldsymbol{1} & \boldsymbol{0} \\ \boldsymbol{0} & \boldsymbol{1 - \frac{t}{R_1 C_1}} \end{bmatrix} \begin{bmatrix} \boldsymbol{U_{0,k}} \\ \boldsymbol{V_{1,k}} \end{bmatrix} + \begin{bmatrix} \boldsymbol{\frac{t}{C_0}} \\ \boldsymbol{\frac{t}{C_1}} \end{bmatrix} \boldsymbol{I_{L,k}} \tag{4.36}$$

$$\boldsymbol{V_{L,k} = V_{oc}(SOC) + V_{1,k} + U_{0,k} + R_s I_{L,k}} \tag{4.37}$$

$\boldsymbol{t}$ is the sampling time.

4.3.4.2. 1st order Thevenin model

Lastly, the Thevenin model may be represented by the following equations as:

$$\begin{bmatrix} SOC_{k+1} \\ V_{1,k+1} \end{bmatrix} = \begin{bmatrix} 1 & 0 \\ 0 & 1 - \dfrac{t}{R_1 C_1} \end{bmatrix} \begin{bmatrix} SOC_k \\ V_{1,k} \end{bmatrix} + \begin{bmatrix} \dfrac{-t * \eta}{Q_n} \\ \dfrac{t}{C_1} \end{bmatrix} I_{L,k} \tag{4.38}$$

$$V_{L,k} = \begin{bmatrix} \dfrac{\partial V_{oc}}{\partial SOC} & -1 \end{bmatrix} \begin{bmatrix} SOC_k \\ V_{1,k} \end{bmatrix} - R_s I_{L,k} \tag{4.39}$$

4.3.4.3. 2nd order Thevenin model

$$\begin{bmatrix} SOC_{k+1} \\ V_{1,k+1} \\ V_{2,k+1} \end{bmatrix} = \begin{bmatrix} 1 & 0 & 0 \\ 0 & 1 - \dfrac{t}{R_1 C_1} & 0 \\ 0 & 0 & 1 - \dfrac{t}{R_2 C_2} \end{bmatrix} \begin{bmatrix} SOC_k \\ V_{1,k} \\ V_{2,k} \end{bmatrix} + \begin{bmatrix} \dfrac{-t * \eta}{Q_n} \\ \dfrac{t}{C_1} \\ \dfrac{t}{C_2} \end{bmatrix} I_{L,k} \tag{4.40}$$

$$V_{L,k} = \begin{bmatrix} \dfrac{\partial V_{oc}}{\partial SOC} & -1 & -1 \end{bmatrix} \begin{bmatrix} SOC_k \\ V_{1,k} \\ V_{2,k} \end{bmatrix} - R_s I_{L,k} \tag{4.41}$$

4.3.4.4. 3rd order Thevenin model

$$\begin{bmatrix} SOC_{k+1} \\ V_{1,k+1} \\ V_{2,k+1} \\ V_{3,k+1} \end{bmatrix} = \begin{bmatrix} 1 & 0 & 0 & 0 \\ 0 & 1 - \dfrac{t}{R_1 C_1} & 0 & 0 \\ 0 & 0 & 1 - \dfrac{t}{R_2 C_2} & 0 \\ 0 & 0 & 0 & 1 - \dfrac{t}{R_3 C_3} \end{bmatrix} \begin{bmatrix} SOC_k \\ V_{1,k} \\ V_{2,k} \\ V_{3,k} \end{bmatrix} + \begin{bmatrix} \dfrac{-t * \eta}{Q_n} \\ \dfrac{t}{C_1} \\ \dfrac{t}{C_2} \\ \dfrac{t}{C_3} \end{bmatrix} I_{L,k} \tag{4.42}$$

$$V_{L,k} = \begin{bmatrix} \dfrac{\partial V_{oc}}{\partial SOC} & -1 & -1 & -1 \end{bmatrix} \begin{bmatrix} SOC_k \\ V_{1,k} \\ V_{2,k} \\ V_{3,k} \end{bmatrix} - R_s I_{L,k} \tag{4.43}$$

4.3.5. OCV-SOC mapping

A unique relationship between OCV and SOC has been experimentally determined, which can be presented with nonlinear function. Therefore, SOC can be mapped OCV through the OCV-SOC relationship.

In Figure (4-6) is shown a mapping OCV-SOC relationship extracted points from experiment and fitted with MATLAB. However, the OCV defined as the terminal voltage without current load and system is in steady state.

However, the OCV can be changed throughout the variation of temperature, in this study the temperature ambient is 25° C.

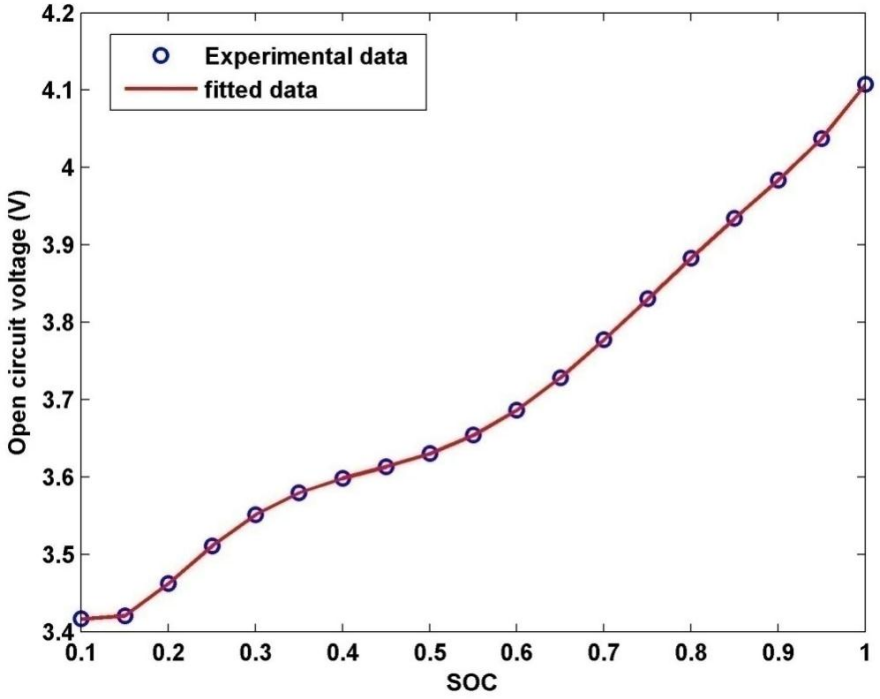

Figure (4-6): OCV-SOC relationship mapping for lithium-ion battery.

4.3.5.1. Partial derivatives

For all battery models, the Jacobians derivatives can be computed by taking partial derivatives of these equations $A_k$and C_k with respect to the states. It is noticeable that the Jacobin of the equation A_k is independent of state of charge, which remains constant.

In the other hand, C_k is relatively dependent in differential terms of V_{oc} and SOC, which can be calculated through Taylor's approximation as presented in the algorithm in Table (4-1).

Table (4-1): Algorithm for computing the partial derivative $\frac{\partial V_{oc}}{\partial SOC}$

Algorithm 1
1: a mapped curve V_{oc} vs SOC with f function 2: **for** k =1,2,…,n **do** **if** $k = 0$ $\frac{\partial V_{oc}}{\partial SOC} = \frac{V_{oc}(SOC_{k+1}) - V_{oc}(SOC_k)}{SOC_{k+1} - SOC_k}$ **else if** $k = n$ $\frac{\partial V_{oc}}{\partial SOC} = \frac{V_{oc}(SOC_k) - V_{oc}(SOC_{k-1})}{SOC_k - SOC_{k-1}}$ **else if** $k = 0$ $V_{oc,forward} = \frac{V_{oc}(SOC_{k+1}) - V_{oc}(SOC_k)}{SOC_{k+1} - SOC_k}$ $V_{oc,backward} = \frac{V_{oc}(SOC_k) - V_{oc}(SOC_{k-1})}{SOC_k - SOC_{k-1}}$ $\frac{\partial V_{oc}}{\partial SOC} = \frac{V_{oc,forward} - V_{oc,backward}}{2}$ **end for**

According to the above algorithm, the $\frac{\partial V_{oc}}{\partial SOC}$ as function of SOC can be depicted as shown is Figure (4-7).

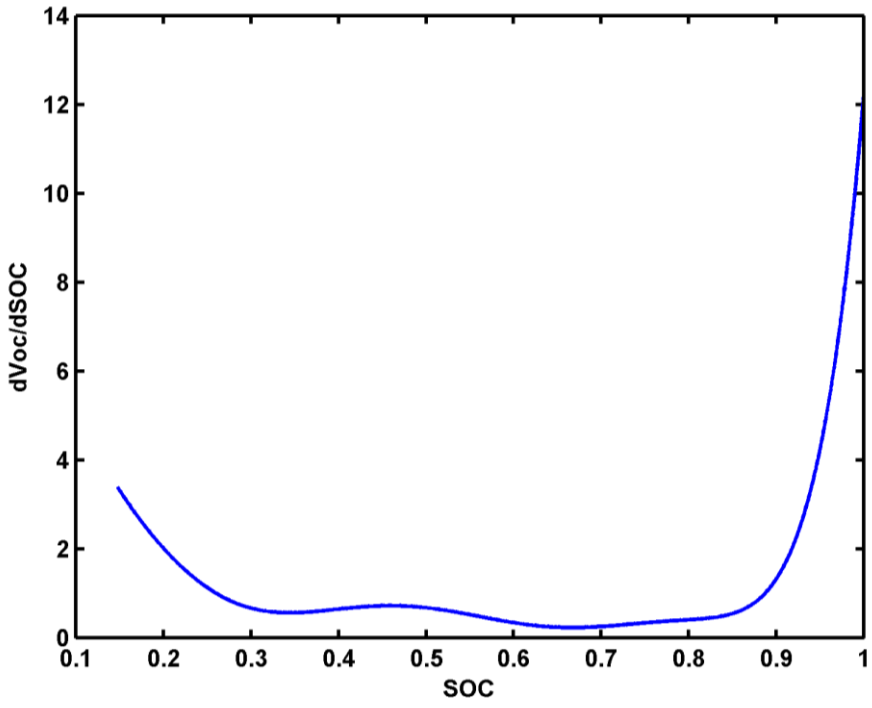

Figure (4-7): Partial derivative of V_{OC} with respect to SOC curve.

The pulse-rest sequences are widely used for characterizing the internal resistance, the diffusion coefficient or the OCV. The measurement of voltage relaxation and the time constants of this electrochemical model and the simulations of the pulse-rest sequences are discussed.

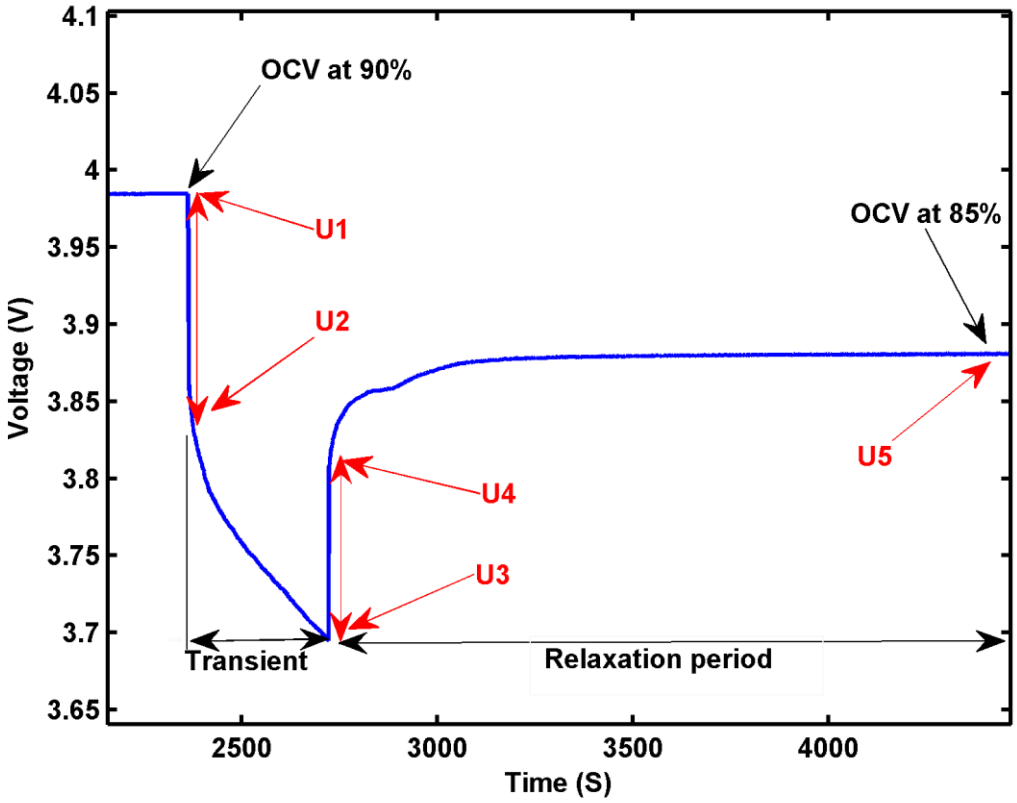

Figure (4-8): The transient response for a pulse discharge curve.

In the literature is reported the simplest equivalent electrical circuit able to simulate approximatively the dynamics of a lithium ion cell's and Lead-acid cell, shown in Figure (3-9). In details, the internal resistance R_s represents the ohmic drop associated to charge transfer. The resistance R_1 and C_1 parallel branch is attributed to physical and chemical phenomena. These electrical components require multiple tests to be identified as function of the SOC.

Consequently, large libraries of resistances and capacitance are created and implemented in the model with a look-up table. Furthermore, such as an example the impulsion reported in Figure (4-8) for the Lithium-Ion battery at 1C-rate, 90 % SOC & 25°C, illustrates the part of the voltage used to identify these electrical components.

In order to identify the parameters of the battery in depicted in Figure (3-9), it is recommended to apply a pulse current and extract them from the transient response. At room of ambient temperature (25°C), a Lithium-ion battery is used in the test, which has a nominal voltage of 3.6 V and a nominal capacity of 10 Ah. A battery testing bench is constructed to settle the experiment, and it consists of a power supply, electronic loads and switches for safety. The testing platform is illustrated in Figure (4-9). The testing prototype can control charging / discharging battery, the data sampling stored into PC host via interface program designed by using the MATLAB/Simulink software.

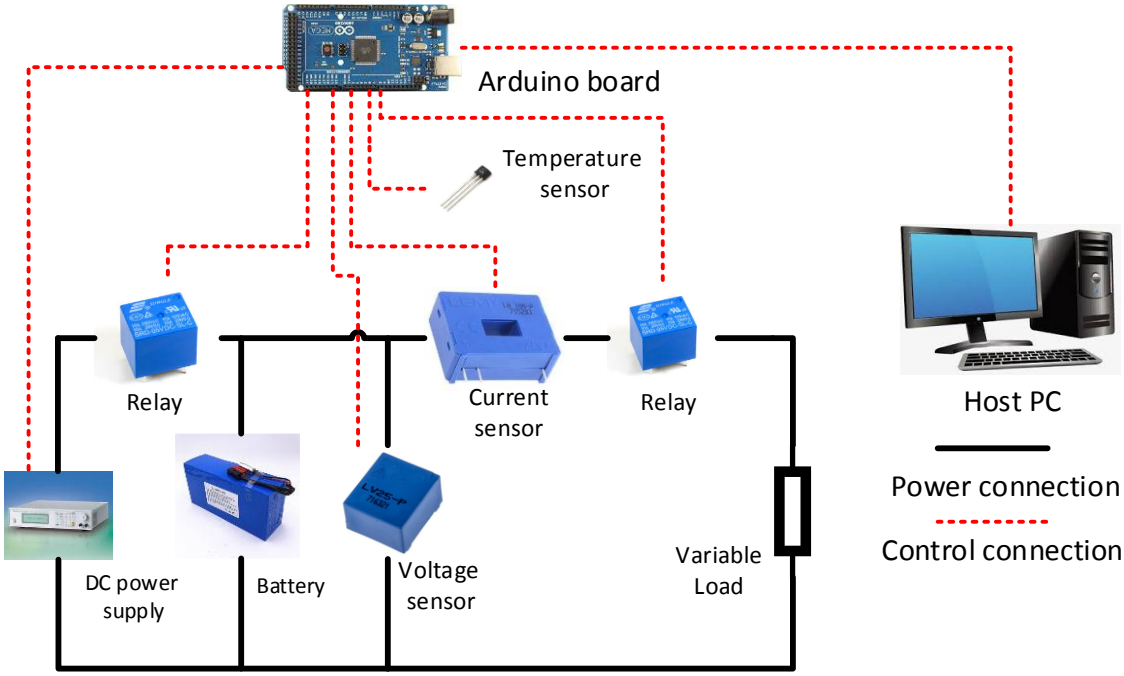

Figure (4-9): The platform of the experiment.

There is off-line parameters identification method, which is widely applied. It is based on minimizing the error between the battery output and the mathematical model with the help of some algorithms. Therefore, this is a robust off-line extraction method, which is used to fit the terminal voltage of the collected data with some mathematical functions.

However, By the aid of the previous principle, a pulse current profile was applied to determine the model parameters. As shown in Figure (4-10), the pulse discharge current consists of 10 sequences of discharge and rest. For the fully charged cell (SOC = 1), each pulse discharge approximate 10% of the nominal capacity equivalent to 10% of the SOC. From the experimental data, the V_{oc} at different SOC can be observed.

Consequently, the nonlinear relationship between the V_{oc} and SOC can be piecewise linearized as a function of SOC as:

$$V_{oc}(SOC) = \alpha_i \, SOC + \beta_i \tag{4.44}$$

where α_i and β_i are constants for each SOC range and theirs values are summarized in Table (4-2).

Table (4-2): Values of relationship between V_{oc}-SOC of Li-ion battery.

SOC	**1-0.9**	**0.9-0.8**	**0.8-0.7**	**0.7-0.6**	**0.6-0.5**	**0.5-0.4**	**0.4-0.3**	**0.3-0.2**	**0.2-0.1**	**0.1-0**
α_i	**1.23**	**1.01**	**1.06**	**0.9**	**0.57**	**0.31**	**0.48**	**0.88**	**0.46**	**0.17**
β_i	**3.40**	**3.371**	**3.287**	**3.407**	**3.475**	**3.345**	**3.147**	**3.035**	**3.075**	**2.87**

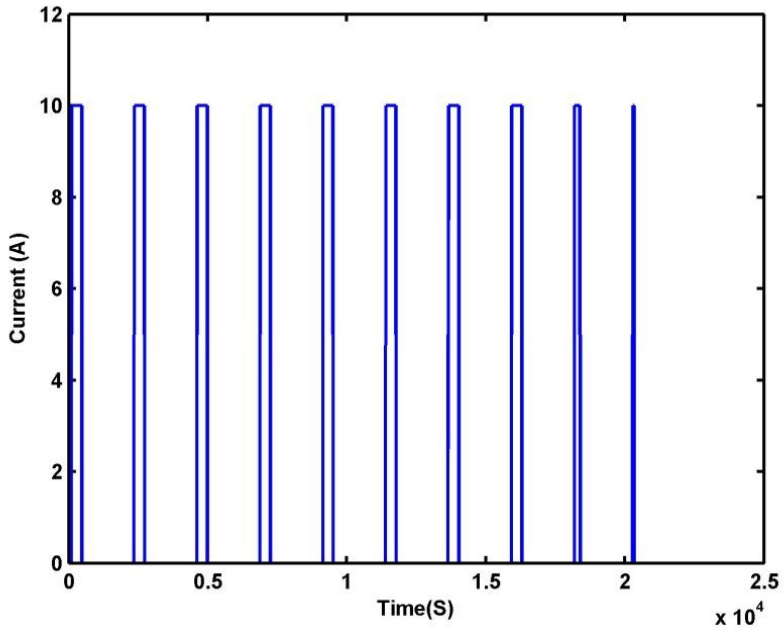

Figure (4-10): Pulse current discharge.

The other parameters of the battery model are determined based on the curve of the terminal voltage as shown in Figure (4-11). To identify the model parameters, the terminal voltage response after 10% SOC for each step discharge is used to extract the 10 sets of circuit parameters. In Figure (4-12), a view of voltage response after a pulse discharge is magnified to present more details.

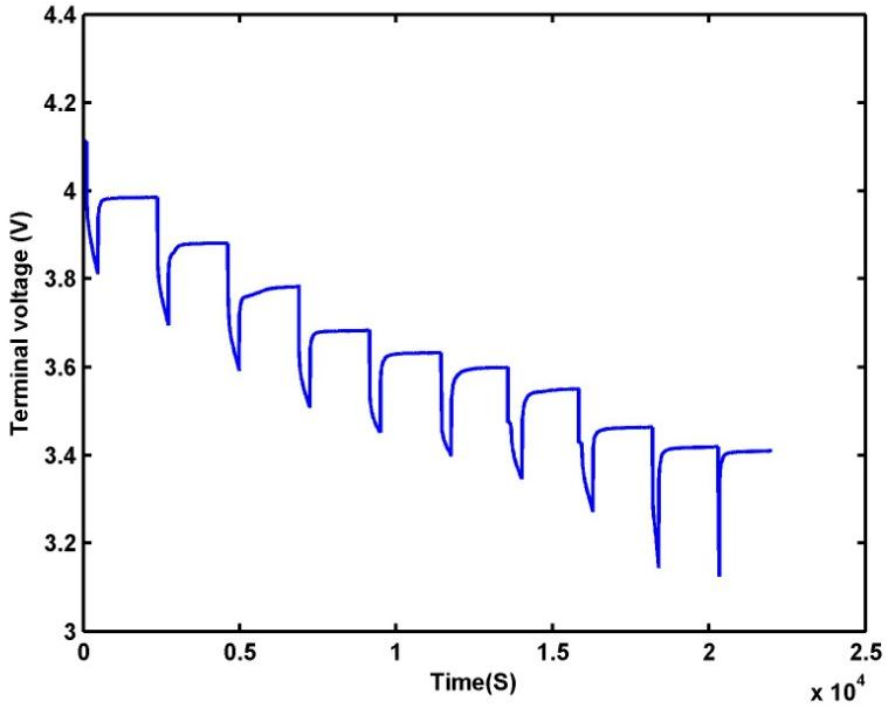

Figure (4-11): The terminal voltage response Li-Ion battery.

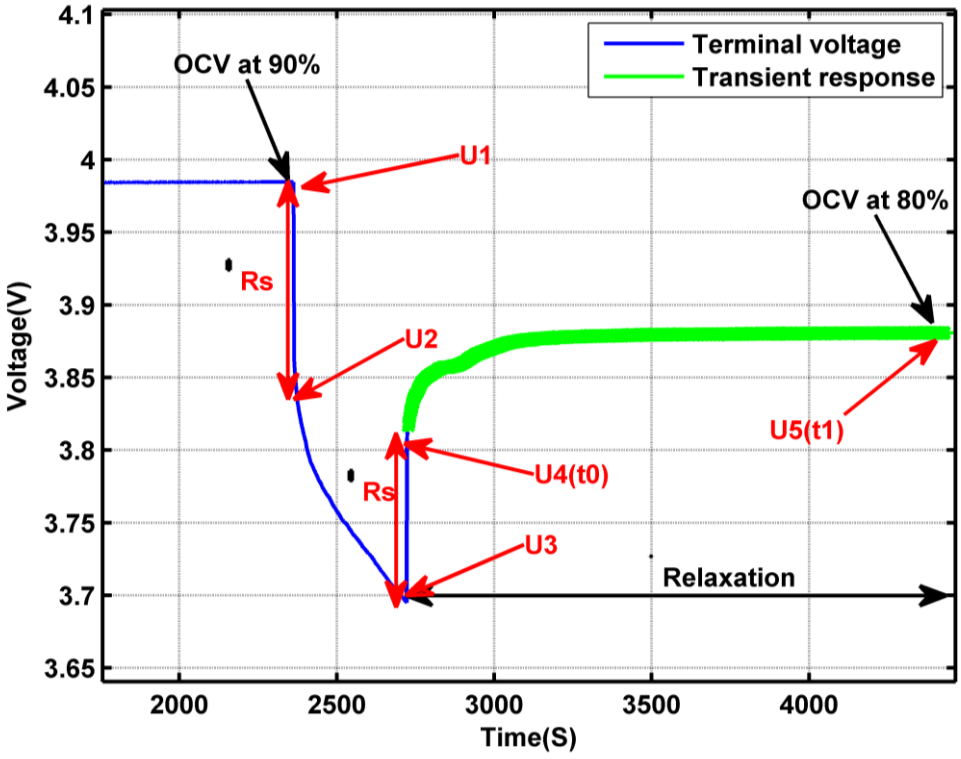

Figure (4-12): The transient response for a pulse discharge.

The R_s resistance is calculated from the instant drop or jump voltage when the current applied or stops. The calculated values for each SOC range are shown in

Figure (4-12). It shows that the R_s change slowly in the range of 0.2 to 1, while it increases rapidly in the rest range. So, the ohmic resistance can be calculated by using the following equation:

$$R_s = \frac{\left|\frac{U_1 - U_2}{I_L}\right| + \left|\frac{U_3 - U_4}{I_L}\right|}{2} \tag{4.45}$$

During the relaxation period as shown in Figure (4-12), in the interval $t_0 \leq t \leq t_1$, the terminal voltage increase slowly to reach the V_{oc} and V_1 denoted as U5 and U4 in Figure (4-12), respectively. So, the terminal voltage can be expressed as:

$$V_L(t) = V_{oc}(SOC) - V_1.e^{-\frac{t0}{\tau}} \tag{4.46}$$

Where $\tau = R_1 C_1$ is the time constant of polarization. The red curve shown in Figure (4-12), it is the terminal response fitted by using the equation (4-46) in MATLAB curve fitting tool. However, the V_1 (U4) was solved by setting the current I_L to zero in equation (3-18)-(3-19) and solve the differential equation, thus, R_1 and C_1 can be calculated as:

$$R_1 = \frac{V_1(t0)}{I_L(t0)(1 - e^{-\frac{t0}{\tau}})} \tag{4.47}$$

$$C_1 = \frac{\tau}{R_1} \tag{4.48}$$

To identify the parameters of the 2nd order Thevenin and 3rd order Thevenin models, the terminal voltage for 2nd order model (Figure (3-11)) is expressed as follow:

$$V_L(t) = V_{oc}(SOC) - V_1.e^{-(\frac{t0}{\tau_1})} - V_2.e^{-(\frac{t0}{\tau_2})} \tag{4.49}$$

Where τ_1 and τ_2 are the time polarization for V_1 and V_2 respectively. The same as previous, the terminal voltage for the 3rd order model (Figure (3-12)) can be presented as:

$$V_L(t) = V_{oc}(SOC) - V_1.e^{-(\frac{t0}{\tau_1})} - V_2.e^{-(\frac{t0}{\tau_2})} - V_3.e^{-(\frac{t0}{\tau_3})} \tag{4.50}$$

After identifying all the model parameters for different SOCs, the parameters can be assumed as constant except in low SOC range. The parameters are presented in Figures (4-13), (4-14) and (4-15) respectively to R_s, R_1, and C_1 for the 1st order Thevenin model.

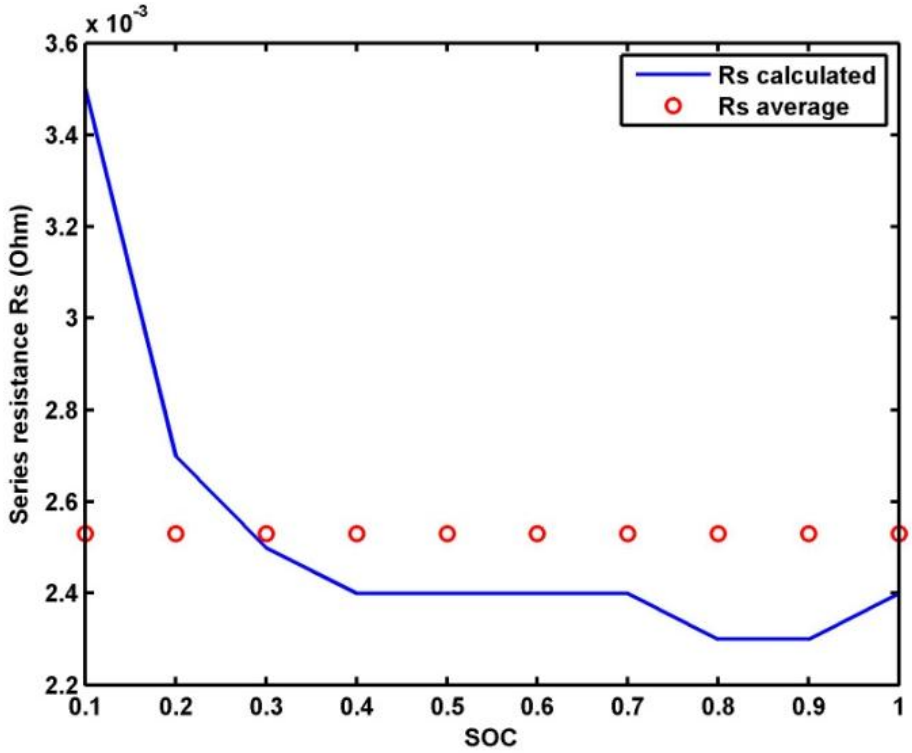

Figure (4-13): The calculated R_s value versus SOC.

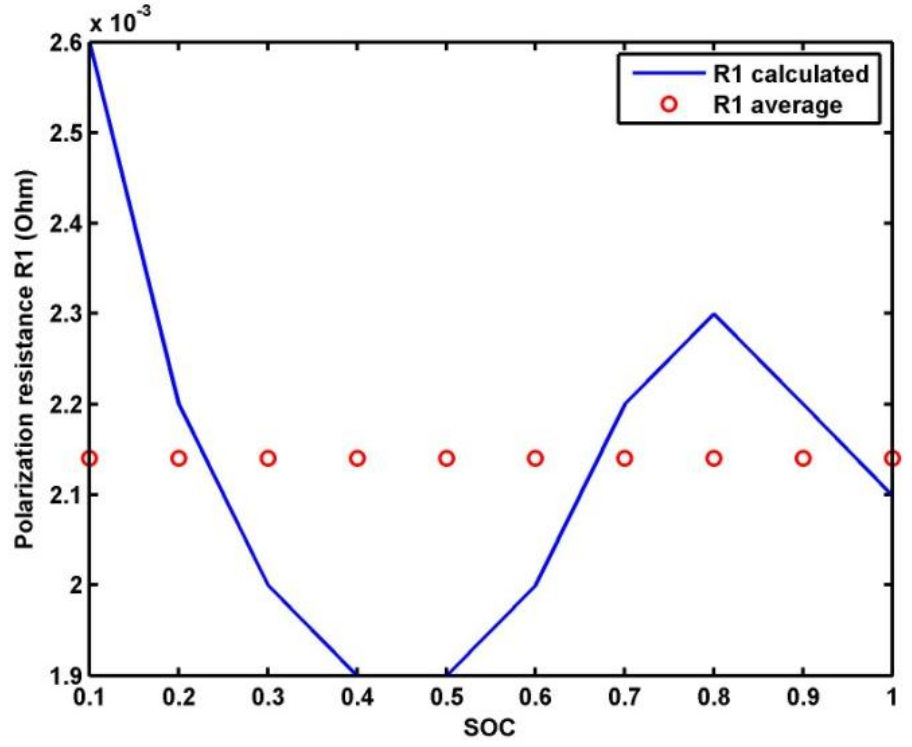

Figure (4-14): The R_1 value versus SOC.

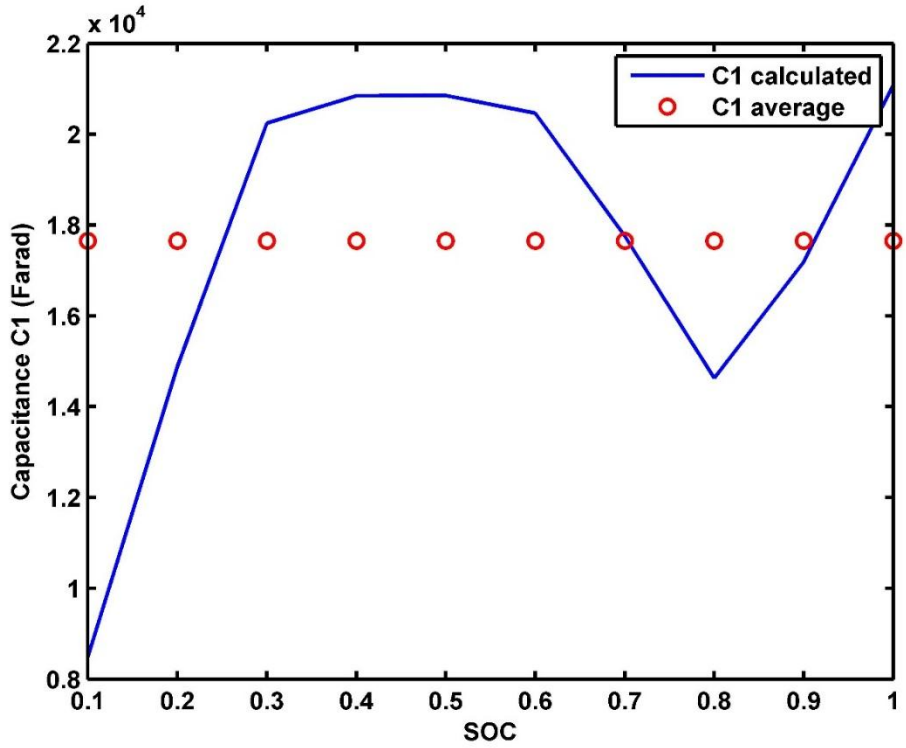

Figure (4-15): The C_1 value versus SOC.

4.3.5.2. Proposed model

Instead of a look-up table, a function of OCV model is proposed. It is designed to fit the OCV-SOC experimental data and capture its behaviour phenomena. The model structure is chosen for online implementation with EKF algorithm, it concerns to enforce the accuracy of SOC estimation.

The OCV of the battery is essential potential, which can give an approximate estimation of the SOC; several models were proposed in the literature [39,45,46]. Some of these models are simple with less parameter, and some are very complex. However, the OCV equations are multiple; in Table (4-3) a review from literature is presented.

Some of them were hard to implement in real-time, as well as, some other models are combined between logarithmic and exponential functions. In fact, some models proved their accuracy as in [13], but their number of parameters needs time-consuming.

Table (4-3): OCV models overview

OCV functions	Reference
$OCV(z) = a_1 z + a_2$	[45]
$OCV(z) = a_1 z^6 + a_2 z^5 + a_3 z^4 + a_4 z^3 + a_5 z^2 + a_6 z + a_7$	[39]
$OCV(z) = a_1 + \frac{a_2}{z} + a_3 z + a_4 \ln(z) + a_5 \ln(1 - z)$	[46]
$OCV(z) = a_1 + \frac{a_2}{z} + a_3 z^2 + a_4 e^{-a_5(1+z)}$	[10,47]

Therefore, proposed a combined analytic model for OCV, in order to create a model that fits closely the OCV closely and also able to deal with the behaviour of the battery dynamics. In this aim, an exponential function combined with logarithm is modelled as well as the root mean square error (RMSE) is taken into consideration. Thereby, the RMSE of other models like the polynomial has high RMSE.

OCV-SOC relationship can be written as:

$$OCV(z) = a_1 e^{a_2 z} + a_3 e^{a_4 z} + a_5 \ln(z) \tag{4.51}$$

The selected OCV model is compared with four different models, which summarized in Table (4-4). The fitted curves are presented in Figure (4-16).

Table (4-4): Candidate OCV models.

Model	Equation of OCV(z)	Number of coefficients
Model 1	$OCV(z) = a_1 z^5 + a_2 z^4 + a_3 z^3 + a_4 z^2 + a_5 z + a_6$	6
Model 2	$OCV(z) = a_1 z^4 + a_2 z^3 + a_3 z^2 + a_4 z + a_5$	5
Model 3	$OCV(z) = a_1 + \frac{a_2}{z} + a_3 z^2 + a_4 e^{-a_5(1+z)}$	5
Model 4	$OCV(z) = a_1 e^{a_2 z} + a_3 e^{a_4 z}$	4
Proposed	$OCV(z) = a_1 e^{a_2 z} + a_3 e^{a_4 z} + a_5 ln(z)$	5

The coefficients of studied models are tabulated in Table (4-5); all the values are obtained by the MATLAB curve fitting toolbox.

Table (4-5): The coefficients of the fitted OCV models.

parameters	Model 1	Model 2	Model 3	Model 4	Proposed
a_1	-6.704	-1.716	3.11	3.368	2.383
a_2	16.72	4.622	- 0.005056	0.1392	0.5472
a_3	-14.01	-3.744	- 0.5843	0.003903	-2.019
a_4	4.69	1.682	0.05521	4.127	-6.563
a_5	0.03277	3.261	-1.681	-	-0.8429
a_6	3.367	-	-	-	-

In [48] , the polynomial model is concluded as the best fit, but when see in Table (4-6) that the proposed model defined in equation (4.48) has a low RMSE value, which presents the best fitting accuracy compared to the other models, and this well shown in Figure (4-16). The experimental points closely stand in the fitted model proposed.

Table (4-6): Comparison between the OCV models' error precision.

	Model 1	Model 2	Model 3	Model 4	Proposed
R-square	0.9977	0.9969	0.9956	0.9945	0.9978
RMSE	0.01188	0.01326	0.01562	0.01696	0.01098

In order to evaluate the effectiveness of our proposed OCV model for SOC estimation, the five OCV models are investigated in this study and show their performances. The Coulomb-counting is used as a reference of SOC estimation where the OCV-SOC relationship is given by look-up table. The SOC estimated is taken as a true SOC and the SOCs estimated by using EKF based on different investigated OCV models.

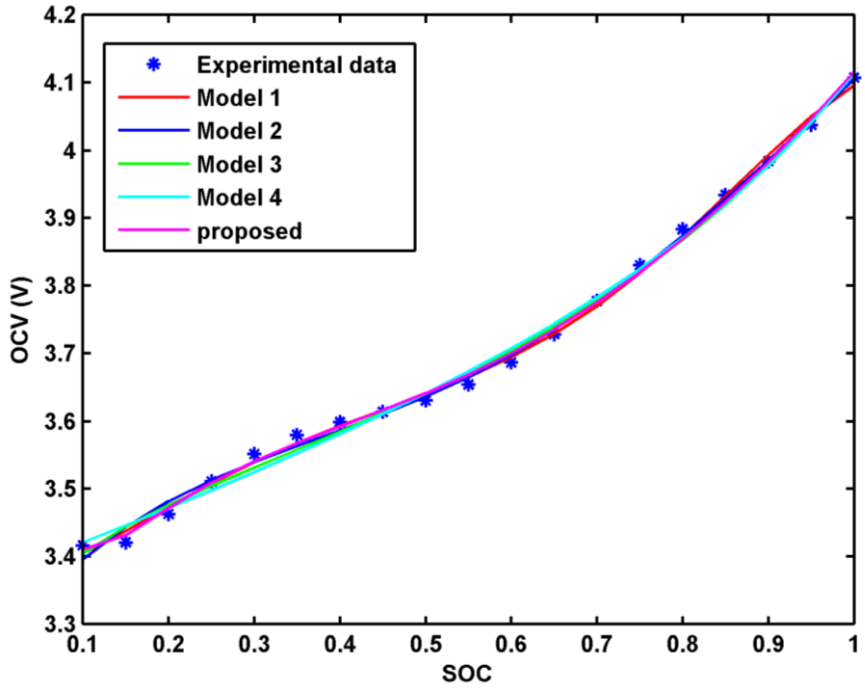

Figure (4-16): fitted OCV results at 25°C.

Actually, a dynamic discharge profile data is loaded and simulated, then, the SOC estimation is observed. The simulated SOCs are plotted for each OCV model as shown in Figure (4-16). The precision of the SOC estimation is computed by comparing the reference curve to the resulting curves as shown in Figure (4-17). In Table (4-6) has been presented the results of corresponding estimation RMSE error.

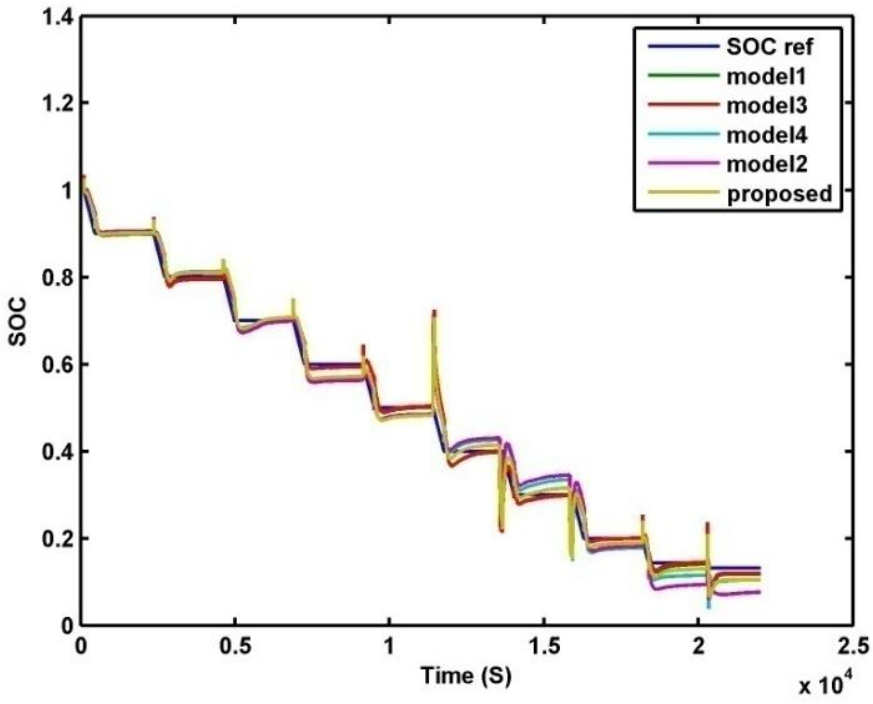

Figure (4-17): EKF simulation based on OCV models.

The AEKF technique is validated by using the pulse discharge tests. The comparative analysis shows the good tracking and matching between experiment and simulated results. The results of simulation and experiment for the pulse discharge test are shown in Figure (4-18), Figure (4-19), Figure (4-20) and Figure (4-21) respectively to the rate of discharge of 0.4 C, 0.5 C and 1C.

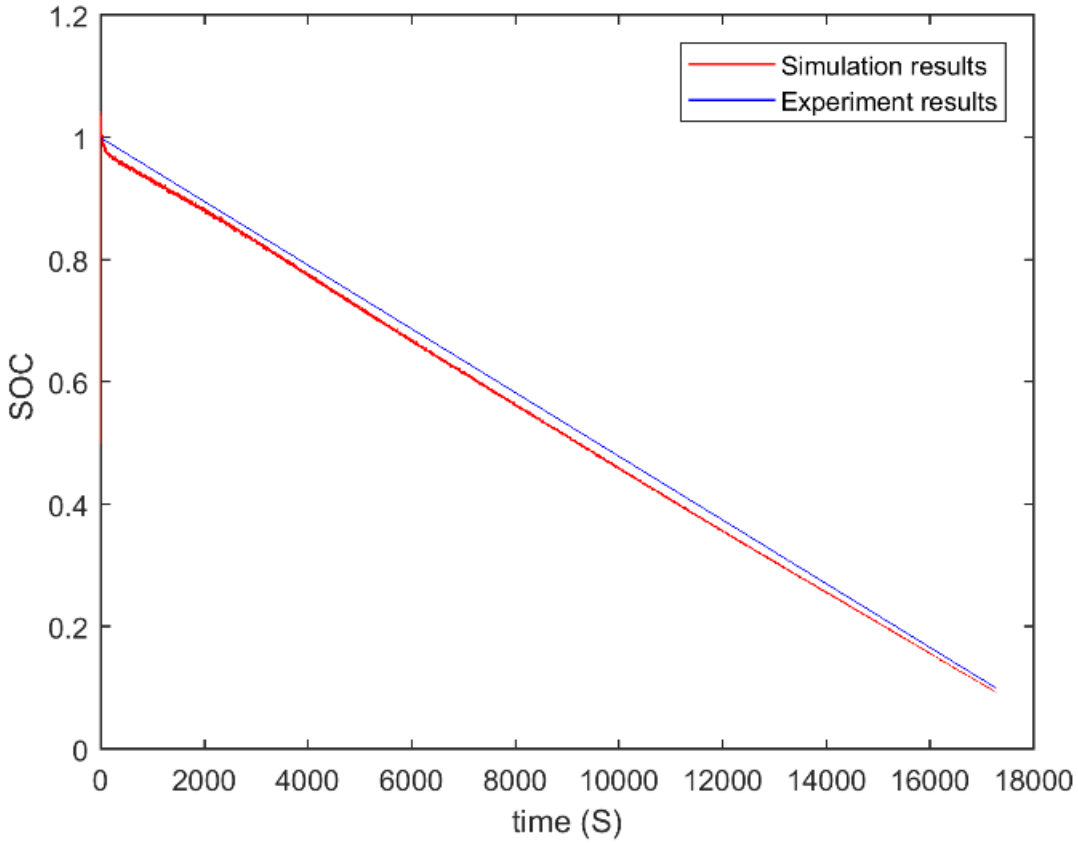

Figure (4-18): Comparison between experimental SOC and AEKF estimated SOC under discharge test.

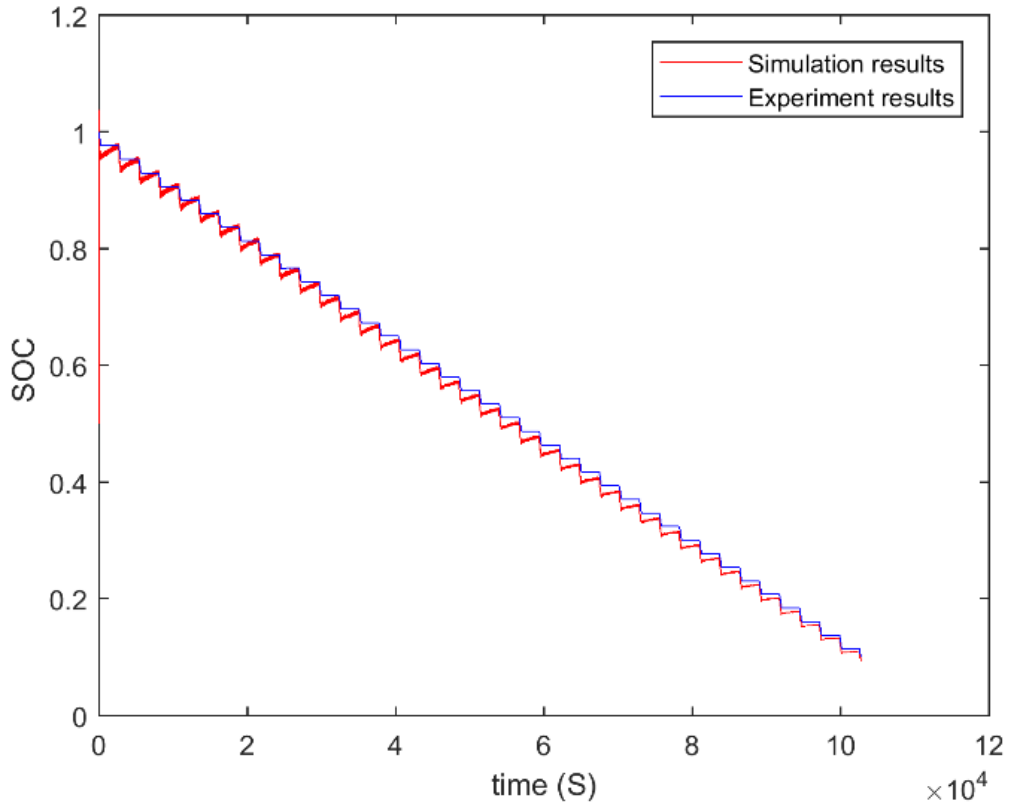

Figure (4-19): Comparison between experimental SOC and EKF estimated SOC under pulse current 0.4 C

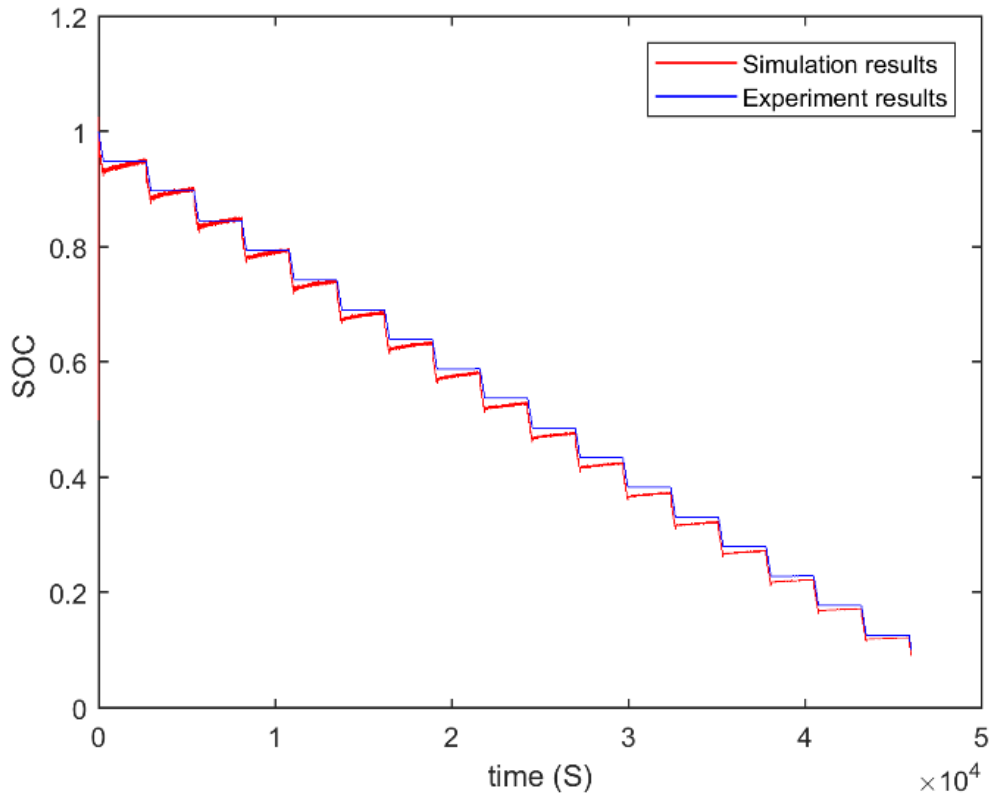

Figure (4-20): Comparison between experimental SOC and EKF estimated SOC under pulse current 0.5 C

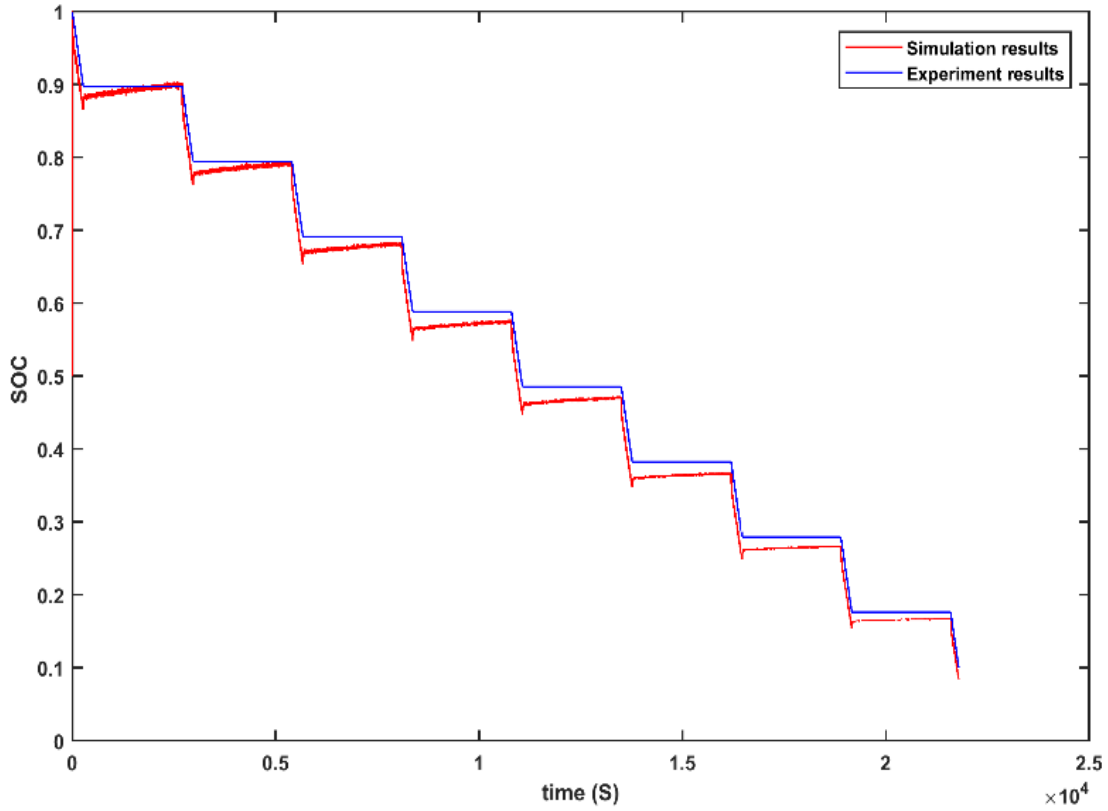

Figure (4-21): Comparison between experimental SOC and EKF estimated SOC under pulse discharge current 1C.

In this test, the actual battery's capacity is ranging in the level of 10%-95%, to protect it from damage. In order to investigate the nonlinear behaviour, 4 different functions [17], [33] for the OCV proposed to fit the OCV-SOC curve. The experimental data shown in Table (4-2) are used to identify the parameters of the proposed functions. The functions descriptive are shown in Table (4-4).

Choosing the right OCV function is the key for better estimation SOC of the battery. Better estimation results were getting when using second order Thevenin model. Therefore, the high n-order Thevenin model gets high accuracy.

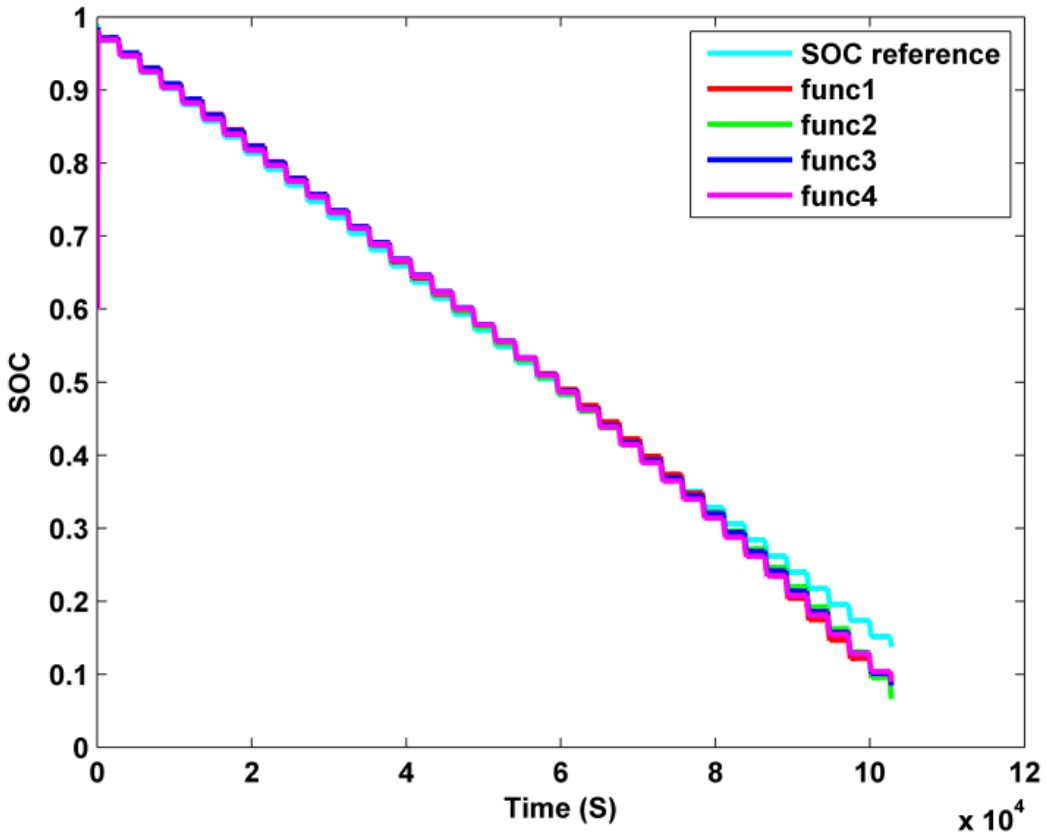

Figure (4-22): The SOC estimation with initial value of 0.6 for first order Thevenin model

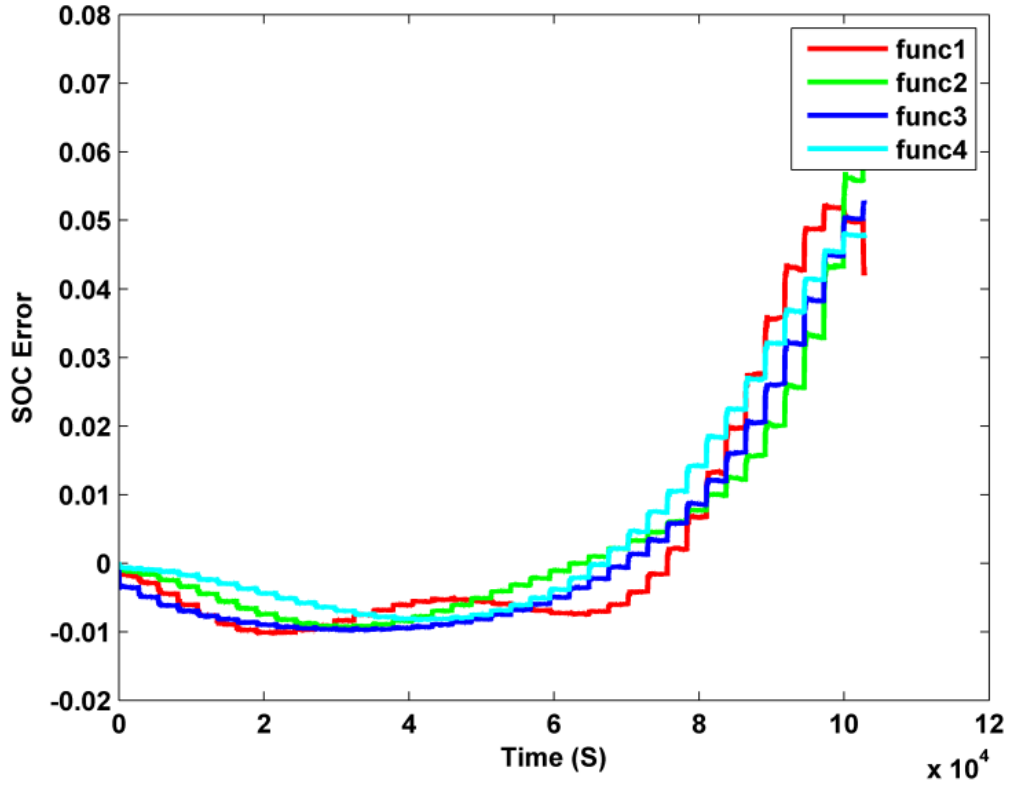

Figure (4-23): The SOC estimation error of first order Thevenin model.

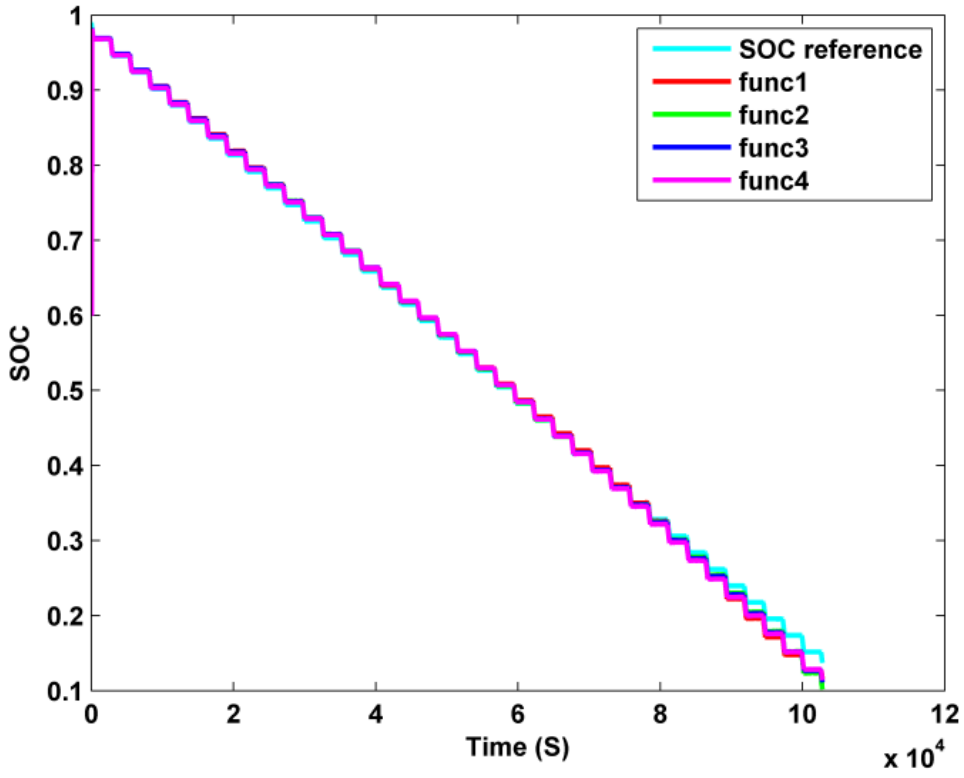

Figure (4-24): The SOC estimation with initial value of 0.6 for second order Thevenin model

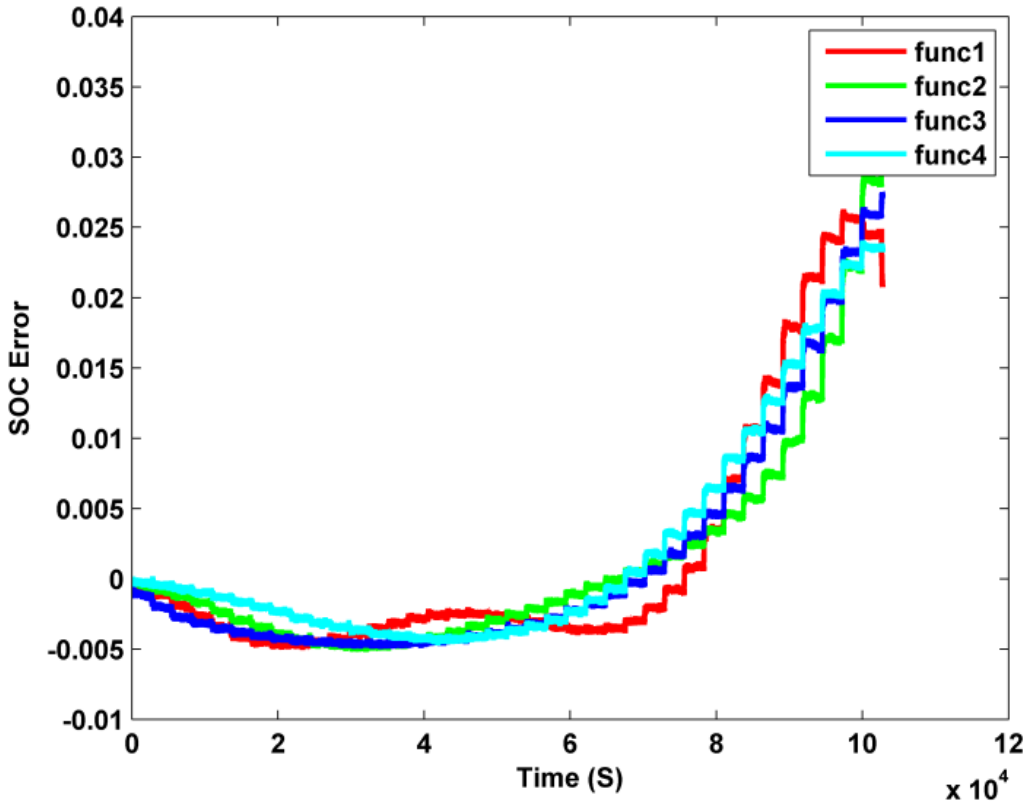

Figure (4-25): The SOC estimation error of second order Thevenin model

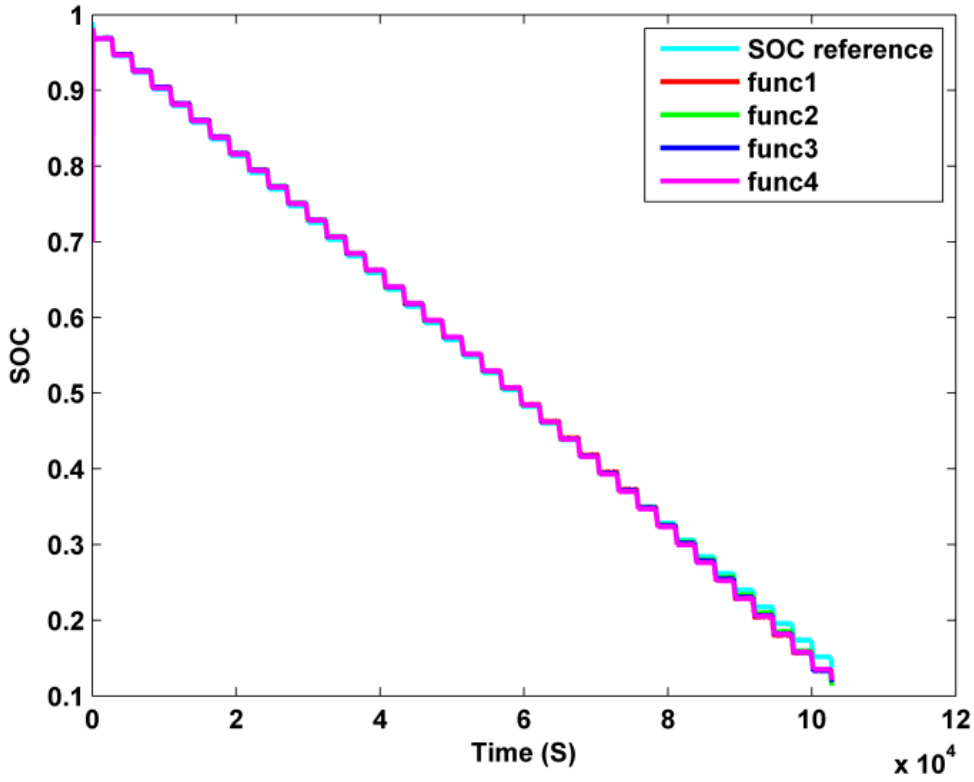

Figure (4-26): The SOC estimation for initial value of 0.6 of third order Thevenin model

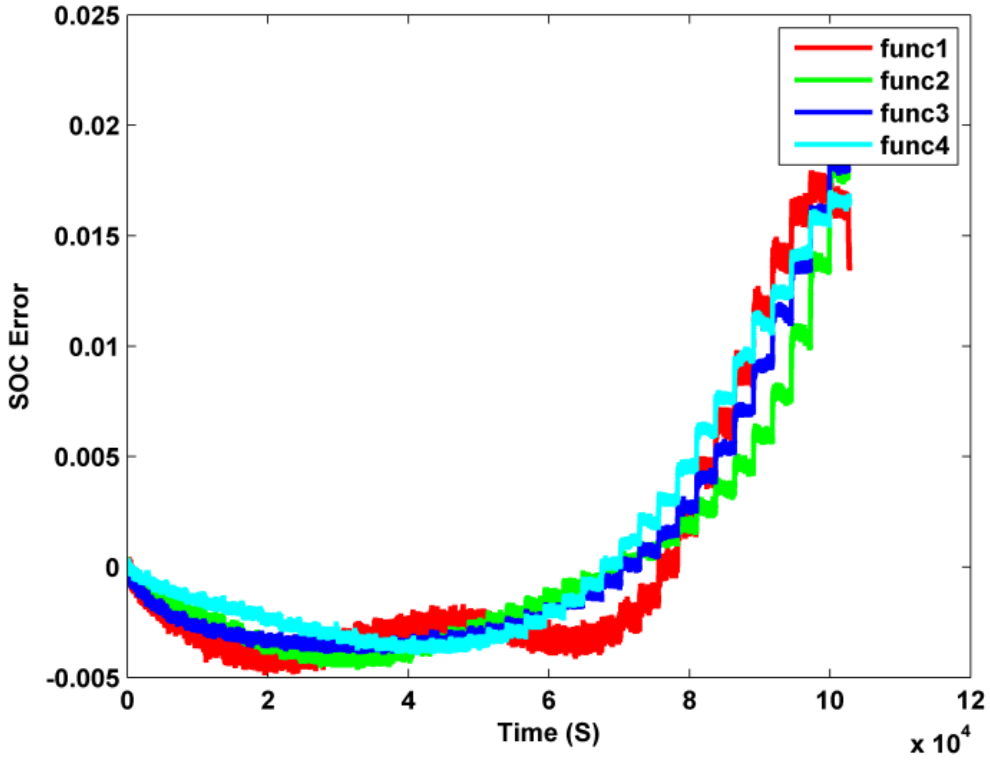

Figure (4-27): The SOC estimation error of third order Thevenin model

In Figure (4-27), it can be seen that the SOC error less than the previous shown in Figure (4-25). The proposed function fits better than the other functions, and the result become better on tracking by using the third-order Thevenin model. The RMSE is summarized in Table (4-7) while the estimated and real terminal voltages were depicted in Figure (4-28).

Table (4-7): The RMSE of SOC estimated for third model-based

Functions	Func1	Func2	Func3	Func4
RMSE	0.0144	0.0168	0.0193	0.0201

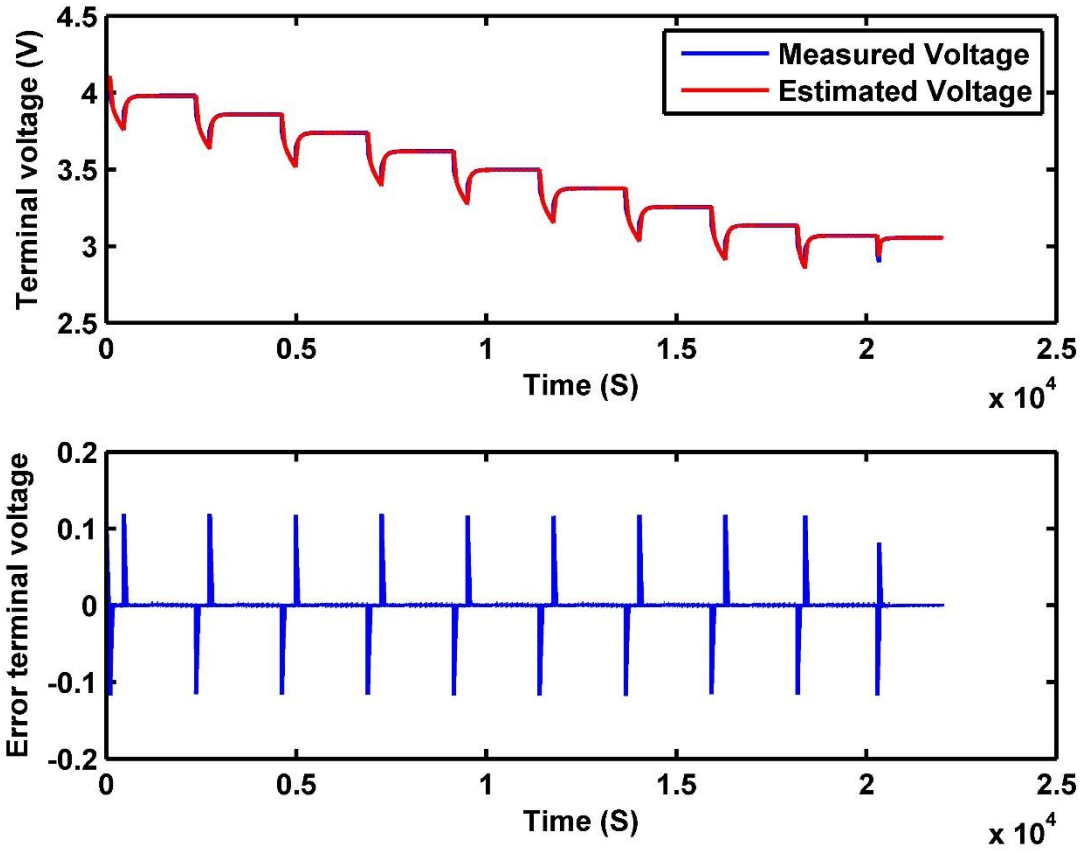

Figure (4-28): The terminal voltage and error of estimation.

4.4. Sliding mode observer

Battery behaviours are known by its highly nonlinear and dynamic model, due to the chemical reactions. Furthermore, the dynamics of the battery may not be fully known, since it is known as a black box and some of parameters appearing in the equations of mathematical model may vary.

For instance, the internal resistance can be change as function of the temperature or aging. Generally, a lot of ECMs models have been widely used to estimate the SOC. However, dynamics, parameters variations, load and sensors disturbances are the main disturbances and uncertainties that can affect the effective estimating of the SOC. Therefore, it will be very difficult to limit these disturbances effectively if linear control methods like KF is adopted [69, 72, 128].

To overcome the aforementioned problems other advanced methods have been proposed [33, 24-25]. These strategies include among others the sliding mode control (SMC). The SMC is a nonlinear control method known to have robust control characteristics under restricted disturbance conditions or when there are limited internal parameter modelling errors [26-29].

The effectiveness of the SMC is guaranteed usually by using a switching control law. Unfortunately, this switching strategy often leads to a chattering phenomenon. In order to reduce the chattering phenomenon, a common method is to use the smooth function instead of the switching function [66-67].

In this section, the EKF have been replaced by SMO. Therefore, first we start by a summary about sliding mode theory, then followed by the application of the sliding mode control to estimate the SOC, based on ECM model.

4.5. Sliding mode control history

The concept of sliding mode control has appeared in Russian literature since the 1950s. So, big work has been done on this concept of control mode until now [68-70].

4.5.1. Basic of sliding mode concepts

Mode Control is a variable structure control consists of an algorithm inherently robust that can change structure and switch between two values according to a very specific

switching logic in parameters, nonlinear models against disturbances and uncertainty. The principle of sliding mode control is to force the system to reach a given surface called the sliding surface and to remain there until it reaches equilibrium. Therefore, when the system moves on the sliding surface or on the line, it is called the system slides.

However, this control is done in two steps: the state trajectory start outside the surface and converges to the sliding surface (the line), then it is restricted to the surface for all subsequent time as depicted in Figure (4-29) [129-131].

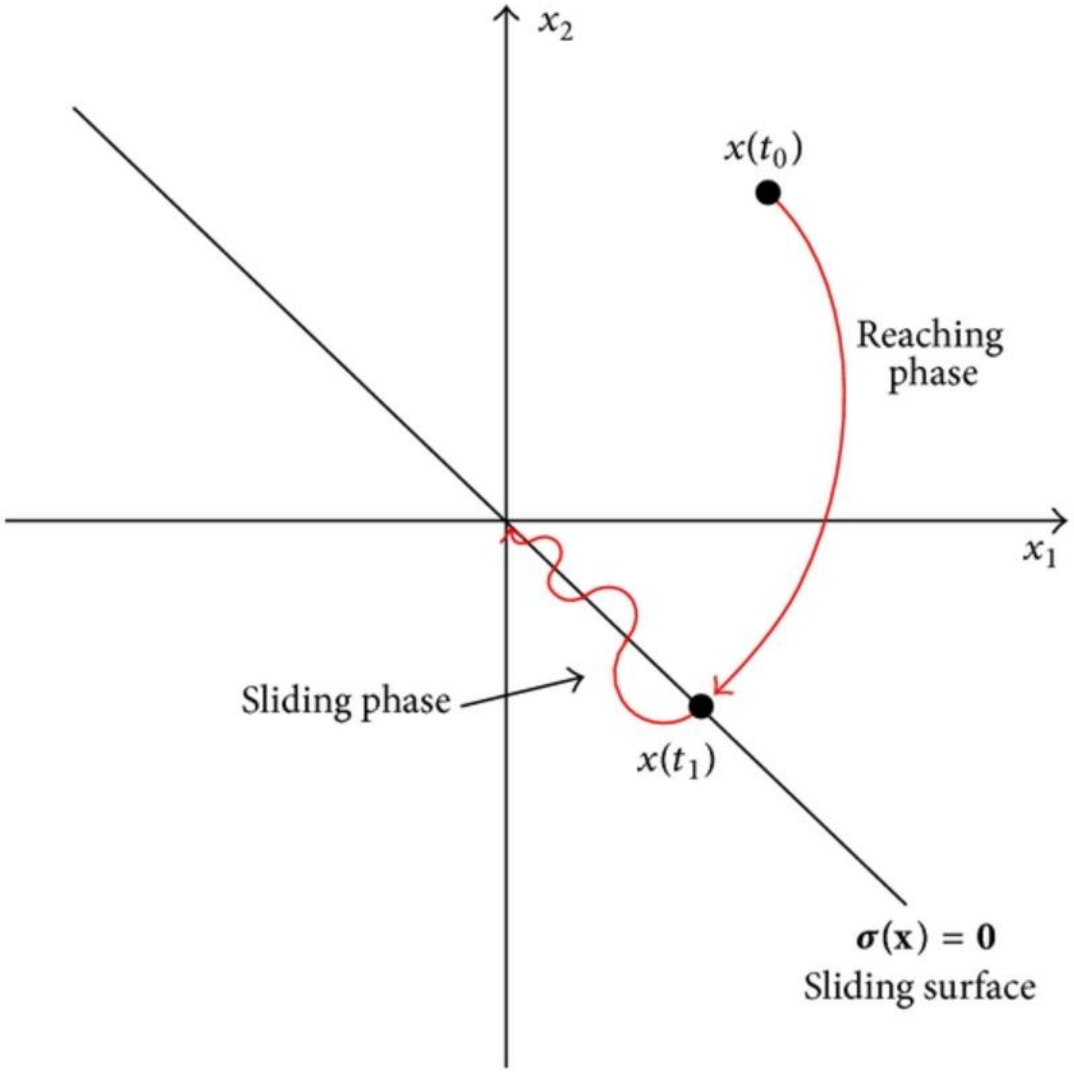

Figure (4-29): Principle concepts of the sliding mode control.

The controller consists of two parts. The first one is continuous representing the dynamics of the system during the sliding mode and also a discontinuous one, which is representing the dynamics of the system during the convergence mode.

The second term of SMC is essential to deal with the nonlinear control, because its role to eliminate or reduce the effects of imprecision and disruption of the model. The combination of this controller can be divided into two steps [129, 130]:

- Choice of a suitable sliding surface so that the dynamic of the system confined to the sliding manifold produces a desired behaviour.
- Design the control law, which forces the system trajectory to the sliding surface and keep it there.

4.5.2. Sliding surface choice

If the sliding surface is a linear combination of the error and its corresponding differentiations, it becomes a linear sliding surface S(x). Otherwise, if it is a nonlinear combination of the error and its corresponding differentiation, it becomes a nonlinear sliding surface $S(x,t)$. This problem is investigated in [132, 133], who's proposed a general form, which consists of a scalar function given by:

$$S(x) = \left(\left(\frac{d}{dt} + \lambda \right)^{r-1} * e(x) \right) \tag{4.52}$$

with $e(x) = x_{ref} - x$

λ : is a positive coefficient.

r: is the relative degree, which is the number of times required to differentiate the surface before the input appears explicitly. Furthermore, for example:

$$\begin{aligned} r = 1 &\Rightarrow S(x) = e(x) \\ r = 2 &\Rightarrow S(x) = \left(\lambda * e(x)\right) + \dot{e}(x) \\ r = 3 &\Rightarrow S(x) = \left(\lambda^2 * e(x)\right) + \left(2\lambda * \dot{e}(x)\right) + \ddot{e}(x) \end{aligned} \tag{4.53}$$

4.6. Conditions of existence and convergence of the sliding mode

The theory of Lyapunov stability provides a dynamic system stable approach. If we can build a positive definite function V_r, so that its derivative $\dot{V}_r$. Therefore, the system is stable if the derivative is always negative. While this kind of method is habitually used to design sliding mode controller [134].

Afterword, the Lyapunov function candidate can be expressed as:

$$V_r = \frac{1}{2} S^2(x) \tag{4.54}$$

The derivative of equation (4.54) is:

$$V_r = S(x)\dot{S}(x) \tag{4.55}$$

The control stability is ensured under the following two conditions:

- The Lyapunov function V_r is positive definite.
- The derivative of the Lyapunov function should be negative $\dot{V}_r < 0$, it is sufficient to ensure that:

$$S(x)\dot{S}(x) < 0 \ (\forall S) \tag{4.56}$$

This method is used to estimate the performance of the control and ensures asymptotically the convergence towards the sliding surface.

4.7. Drawback of sliding mode control

The sliding mode control is designed in way to force the variables to arrive at sliding mode surface $S = 0$ from the initial value after a period time. The sliding mode trajectory is shown in Figure (4-30).

Thereby, From the Figure (4-30) appears the drawback of chattering problem due to the discontinuous control law acting on the sliding mode when system goes into sliding mode state. This phenomenon can increase the loss and reduce the estimation strategy. Therefore, it should be overcome as possible as we can [135].

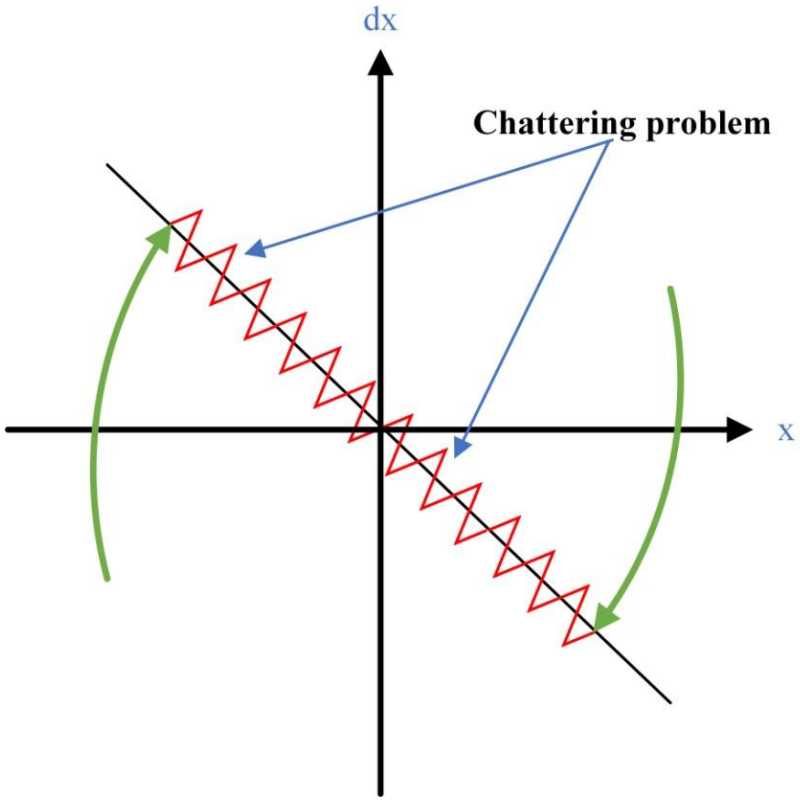

Figure (4-30): Problem of chattering phenomenon.

4.8. Sliding Mode Observer structure

The sliding mode observer (SMO) is based on the same idea of sliding mode control. This type of observer uses the model of the system, employs high frequency switching to force the trajectory of the estimated variables to remain in the sliding surface [136, 137]. Figure (4-31) shows the general structure of sliding mode observer.

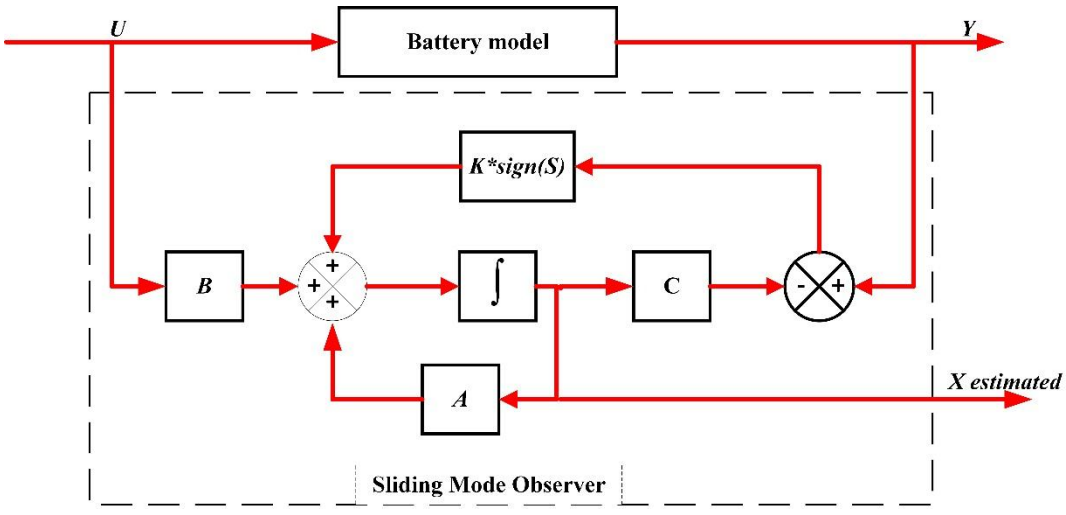

Figure (4-31): Sliding mode observer structure.

The sliding surface is chosen to ensure the observed states converge to the actual states. Therefore, once the sliding mode is achieved, the SMO can reject certain external disturbances and internal parameter uncertainties. Afterword, The SMO synthesis is based on the comparison between observed and measured variables as expressed:

$$e = y - \hat{y} \tag{4.57}$$

The design of the SMO consists of reduce the error (e) between the measured outputs of the system by using switching function to get high convergence. The SMO is modelled in the following form:

$$\begin{aligned} \dot{\hat{x}} &= f(\hat{x}, u) + k * sign(y - \hat{y}) \\ \hat{y} &= C(\hat{x}) \end{aligned} \tag{4.58}$$

with:

$\hat{x}$: represents the estimated state

y and $\hat{y}$: represent the real output and its estimated.

k : is the switching gain.

So, by using the equation (4.54) it is easy, simple and non-complex implementation to estimate the state of the system. This is the reason why the SMO is widely used, and duo to its robustness against parameter variations, disturbances and noise.

4.9. Solving the chattering problem

The chattering problem has become the famous and biggest obstacle depending on the sliding mode control. The academics have continued their developing to weaken or avoid the chattering without interruption. In order to reduce or eliminate the chattering phenomena, a large number of researches have been using: smooth function, smooth function, filters (by adopt a low-pass filter), saturation function, observer, neural sliding, fuzzy sliding mode and higher-order sliding mode [138]. The saturation function has been chosen in order to limit the effect of chattering due to its simplicity and give a better response.

4.10. Application of sliding mode in battery SOC estimation

Normally, battery ECM models used for estimating the SOC can be easily extended to form into SMO application. For each model, the SOC estimation requires only voltages and currents, which are measured by using its sensors.

In this section, a sliding mode observer based on Thevenin model is presented to estimate directly the SOC by using voltages as output and current as input. Using the Thevenin model and based on the sliding mode structure theory, the proposed sliding mode observer is designed as:

The terminal voltage V_L mathematical characteristics can be presented by the governing equations as follows:

$$\dot{V}_1 = -\frac{1}{R_1 C_1} V_1 + \frac{1}{C_1} I_L \tag{4.59}$$

$$V_L = V_{oc}(z) - R_s I_L - V_1 \tag{4.60}$$

Where:

V_L terminal voltage.

V_{oc} bridge relationship between OCV and SOC

$R_1 C_1$ polarization time.

V_1 polarisation voltage across the RC branch.

R_s internal resistance.

z the state of charge (SOC).

I_L current of the battery.

While, the SOC defined as the ratio of remain capacity of a battery, and it can be presented in mathematical formula as:

$$z(t) = (z_0 - \int_0^t \frac{\eta I_L(\tau)}{Q_n}) * 100 \tag{4.61}$$

where z_0 is the initial SOC of the battery. $I_L(\tau)$ is the current in a short time, while it is considered positive for discharge and negative for the charge. Q_n is the nominal capacity of the battery. η denotes the coulomb efficiency is this study taken as one, which is affected by the current range and temperature.

For a small variation of SOC, the derivative form can be expressed as follow:

$$\dot{z} = (-\frac{I_L}{Q_n}) * 100 \tag{4.62}$$

The OCV-SOC relationship can be extracted from charge discharge process; the average can be piecewise linearized in 20 sequences as depicted in Table (4-2), and presented in equation (4.59):

$$V_{oc}(z) = (\alpha_i * z) + \beta_i \tag{4.63}$$

4.10.1. Conventional sliding mode observer design

There are two important stages required to design a sliding mode observer. Step one is choosing the sliding surface. The second step is designing a control law, which will conduct the state variables to the sliding surface and keeping them onto the surface.

Define $e = \hat{V}_L - V_L$ as the battery terminal voltage estimator error. So, the following sliding surface is defined as:

$$S = e = V_L - \hat{V}_L \tag{4.64}$$

where V_L, $\hat{V}_L$ are the terminal voltage and estimated terminal voltage respectively.

The conventional sliding mode observer (CSMO) can be modelled as following:

$$\begin{cases} \dot{\hat{x}} = f(\hat{x}, u) + g * sign(y - \hat{y}) \\ \hat{y} = C(\hat{x}) \end{cases} \tag{4.65}$$

where $sign(.)$ is signum function. g is the switching gain. y and $\hat{y}$ denote the true terminal voltage and estimated terminal voltage V_L, $\hat{V}_L$, respectively. u is the input control, which represent the current I_L . $\hat{x}$ is the estimated states. C is the matrix of control.

Therefore, based on equation (4.59), (4.60), (4.62) and (4.63), the battery system can be formulated by the following steps, for fast sampling frequency in SOC estimation, the current change rate $\dot{I}_L$ can be disregarded. We substitute equation (4.59) and (4.62) into the derivative of equation (4.64) and rearrange to differential equation:

$$\dot{V}_L = -\alpha_i \left(\frac{I_L}{Q_n}\right) + \left(\frac{V_1}{R_1.C_1}\right) - \left(\frac{I_L}{C_1}\right) \tag{4.66}$$

Solving equation (4.60) for I_L and rearranging it as follows:

$$I_L = -\left(\frac{V_L}{R_s}\right) + \left(\frac{V_{oc}}{R_s}\right) - (\frac{V_1}{R_s}) \tag{4.67}$$

And from equation (4.60), substitute into (4.63) and rearranging:

$$\dot{V}_L = -a_1 V_L + a_1 V_{oc} - b_1 I_L \tag{4.68}$$

Substitute equation (4.67) into (4.62) result:

$$\dot{z} = a_2 V_L - a_2 V_{oc} + b_2 V_1 \tag{4.69}$$

where $a_1 = 1/R_1 C_1$, $a_2 = 1/R_s Q_n$, $b_1 = \frac{\alpha_i}{C_n} + \frac{R_s}{R_1 C_1} + \frac{1}{C_1}$ and $b_2 = 1/C_1$.

Thus, the final state-space of the system is expressed as follows:

$$\begin{cases} \dot{V}_L = -a_1 V_L + a_1 V_{oc} - b_1 I_L \\ \dot{z} = a_2 V_L - a_2 V_{oc} + a_2 V_1 \\ \dot{V}_1 = -a_1 V_1 + b_2 I_L \end{cases} \tag{4.70}$$

where the CSMO observer can be presented as:

$$\begin{cases} \begin{bmatrix} \dot{V}_L \\ \dot{\hat{z}} \\ \dot{V}_1 \end{bmatrix} = \begin{bmatrix} -a_1 & a_1\alpha_i & 0 \\ a_2 & -a_2\alpha_i & a_2 \\ 0 & 0 & -a_1 \end{bmatrix} \begin{bmatrix} V_L \\ z \\ V_1 \end{bmatrix} + \begin{bmatrix} -b_1 \\ 0 \\ b_2 \end{bmatrix} u + \begin{bmatrix} a_1\beta_i \\ -a_2\beta_i \\ 0 \end{bmatrix} + \begin{bmatrix} g_1 sign(e_{VL}) \\ g_2 sign(e_z) \\ g_3 sign(e_{V1}) \end{bmatrix} \\ y = [1 \quad 0 \quad 0] \begin{bmatrix} V_L \\ z \\ V_1 \end{bmatrix} \end{cases} \tag{4.71}$$

where the errors of states calculated as:

$$\begin{cases} e_{VL} = V_L - \hat{V}_L \\ e_z = V_{oc}(z) - V_{oc}(\hat{z}) = \alpha_i(z - \hat{z}) \\ e_{V1} = V_1 - \hat{V}_1 \end{cases} \tag{4.72}$$

with $g_1,\ g_2\ and\ g_3$ are the switching gains. e_{VL} represents the error committed between real output and estimated, as well as e_z and e_{V1} errors of SOC and polarization voltage respectively.

Conventional sliding mode observer (CSMO) with constant switching gains for SOC estimation have applied and its robustness proved against error modelling and uncertainties with selected gains. However, lower gains caused poor tracking and reduce chattering phenomena, in opposite high gains the tracking is better but caused undesired chattering as illustrated in Figures (4-32) and (4-33).

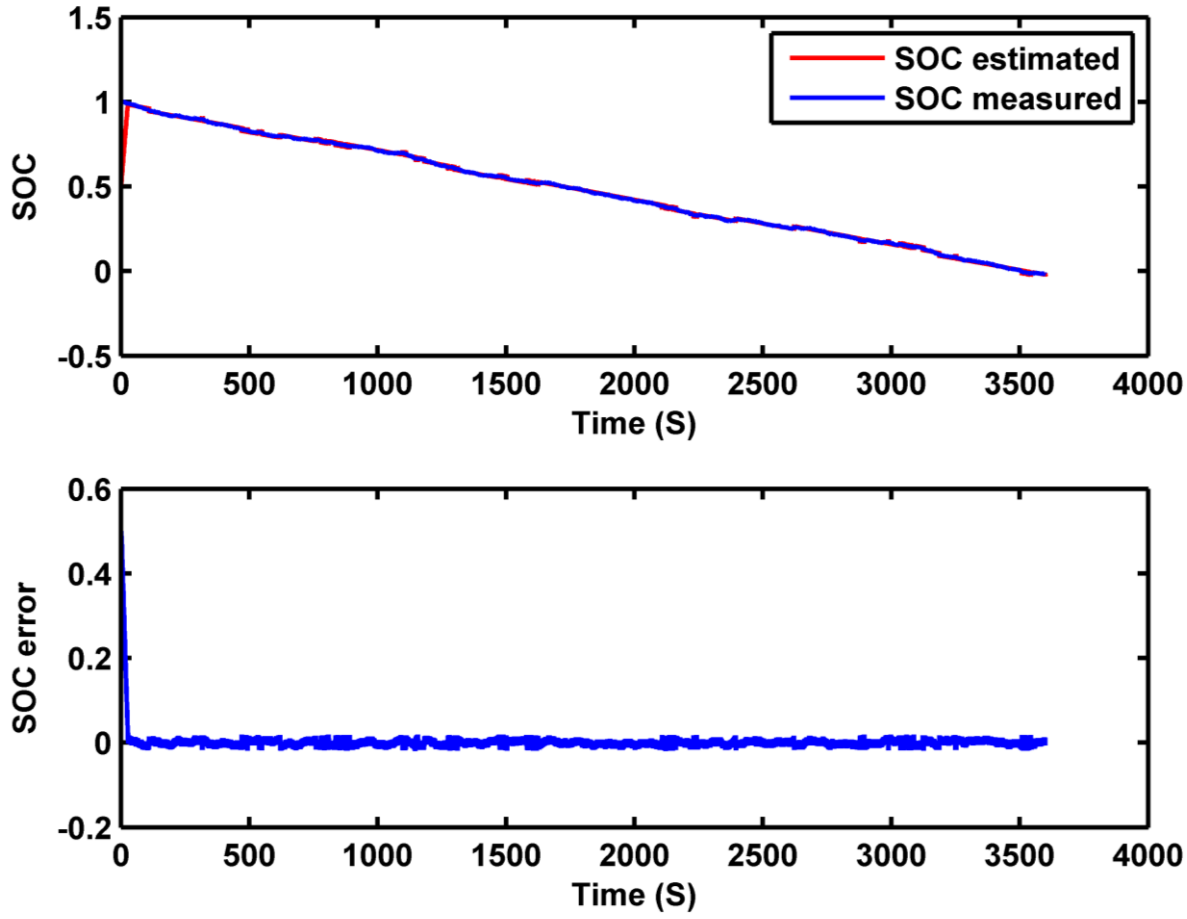

Figure (4-32): CSMO based SOC estimation with large gains.

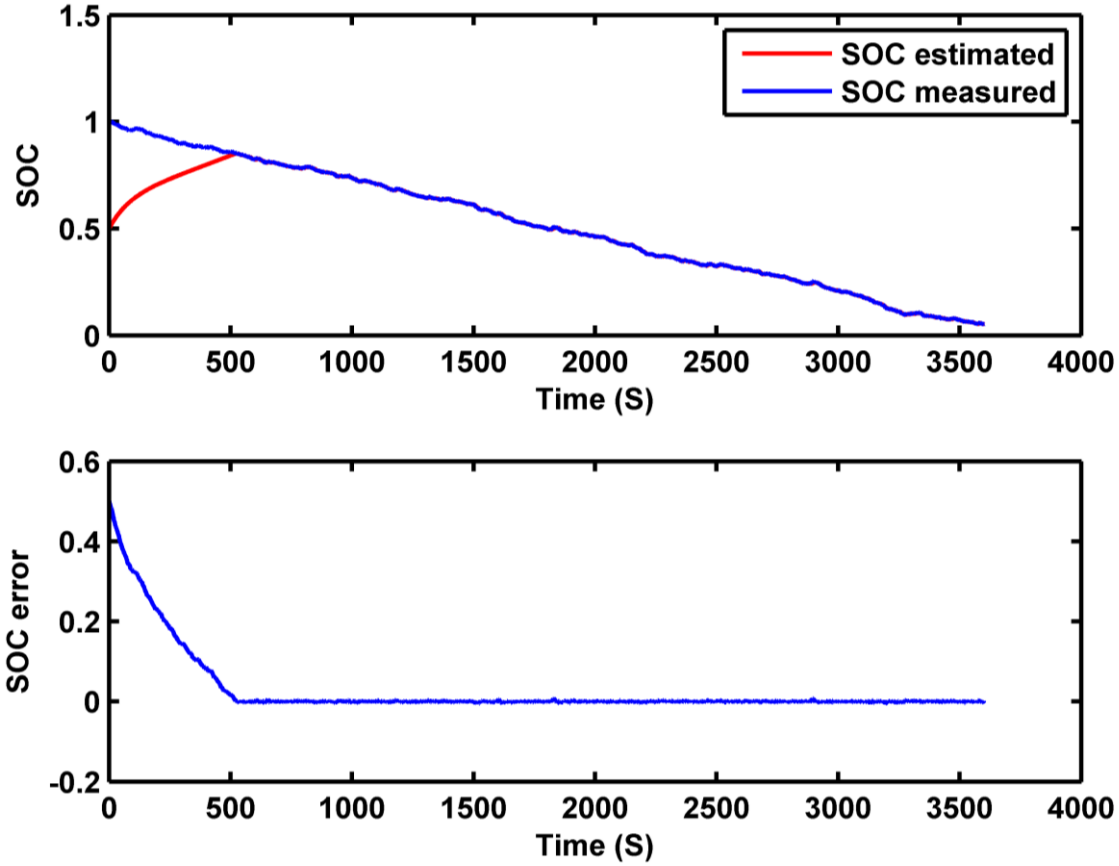

Figure (4-33): CSMO based SOC estimation with low gains.

4.10.2. Modified sliding mode observer design

The system states of the equivalent circuit can be improved through adaptive switching gains. Based on the CSMO and equivalent circuit model, we propose a modified gain for sliding mode observer (SMO). The states are estimated by the following equations as:

$$\begin{cases} \dot{\hat{V}}_L = -a_1\hat{V}_L + a_1\hat{V}_{oc} - b_1 I_L + \sqrt{g_1}sign(e_{VL}) \\ \dot{\hat{z}} = a_2\hat{V}_L - a_2\hat{V}_{oc} + b_2\hat{V}_1 + \sqrt{g_2}sign(e_z) \\ \dot{\hat{V}}_1 = -a_1\hat{V}_1 + b_2 I_L + \sqrt{g_3}sign(e_{V1}) \end{cases} \quad (4.73)$$

with $\sqrt{g_1}$, $\sqrt{g_2}$ and $\sqrt{g_3}$ are the switching gains of the new SMO. The error dynamics of the terminal voltage error e_{VL} , e_z and e_{V1} are computed by:

$$\begin{cases} \dot{e}_{VL} = -a_1 e_{VL} + a_1 \alpha_i e_z + a_1 \beta_i - \sqrt{g_1} sign(e_{VL}) \\ \dot{e}_z = a_2 e_{VL} - a_2 \alpha_i e_z - a_2 \beta_i + a_2 e_{V1} - \sqrt{g_2} sign(e_z) \\ \dot{e}_{V1} = -a_1 e_{V1} - \sqrt{g_3} sign(e_{V1}) \end{cases} \quad (4.74)$$

Where sign(.) is singum function defined as:

$$sign(e_{VL}) = \begin{cases} +1 & e_{VL} > 0 \\ 0 & e_{VL} = 0 \\ -1 & e_{VL} < 0 \end{cases} \quad (4.75)$$

Remark:

Since the voltage and current of output and input are bounded, the whole system is bounded.

Stability proof:

Select the candidate Lyapunov function as:

$$V_r(e) = 0.5\, e_{VL}^2 \quad (4.76)$$

The stability is ensured under two conditions as:

- The Lyapunov function V_r is positive definite.
- The derivative of the sliding function has to be negative.

$$\begin{aligned} \dot{V}_r(e) &= e_{VL} \dot{e}_{VL} \\ &= e_{VL}(-a_1 e_{VL} + a_1 \alpha_i e_z + a_1 \beta_i - \sqrt{g_1} sign(e_{VL})) \end{aligned} \quad (4.77)$$

There exists an unknown finite positive switching gain g_1 leads to $\dot{V}_r < 0$, satisfy $g_1 > a_1(\alpha_i e_z + \beta_i)$ and validate the Lyapunov stability theory.

Thus, in order to eliminate the chattering phenomena and higher the response of the SMO, the control switching gains are formed by using a saturation function.

The saturation function illustrated in Figure (4-34), and expressed as follows[139]:

$$sat(e_{VL}) = \begin{cases} sign(e_{VL}) & if\ |e_{VL}| > sigma \\ \dfrac{e_{VL}}{sigma} & if\ |e_{VL}| < sigma \end{cases} \quad (4.78)$$

with sigma is the boundary of width.

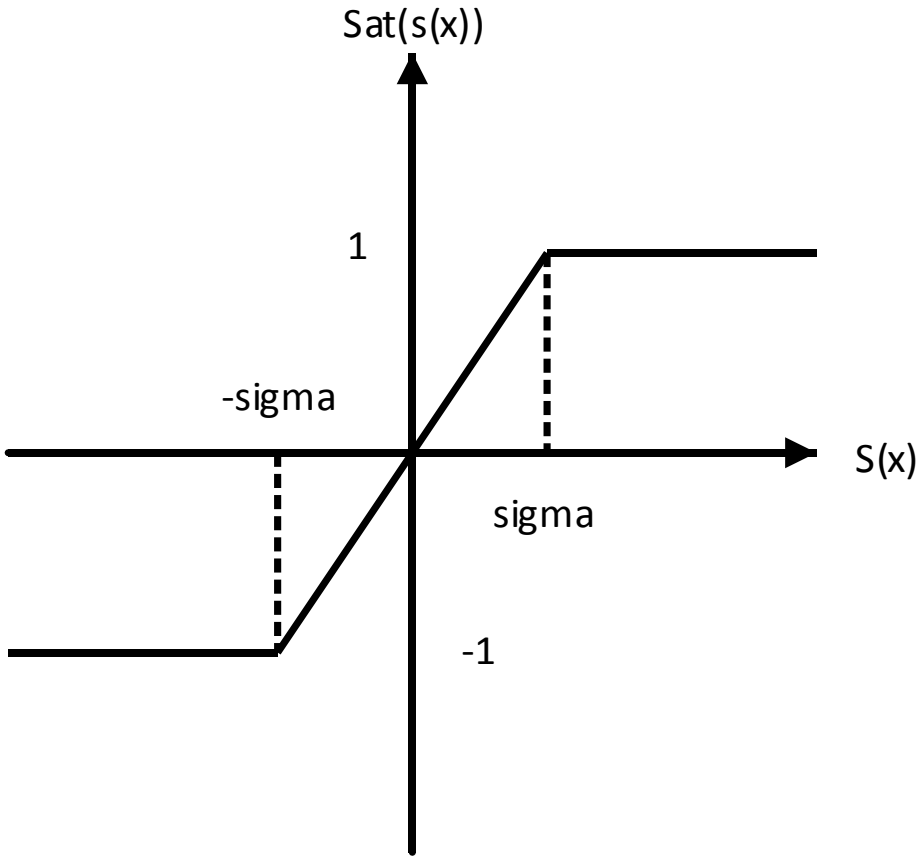

Figure (4-34): Saturation function

4.11. Comparison between EKF and SMO

To evaluate the robustness and figure out the high precision of the proposed observer, a mean value of noise with standard deviation of 0.01 is applied. Figure (4-35) and Figure (4-36) illustrate comparison estimation of SOC based on SMO and EKF. The SOC estimation results based on EKF and SMO and theirs committed errors of the observers, for continuous current discharge.

The same experience repeated with pulse discharge is shown in Figure (4-35) and Figure (4-36) with sequences of pulse discharge current.

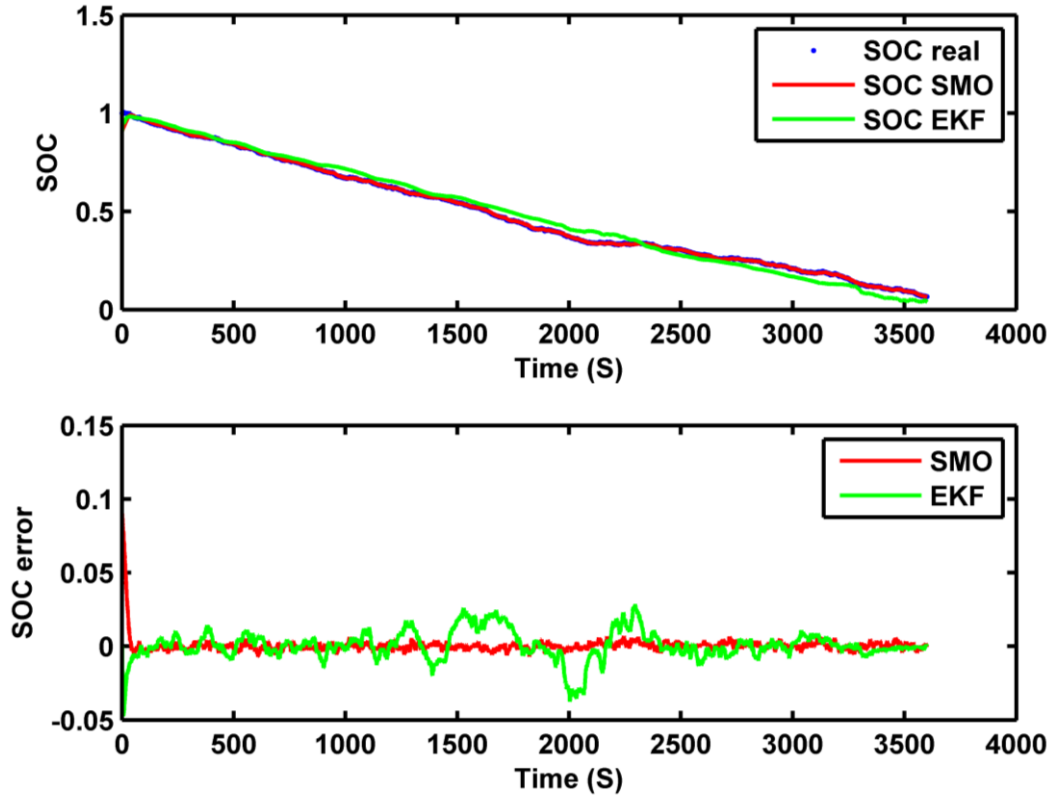

Figure (4-35): SOC estimated under 1C-rate current profile.

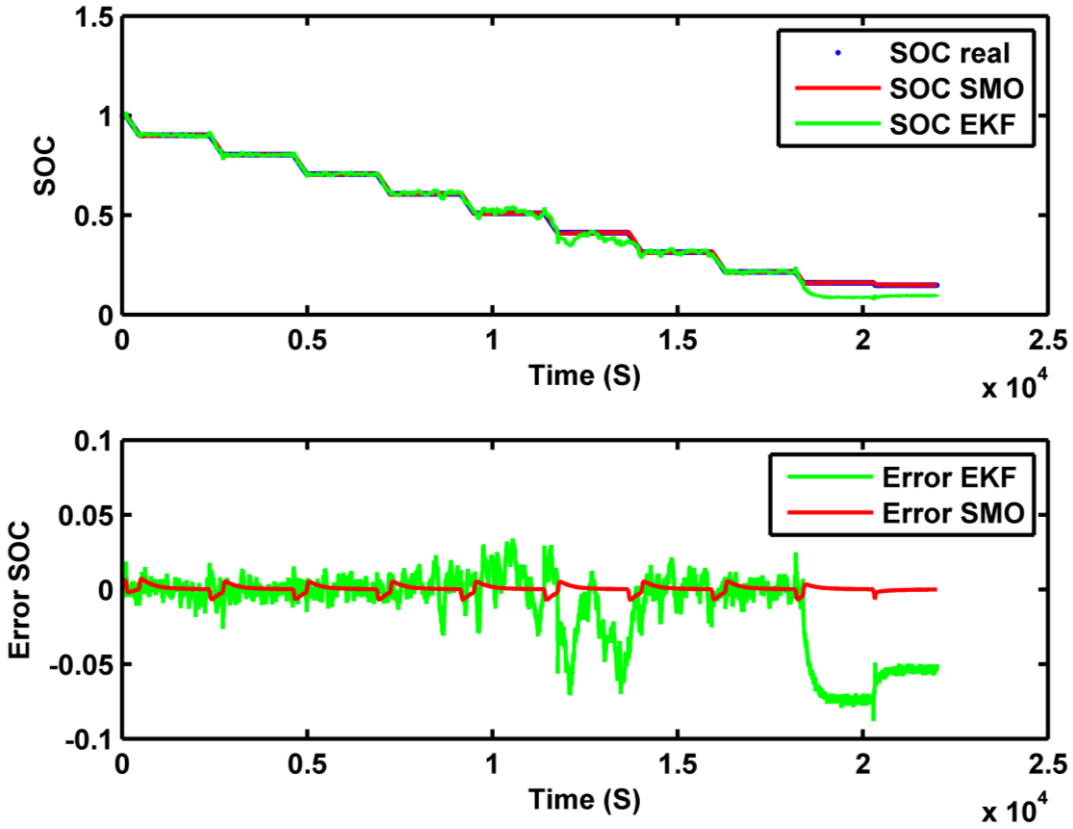

Figure (4-36): SOC estimated under 1C-rate pulse current profile.

Therefore, the SMO has shown better tracking capability to the real SOC, also has a smooth error during the estimation, which means suitable and robustness technique. Table (4-8) summarized the corresponding RMSE and the settling times for two simulations, also the proposed algorithm shows strong robustness against low SOC estimation in the range of 0.1 to 0.

Moreover, it is clear that SMO is fast than EKF in time consumption and convergence as shows the comparison.

Table (4-8): Comparison between EKF and MSMO techniques.

Technique	Pulse discharge		Continuous discharge	
	RMSE	Time computation	RMSE	Time computation
EKF	0.0176	0.726 S	0.0276	11.13 S
SMO	0.0084	0.171 S	0.0038	1.429 S

In addition, Table (4-9) present SOC convergence comparison between EKF and SMO at different initial SOCs, these results show the strong performance against wrong initial SOC.

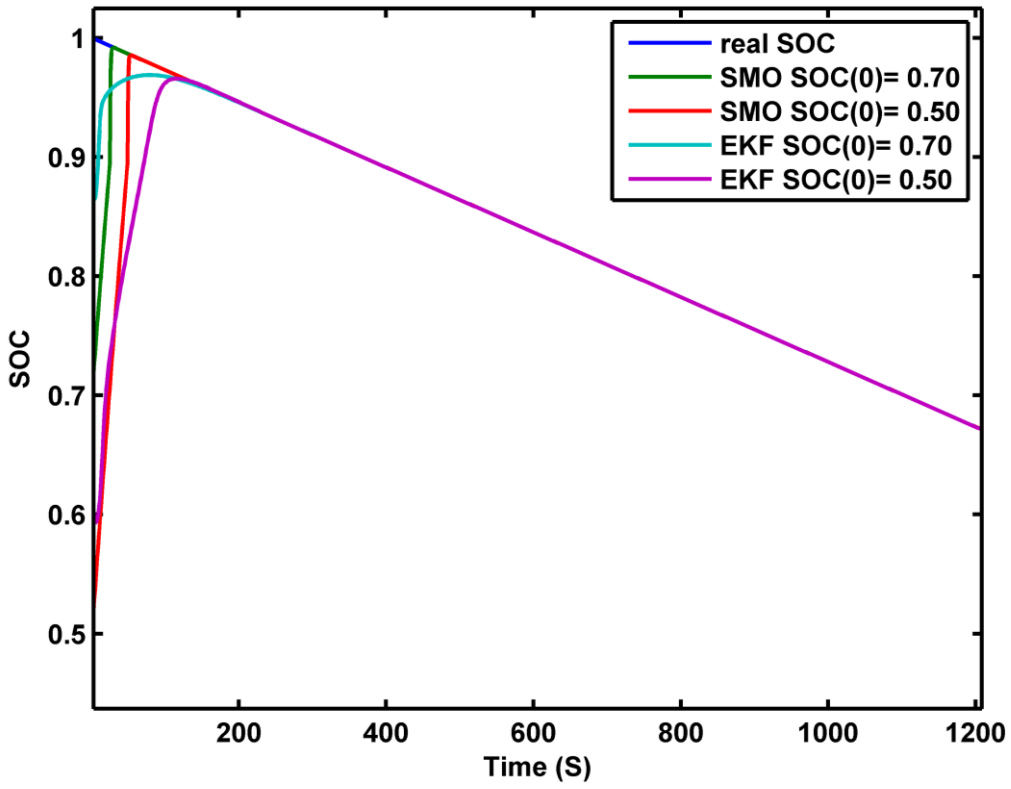

Figure (4-37): SOC convergence for both algorithms at different initial SOCs.

Therefore, it is clear that the convergence time for the SMO is less than the EKF more than 3 times. Thereby, the quick convergence helps to reduce error and gives better SOC tracking as depicted in Figure (4-37).

Table (4-9): Convergence time at different initial SOCs

Technique	SOC_0= 0.50	SOC_0= 0.70
EKF	131 S	150 S
SMO	55 S	30 S

4.12. Conclusion

In this section, an adaptive SOC technique has been developed for lithium-ion batteries. The proposed technique based on control theory to achieve robustness for SOC estimation. The strategy shows that the SOC can be determined with high accuracy based on the measurements of the battery voltage and current. Moreover, Lyapunov theory of stability analysis provides the convergence and stability of the proposed algorithm. The SMO has been established using the first-order Thevenin battery equivalent circuit model, the proposed algorithm shows performance to solve the problem of chattering and improvement of the convergence of the technique. The simulation and experimental results highlight the performance of the SMO in the context of SOC with high robustness for constant and pulse currents, which demonstrate the effectiveness of this adaptive technical estimation.

In first step, the Extended Kalman Filter is used for SOC estimation. The benefit of EKF based ECMs models is the improvement of the system dynamics, which increase the accuracy of SOC estimations. The accuracy is increasing by using different ECMs model, which is include of RC branches. While in the sliding mode observer is used to enhance the estimation and to guarantee the system stability. The SOC is estimated by using a sliding mode observer based on first-order Thevenin model of the battery. The effectiveness of the proposed observer approaches has been verified through extensive computer simulations and compared with EKF.

Simulation results have demonstrated not only truly SOC estimation but also many improvements on the dynamic responses as well as the steady state performances, in terms of time response, accuracy. In addition, the simulation results show that, the stochastic EKF has a great robustness during the application of third-order battery model. The reversal

mode, and during the measurement noise on the voltages and currents, which is generated by sensors. On the other hand, the added value of the SMO based on first-order Thevenin model is the amelioration in the system dynamics through the accuracy with less parameters and SOC estimation.

Indeed, the obtained simulation results show better speed tracking performance at dynamic and steady states, acceptable estimations errors, robustness in different tests including pulse discharge. Therefore, these results affirm the ability of the proposed observer to guarantee good estimations in steady state and transients as well.

General conclusion

Summary of research

A comparative study between different battery models and state of charge (SOC) estimation techniques was performed. Three categories of battery models were considered in this study based on equivalent circuit models. The SOC was estimated using two estimation strategies, namely the adaptive Extended Kalman filter (EKF) and adaptive sliding mode observer (SMO). The models and SOC estimation strategies were applied to experimental data provided by a prototype designed in the laboratory of LGEER of Chlef University. The results were validated using simulation models obtained from MATLAB/SIMULINK software platform.

This thesis provided a detailed overview of Behavioural models and their implementation. The Behavioural models simulate the terminal voltage behaviour of the batteries without the need for the specification of the underlying physical or electrochemical reactions. These models can be simple starting with one state to capture the SOC, and progressively become more complex with more than one state used to capture the internal battery dynamics. The ECM models parameters were determined using experimental data and optimized using the MATLAB curve fitting toolbox. The EKF were applied to three different equivalent circuit models, and the SOC was estimated. The results were compared based on the SOC root mean squared error (RMSE).

The three Equivalent circuit models and their implementation were considered due to these models are widely used, they are relatively simple and have fewer parameters to tune, and also they are easy to implement. The Equivalent circuit models consist of first-order, second-order, or third-order resistance-capacitance (RC) models.

The greatest RMSE difference occurred when applying the estimation methods on the third-order Thevenin Model. The EKF estimation results were consistent throughout all 3 models (i.e., the SOC estimation error varied by under 0.5%). The EKF application results were less consistent; the SOC estimation error varied by upwards of 2.5%. The differences in consistency were likely due to the sensitivity of the EKF to modelling uncertainties.

Furthermore, the results of applying both the EKF and SMO estimation strategies on the Equivalent circuit models were shown and discussed. The SMO strategy used to estimate SOC yielded the better performance in terms of estimation accuracy. Similar to the Behavioural models, the SOC estimation RMSE was improved by 15 to 60%, depending on

the model used. The most accurate model was the third-order RC model based on EKF observer but a bit slow due to large matrix. In opposite, the SMO algorithm was concluded that the first-order Thevenin model provides a better performance in tracking the SOC accurately then using EKF with the third order Thevenin model, beside very fast and simple in programming.

Recommendations and future work

A trade-off exists between model complexity, accuracy, and parameterization. It is recommended that the selection of a battery model should be made based on the required accuracy and the available computation power. For example, in some situations a simple first-order RC model may suffice; such as in simple, low current operating conditions. However, a more complicated model is required to capture nonlinearities present in environments involving fast transients or in order to capture more internal states depending on the state of health information.

The first recommendation for new research involves further into including the temperature, which is dependent of model parameters were not considered in this thesis. Future studies can include energy balance equations in the models to incorporate temperature information and its effects on the system. Additionally, the temperature sensor placed for the cell along with sensors for terminal voltage and current. It will add more information to the experimental setup, which can be considered in modelling and SOC estimation.

Furthermore, it is important to note that in most cases, the ECM is considered to be one dimensional model. The recommendation for new research involves focusing more in electro-chemical models, which can be extended to higher dimension (2-3). Therefore, a strategy could be developed to create more robust ECM models.

Moreover, the aging effect of the cell was ignored in this work. A very important recommendation for future work includes the study of aging and its effects on a battery cell. This work is important because it may yield more accurate estimation for battery state of health (SOH) by lining temperature with model parameters and study its effects on the system.

Appendices

Appendix A

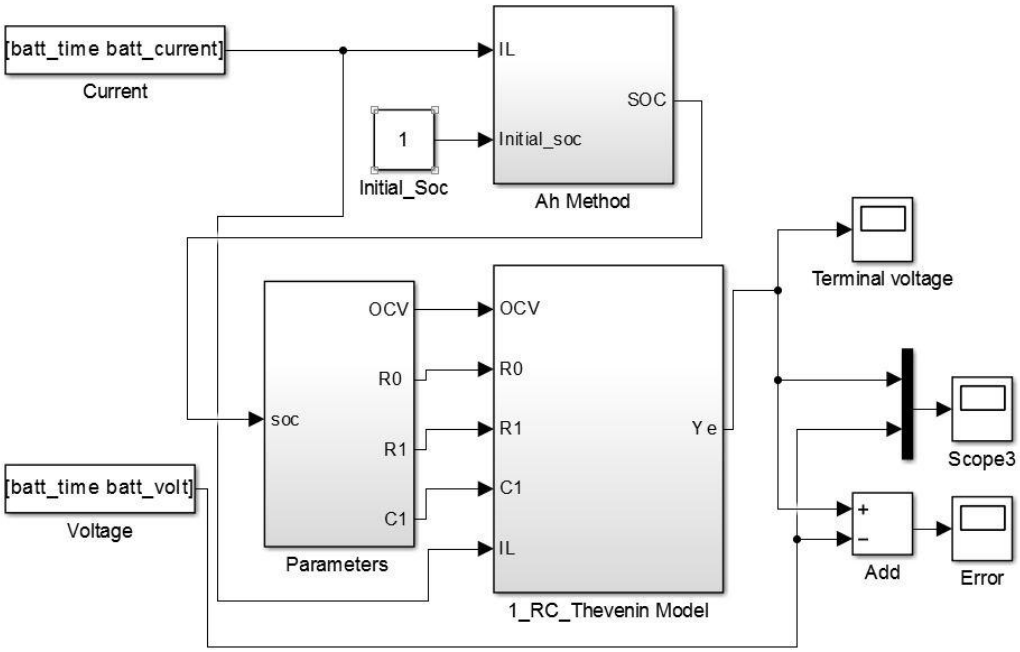

Figure (A-1): Schema block of the battery model in Matlab/Simulink.

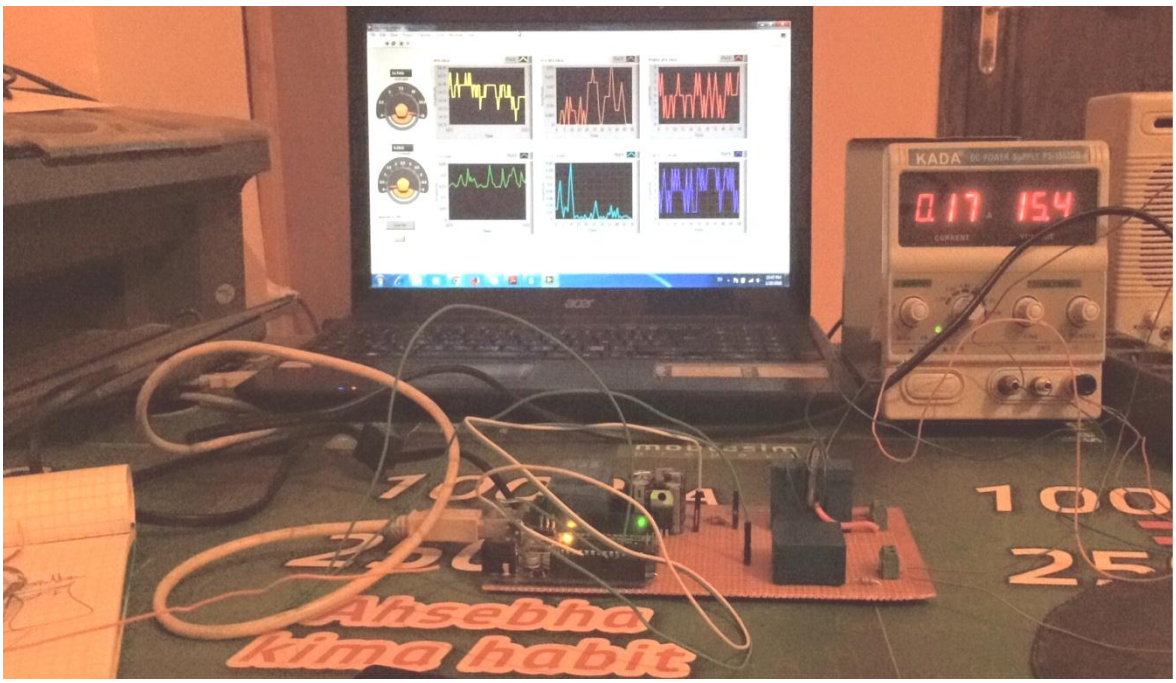

Figure (A-2): a view of the acquisition program used in collecting experimental data.

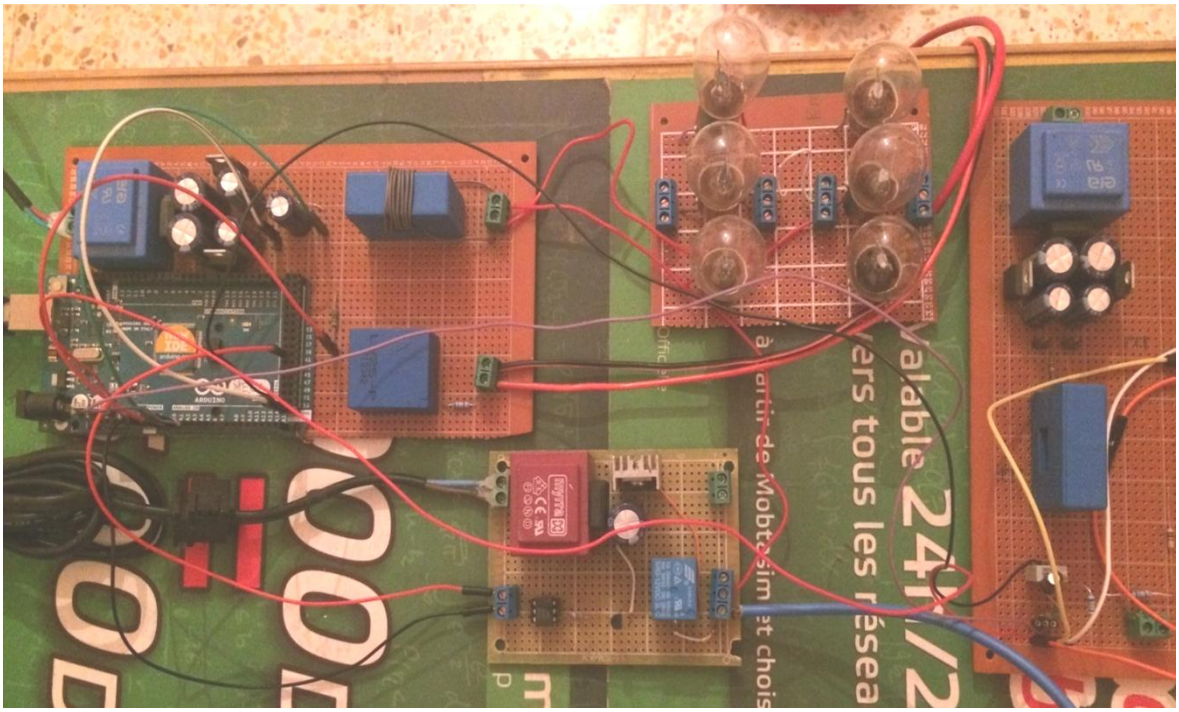

Figure (A-3): Photo of the test bench of the experiment

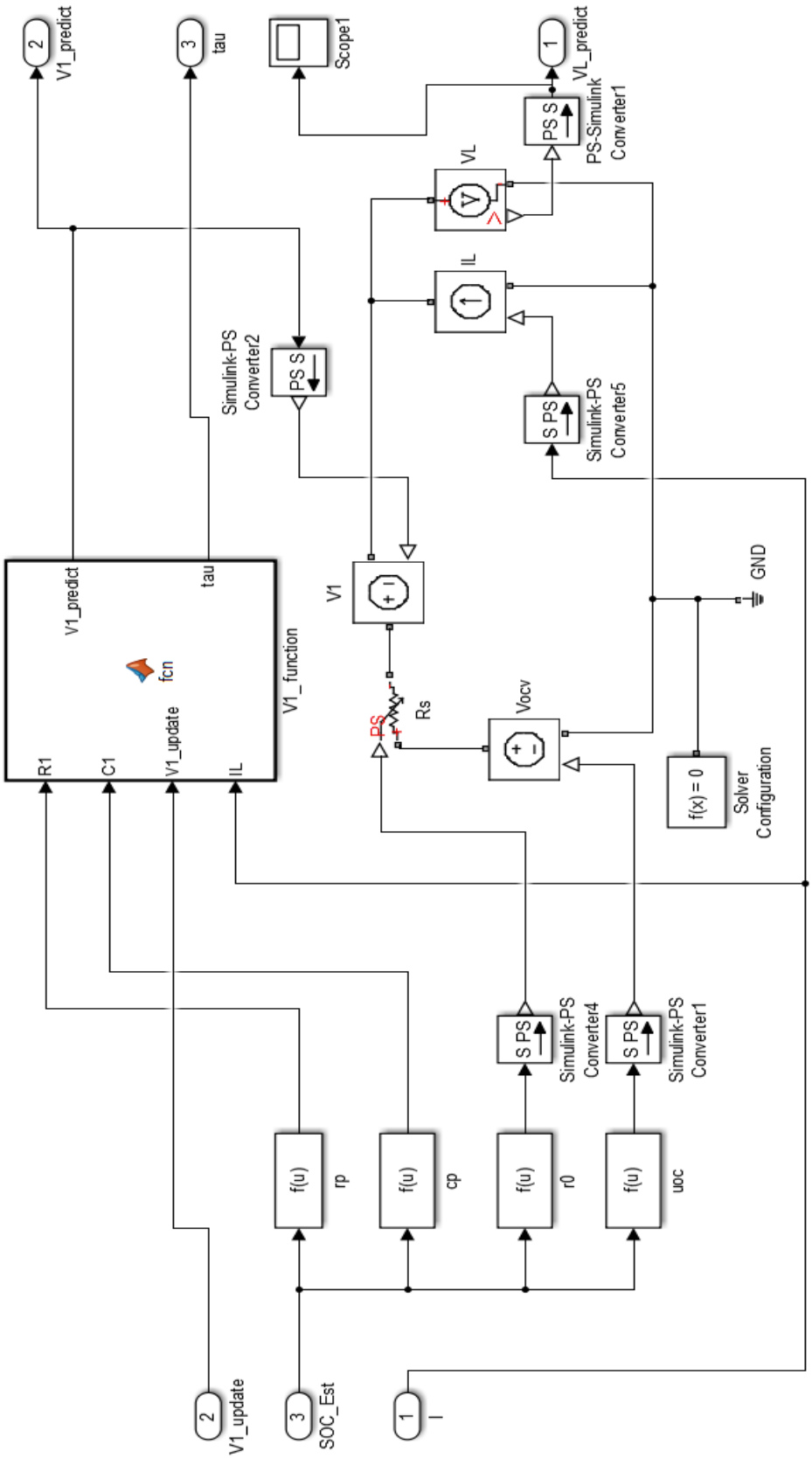

Figure (A-4): Matlab/Simulink schematic blocks of experiment.

Appendix B

LEM

Current Transducer LA 55-P

I_{PN} = 50 A

For the electronic measurement of currents: DC, AC, pulsed..., with galvanic isolation between the primary circuit (high power) and the secondary circuit (electronic circuit).

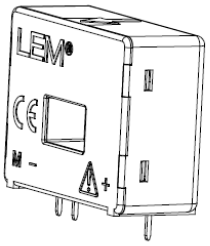

16019

Electrical data

I_{PN}	Primary nominal current rms				50		A
I_{PM}	Primary current, measuring range				0 .. ± 70		A
R_M	Measuring resistance		T_A = 70°C		T_A = 85°C		
			$R_{M\,min}$	$R_{M\,max}$	$R_{M\,min}$	$R_{M\,max}$	
	with ± 12 V	@ ± 50 A_{max}	10	100	60	95	Ω
		@ ± 70 A_{max}	10	50	60 [1]	60 [1]	Ω
	with ± 15 V	@ ± 50 A_{max}	50	160	135	155	Ω
		@ ± 70 A_{max}	50	90	135 [2]	135 [2]	Ω
I_{SN}	Secondary nominal current rms				50		mA
K_N	Conversion ratio				1 : 1000		
V_C	Supply voltage (± 5 %)				± 12 .. 15		V
I_C	Current consumption				10 (@ ± 15 V) + I_S		mA

Accuracy - Dynamic performance data

X	Accuracy @ I_{PN}, T_A = 25°C	@ ± 15 V (± 5 %)	± 0.65		%
		@ ± 12 .. 15 V (± 5 %)	± 0.90		%
ε_L	Linearity error		< 0.15		%
			Typ	Max	
I_O	Offset current @ I_P = 0, T_A = 25°C			± 0.2	mA
I_{OM}	Magnetic offset current [3] @ I_P = 0 and specified R_M, after an overload of 3 x I_{PN}			± 0.3	mA
I_{OT}	Temperature variation of I_O	- 25°C .. + 85°C	± 0.1	± 0.6	mA
		- 40°C .. - 25°C	± 0.2	± 1.0	mA
t_{ra}	Reaction time to 10 % of I_{PN} step		< 500		ns
t_r	Response time to 90 % of I_{PN} step		< 1		µs
di/dt	di/dt accurately followed		> 200		A/µs
BW	Frequency bandwidth (- 1 dB)		DC .. 200		kHz

General data

T_A	Ambient operating temperature		- 40 .. + 85	°C
T_S	Ambient storage temperature		- 40 .. + 90	°C
R_S	Secondary coil resistance	@ T_A = 70°C	80	Ω
		@ T_A = 85°C	85	Ω
m	Mass		18	g
	Standards		EN 50178: 1997	

Notes: [1] Measuring range limited to ± 60 A_{max}
[2] Measuring range limited to ± 55 A_{max}
[3] Result of the coercive field of the magnetic circuit.

Features

- Closed loop (compensated) current transducer using the Hall effect
- Printed circuit board mounting
- Isolated plastic case recognized according to UL 94-V0.

Advantages

- Excellent accuracy
- Very good linearity
- Low temperature drift
- Optimized response time
- Wide frequency bandwidth
- No insertion losses
- High immunity to external interference
- Current overload capability.

Applications

- AC variable speed drives and servo motor drives
- Static converters for DC motor drives
- Battery supplied applications
- Uninterruptible Power Supplies (UPS)
- Switched Mode Power Supplies (SMPS)
- Power supplies for welding applications.

Application domain

- Industrial.

Figure (B-1): Datasheet of current sensor LA55.

LEM

Voltage Transducer LV 25-P

For the electronic measurement of currents: DC, AC, pulsed..., with galvanic isolation between the primary circuit and the secondary circuit.

16084

Electrical data

I_{PN}	Primary nominal current rms		10		mA
I_{PM}	Primary current, measuring range		0 .. ± 14		mA
R_M	Measuring resistance		$R_{M\,min}$	$R_{M\,max}$	
	with ± 12 V	@ ± 10 mA $_{max}$	30	190	Ω
		@ ± 14 mA $_{max}$	30	100	Ω
	with ± 15 V	@ ± 10 mA $_{max}$	100	350	Ω
		@ ± 14 mA $_{max}$	100	190	Ω
I_{SN}	Secondary nominal current rms		25		mA
K_N	Conversion ratio		2500 : 1000		
V_C	Supply voltage (± 5 %)		± 12 .. 15		V
I_C	Current consumption		10 (@ ± 15 V) + I_S		mA

Accuracy - Dynamic performance data

X_G	Overall accuracy @ I_{PN}, T_A = 25°C	@ ± 12 .. 15 V	± 0.9		%
		@ ± 15 V (± 5 %)	± 0.8		%
ε_L	Linearity error		< 0.2		%
			Typ	Max	
I_O	Offset current @ I_P = 0, T_A = 25°C			± 0.15	mA
I_{OT}	Temperature variation of I_O	0°C .. + 25°C	± 0.06	± 0.25	mA
		+ 25°C .. + 70°C	± 0.10	± 0.35	mA
t_r	Response time [1] to 90 % of I_{PN} step		40		µs

General data

T_A	Ambient operating temperature		0 .. + 70	°C
T_S	Ambient storage temperature		- 25 .. + 85	°C
R_P	Primary coil resistance	@ T_A = 70°C	250	Ω
R_S	Secondary coil resistance	@ T_A = 70°C	110	Ω
m	Mass		22	g
	Standard		EN 50178: 1997	

Note: [1] R_t = 25 kΩ (L/R constant, produced by the resistance and inductance of the primary circuit).

I_{PN} = 10 mA

V_{PN} = 10 .. 500 V

Features

- Closed loop (compensated) current transducer using the Hall effect
- Isolated plastic case recognized according to UL 94-V0.

Principle of use

- For voltage measurements, a current proportional to the measured voltage must be passed through an external resistor R_1 which is selected by the user and installed in series with the primary circuit of the transducer.

Advantages

- Excellent accuracy
- Very good linearity
- Low thermal drift
- Low response time
- High bandwidth
- High immunity to external interference
- Low disturbance in common mode.

Applications

- AC variable speed drives and servo motor drives
- Static converters for DC motor drives
- Battery supplied applications
- Uninterruptible Power Supplies (UPS)
- Power supplies for welding applications.

Application domain

- Industrial.

Figure (B-2): Datasheet of voltage sensor LV25.

References

References

[1] R. Xiong, J. Cao, Q. Yu, H. He, and F. Sun, "Critical review on the battery state of charge estimation methods for electric vehicles," Ieee Access, vol. 6, pp. 1832-1843, 2017.

[2] K. Liu, K. Li, Q. Peng, and C. Zhang, "A brief review on key technologies in the battery management system of electric vehicles," Frontiers of Mechanical Engineering, vol. 14, pp. 47-64, 2019.

[3] N. Watrin, B. Blunier, and A. Miraoui, "Review of adaptive systems for lithium batteries state-of-charge and state-of-health estimation," in 2012 IEEE Transportation Electrification Conference and Expo (ITEC), 2012, pp. 1-6.

[4] N. Karami, "Control of a hybrid system based PEMFC and photovoltaic panels," PhD thesis, Aix-Marseille university, France, 2013.

[5] solar pv roof. Available: https://www.trayamtechnologies.com/solar-pv-roof-top-and-ground-mounting/

[6] A. Goetzberger and V. U. Hoffmann, Photovoltaic solar energy generation vol. 112: Springer Science & Business Media, 2005.

[7] B. Bhandari, K.-T. Lee, C. S. Lee, C.-K. Song, R. K. Maskey, and S.-H. Ahn, "A novel off-grid hybrid power system comprised of solar photovoltaic, wind, and hydro energy sources," Applied Energy, vol. 133, pp. 236-242, 2014.

[8] T. Markvart, A. McEvoy, and L. Castaner, Practical handbook of photovoltaics: fundamentals and applications: Elsevier, 2003.

[9] M. Girma, A. Assefa, and M. Molinas, "Feasibility study of a solar photovoltaic water pumping system for rural Ethiopia," AIMS Environmental Science, vol. 2, pp. 697-717, 2015.

[10] on grid pv system shceme. Available: http://www.apricus.com/solar-pv-systems-29/#.Xt4jIlUzbIU

[11] A. P. U. Siahaan, "Photovoltaic Design on Robotic Mobile Surveillance System in Saving Electricity," international Journal of Civil Engineering and Technology (IJCIET), vol. 9, pp. 2045-2053, 2018.

[12] B. K. S. Vastav, S. Nema, P. Swarnkar, and D. Rajesh, "Automatic solar tracking system using DELTA PLC," in 2016 International Conference on Electrical Power and Energy Systems (ICEPES), 2016, pp. 16-21.

[13] M. Louzazni, A. Crãciunescu, and A. Dumitrache, "Identification of Solar Cell Parameters with Firefly Algorithm," in 2015 Second International Conference on Mathematics and Computers in Sciences and in Industry (MCSI), 2015, pp. 7-12.

[14] N. F. A. Hamid, N. A. Rahim, and J. Selvaraj, "Solar cell parameters extraction using particle swarm optimization algorithm," in 2013 IEEE conference on clean energy and technology (CEAT), 2013, pp. 461-465.

[15] A. M. Humada, M. Hojabri, S. Mekhilef, and H. M. Hamada, "Solar cell parameters extraction based on single and double-diode models: A review," Renewable and Sustainable Energy Reviews, vol. 56, pp. 494-509, 2016.

[16] M. Jamadi, F. Merrikh-Bayat, and M. Bigdeli, "Very accurate parameter estimation of single-and double-diode solar cell models using a modified artificial bee colony algorithm," International Journal of Energy and Environmental Engineering, vol. 7, pp. 13-25, 2016.

[17] K. W. E. Cheng, B. Divakar, H. Wu, K. Ding, and H. F. Ho, "Battery-management system (BMS) and SOC development for electrical vehicles," IEEE transactions on vehicular technology, vol. 60, pp. 76-88, 2010.

[18] A. Poullikkas, "A comparative overview of large-scale battery systems for electricity storage," Renewable and Sustainable Energy Reviews, vol. 27, pp. 778-788, 2013.

[19] J. Garche, P. Moseley, and E. Karden, "Lead–acid batteries for hybrid electric vehicles and battery electric vehicles," in Advances in Battery Technologies for Electric Vehicles, ed: Elsevier, 2015, pp. 75-101.

[20] S. E. Sloop, J. B. Kerr, and K. Kinoshita, "The role of Li-ion battery electrolyte reactivity in performance decline and self-discharge," Journal of power sources, vol. 119, pp. 330-337, 2003.

[21] D. Linden, "Thomas. B Reddy, Handbook of Batteries," ed: McGraw Hill, New York, 2002.

[22] J. JONES, "Study of electrodes/elctrolyte interfaces and solubility phenomenons in the lithium-ion battery," Ph.D thesis, Ecole doctorale Santé, sciences, technologies (Tours), France, 2010.

[23] Y. Zhu, X. He, and Y. Mo, "First principles study on electrochemical and chemical stability of solid electrolyte–electrode interfaces in all-solid-state Li-ion batteries," Journal of Materials Chemistry A, vol. 4, pp. 3253-3266, 2016.

[24] I. Buchmann, "Batteries in a portable world. 2007," Richmond: Cadex Electronics, 2010.

[25] D. Pavlov, Lead-acid batteries: science and technology: Elsevier, 2011.

[26] D. Berndt and D. Berndt, Maintenance-free batteries: lead-acid, nickel/cadmium, nickel/metal hydride: a handbook of battery technology: Research Studies Press, 1997.

[27] A. Green, "The characteristics of the nickel-cadmium battery for energy storage," Power engineering journal, vol. 13, pp. 117-121, 1999.

[28] C. J. Rydh and M. Karlström, "Life cycle inventory of recycling portable nickel–cadmium batteries," Resources, Conservation and Recycling, vol. 34, pp. 289-309, 2002.

[29] T. P. Crompton, Battery reference book: Elsevier, 2000.

[30] G. Pistoia, Battery operated devices and systems: From portable electronics to industrial products: Elsevier, 2008.

[31] A. Jha, Next-generation batteries and fuel cells for commercial, military, and space applications: CRC Press, 2016.

[32] K. E. Aifantis, S. A. Hackney, and R. V. Kumar, High energy density lithium batteries: materials, engineering, applications: John Wiley & Sons, 2010.

[33] Z. Zhang and S. Zhang, "Rechargeable Batteries," Nature Communications, vol. 4, 2015.

[34] M. Yoshio, R. J. Brodd, and A. Kozawa, Lithium-ion batteries vol. 1. New York: Springer, 2009.

[35] J. Christensen, P. Albertus, R. S. Sanchez-Carrera, T. Lohmann, B. Kozinsky, R. Liedtke, J. Ahmed, and A. Kojic, "A critical review of Li/air batteries," Journal of the Electrochemical Society, vol. 159, pp. R1-R30, 2011.

[36] B. Scrosati, K. Abraham, W. A. van Schalkwijk, and J. Hassoun, Lithium batteries: advanced technologies and applications vol. 58: John Wiley & Sons, 2013.

[37] S. Park, A. Savvides, and M. B. Srivastava, "Battery capacity measurement and analysis using lithium coin cell battery," in ISLPED'01: Proceedings of the 2001 International Symposium on Low Power Electronics and Design (IEEE Cat. No. 01TH8581), 2001, pp. 382-387.

[38] O. Tremblay, L.-A. Dessaint, and A.-I. Dekkiche, "A generic battery model for the dynamic simulation of hybrid electric vehicles," in 2007 IEEE Vehicle Power and Propulsion Conference, 2007, pp. 284-289.

[39] L. Lu, X. Han, J. Li, J. Hua, and M. Ouyang, "A review on the key issues for lithium-ion battery management in electric vehicles," Journal of power sources, vol. 226, pp. 272-288, 2013.

[40] K. S. Ng, C.-S. Moo, Y.-P. Chen, and Y.-C. Hsieh, "Enhanced coulomb counting method for estimating state-of-charge and state-of-health of lithium-ion batteries," Applied energy, vol. 86, pp. 1506-1511, 2009.

[41] V. Pop, H. J. Bergveld, D. Danilov, P. P. Regtien, and P. H. Notten, "State-of-the-art of battery state-of-charge determination," Battery Management Systems: Accurate State-of-Charge Indication for Battery-Powered Applications, pp. 11-45, 2008.

[42] S. Watanabe, M. Kinoshita, T. Hosokawa, K. Morigaki, and K. Nakura, "Capacity fade of LiAlyNi1− x− yCoxO2 cathode for lithium-ion batteries during accelerated calendar and cycle life tests (surface analysis of LiAlyNi1− x− yCoxO2 cathode after

cycle tests in restricted depth of discharge ranges)," Journal of power sources, vol. 258, pp. 210-217, 2014.

[43] W. Shen, "Optimally sizing of solar array and battery in a standalone photovoltaic system in Malaysia," Renewable energy, vol. 34, pp. 348-352, 2009.

[44] B. S. Bhangu, P. Bentley, D. A. Stone, and C. M. Bingham, "Nonlinear observers for predicting state-of-charge and state-of-health of lead-acid batteries for hybrid-electric vehicles," IEEE transactions on vehicular technology, vol. 54, pp. 783-794, 2005.

[45] H. Rahimi-Eichi, U. Ojha, F. Baronti, and M.-Y. Chow, "Battery management system: An overview of its application in the smart grid and electric vehicles," IEEE Industrial Electronics Magazine, vol. 7, pp. 4-16, 2013.

[46] J. Alzieu, P. Gagnol, and H. Smimite, "Development of an on-board charge and discharge management system for electric-vehicle batteries," Journal of power sources, vol. 53, pp. 327-333, 1995.

[47] G. L. Plett, "Extended Kalman filtering for battery management systems of LiPB-based HEV battery packs: Part 3. State and parameter estimation," Journal of power sources, vol. 134, pp. 277-292, 2004.

[48] F. Zhong, H. Li, S. Zhong, Q. Zhong, and C. Yin, "An SOC estimation approach based on adaptive sliding mode observer and fractional order equivalent circuit model for lithium-ion batteries," Communications in Nonlinear Science and Numerical Simulation, vol. 24, pp. 127-144, 2015.

[49] G. L. Plett, "Sigma-point Kalman filtering for battery management systems of LiPB-based HEV battery packs: Part 2: Simultaneous state and parameter estimation," Journal of power sources, vol. 161, pp. 1369-1384, 2006.

[50] E. Koutroulis and K. Kalaitzakis, "Novel battery charging regulation system for photovoltaic applications," IEE Proceedings-Electric Power Applications, vol. 151, pp. 191-197, 2004.

[51] V. Pop, H. J. Bergveld, D. Danilov, P. P. Regtien, and P. H. Notten, Battery management systems: Accurate state-of-charge indication for battery-powered applications vol. 9: Springer Science & Business Media, 2008.

[52] L.-R. Chen, R. C. Hsu, and C.-S. Liu, "A design of a grey-predicted Li-ion battery charge system," IEEE Transactions on Industrial Electronics, vol. 55, pp. 3692-3701, 2008.

[53] A. Hoke, A. Brissette, D. Maksimović, A. Pratt, and K. Smith, "Electric vehicle charge optimization including effects of lithium-ion battery degradation," in 2011 IEEE Vehicle Power and Propulsion Conference, 2011, pp. 1-8.

[54] G. Sikha, P. Ramadass, B. Haran, R. E. White, and B. N. Popov, "Comparison of the capacity fade of Sony US 18650 cells charged with different protocols," Journal of power sources, vol. 122, pp. 67-76, 2003.

[55] J. Li, "Adaptive model-based state monitoring and prognostics for lithium-ion batteries," Ph.D thesis, University Ulm, Germany, 2016.

[56] Y.-M. Jeong, Y.-K. Cho, J.-H. Ahn, S.-H. Ryu, and B.-K. Lee, "Enhanced Coulomb counting method with adaptive SOC reset time for estimating OCV," in 2014 IEEE Energy Conversion Congress and Exposition (ECCE), 2014, pp. 1313-1318.

[57] L. Zhao, M. Lin, and Y. Chen, "Least-squares based coulomb counting method and its application for state-of-charge (SOC) estimation in electric vehicles," International Journal of Energy Research, vol. 40, pp. 1389-1399, 2016.

[58] A. Purwadi, A. Rizqiawan, A. Kevin, and N. Heryana, "State of Charge estimation method for lithium battery using combination of Coulomb Counting and Adaptive System with considering the effect of temperature," in The 2nd IEEE Conference on Power Engineering and Renewable Energy (ICPERE) 2014, 2014, pp. 91-95.

[59] S. Lee, J. Kim, J. Lee, and B. H. Cho, "The state and parameter estimation of an Li-ion battery using a new OCV-SOC concept," in 2007 IEEE Power Electronics Specialists Conference, 2007, pp. 2799-2803.

[60] Y. Zou, X. Hu, H. Ma, and S. E. Li, "Combined state of charge and state of health estimation over lithium-ion battery cell cycle lifespan for electric vehicles," Journal of power sources, vol. 273, pp. 793-803, 2015.

[61] Y. Xing, W. He, M. Pecht, and K. L. Tsui, "State of charge estimation of lithium-ion batteries using the open-circuit voltage at various ambient temperatures," Applied energy, vol. 113, pp. 106-115, 2014.

[62] J. Zhang, Y. Tang, C. Song, J. Zhang, and H. Wang, "PEM fuel cell open circuit voltage (OCV) in the temperature range of 23 C to 120 C," Journal of power sources, vol. 163, pp. 532-537, 2006.

[63] R. Van Der Merwe, E. Wan, and S. Julier, "Sigma-point Kalman filters for nonlinear estimation and sensor-fusion: Applications to integrated navigation," in AIAA Guidance, Navigation, and Control Conference and Exhibit, 2004, p. 5120.

[64] F. Yang, Y. Xing, D. Wang, and K.-L. Tsui, "A comparative study of three model-based algorithms for estimating state-of-charge of lithium-ion batteries under a new combined dynamic loading profile," Applied energy, vol. 164, pp. 387-399, 2016.

[65] N. Omar, P. Bossche, T. Coosemans, and J. Mierlo, "Peukert revisited—Critical appraisal and need for modification for lithium-ion batteries," energies, vol. 6, pp. 5625-5641, 2013.

[66] J. Meng, G. Luo, and F. Gao, "Lithium polymer battery state-of-charge estimation based on adaptive unscented Kalman filter and support vector machine," IEEE Transactions on Power Electronics, vol. 31, pp. 2226-2238, 2015.

[67] H. He, R. Xiong, X. Zhang, F. Sun, and J. Fan, "State-of-charge estimation of the lithium-ion battery using an adaptive extended Kalman filter based on an improved Thevenin model," IEEE transactions on vehicular technology, vol. 60, pp. 1461-1469, 2011.

[68] Y. Xiong and M. Saif, "Sliding mode observer for nonlinear uncertain systems," IEEE transactions on automatic control, vol. 46, pp. 2012-2017, 2001.

[69] I.-S. Kim, "The novel state of charge estimation method for lithium battery using sliding mode observer," Journal of power sources, vol. 163, pp. 584-590, 2006.

[70] I.-S. Kim, "Nonlinear state of charge estimator for hybrid electric vehicle battery," IEEE Transactions on Power Electronics, vol. 23, pp. 2027-2034, 2008.

[71] X. Chen, W. Shen, Z. Cao, and A. Kapoor, "A novel approach for state of charge estimation based on adaptive switching gain sliding mode observer in electric vehicles," Journal of power sources, vol. 246, pp. 667-678, 2014.

[72] D. Kim, K. Koo, J. Jeong, T. Goh, and S. Kim, "Second-order discrete-time sliding mode observer for state of charge determination based on a dynamic resistance Li-ion battery model," Energies, vol. 6, pp. 5538-5551, 2013.

[73] X. Liu, Z. Chen, C. Zhang, and J. Wu, "A novel temperature-compensated model for power Li-ion batteries with dual-particle-filter state of charge estimation," Applied energy, vol. 123, pp. 263-272, 2014.

[74] F. Gustafsson, F. Gunnarsson, N. Bergman, U. Forssell, J. Jansson, R. Karlsson, and P.-J. Nordlund, "Particle filters for positioning, navigation, and tracking," IEEE Transactions on signal processing, vol. 50, pp. 425-437, 2002.

[75] Q. Miao, L. Xie, H. Cui, W. Liang, and M. Pecht, "Remaining useful life prediction of lithium-ion battery with unscented particle filter technique," Microelectronics Reliability, vol. 53, pp. 805-810, 2013.

[76] M. Ye, H. Guo, and B. Cao, "A model-based adaptive state of charge estimator for a lithium-ion battery using an improved adaptive particle filter," Applied energy, vol. 190, pp. 740-748, 2017.

[77] D. Liu, X. Yin, Y. Song, W. Liu, and Y. Peng, "An on-line state of health estimation of lithium-ion battery using unscented particle filter," Ieee Access, vol. 6, pp. 40990-41001, 2018.

[78] G. Didinsky, Z. Pan, and T. Başar, "Parameter identification for uncertain plants using H∞ methods," Automatica, vol. 31, pp. 1227-1250, 1995.

[79] W.-J. Yang, D.-H. Yu, and Y.-B. Kim, "Parameter estimation of lithium-ion batteries and noise reduction using an H∞ filter," Journal of Mechanical Science and Technology, vol. 27, pp. 247-256, 2013.

[80] R. Xiong, Q. Yu, L. Y. Wang, and C. Lin, "A novel method to obtain the open circuit voltage for the state of charge of lithium ion batteries in electric vehicles by using H infinity filter," Applied energy, vol. 207, pp. 346-353, 2017.

[81] C. Lin, H. Mu, R. Xiong, and W. Shen, "A novel multi-model probability battery state of charge estimation approach for electric vehicles using H-infinity algorithm," Applied energy, vol. 166, pp. 76-83, 2016.

[82] Y. Zhang, R. Xiong, H. He, and W. Shen, "Lithium-ion battery pack state of charge and state of energy estimation algorithms using a hardware-in-the-loop validation," IEEE Transactions on Power Electronics, vol. 32, pp. 4421-4431, 2016.

[83] L. Zheng, L. Zhang, J. Zhu, G. Wang, and J. Jiang, "Co-estimation of state-of-charge, capacity and resistance for lithium-ion batteries based on a high-fidelity electrochemical model," Applied energy, vol. 180, pp. 424-434, 2016.

[84] Z. Wei, S. Meng, B. Xiong, D. Ji, and K. J. Tseng, "Enhanced online model identification and state of charge estimation for lithium-ion battery with a FBCRLS based observer," Applied energy, vol. 181, pp. 332-341, 2016.

[85] J. Xu, C. C. Mi, B. Cao, J. Deng, Z. Chen, and S. Li, "The state of charge estimation of lithium-ion batteries based on a proportional-integral observer," IEEE Transactions on Vehicular Technology, vol. 63, pp. 1614-1621, 2013.

[86] T. Zhao, J. Jiang, C. Zhang, L. Zheng, and F. Wen, "Error analysis of SOC estimation based on PI observer," in 2014 IEEE Conference and Expo Transportation Electrification Asia-Pacific (ITEC Asia-Pacific), 2014, pp. 1-5.

[87] S. Haykin, Kalman filtering and neural networks vol. 47: John Wiley & Sons, 2004.

[88] D. Andre, A. Nuhic, T. Soczka-Guth, and D. U. Sauer, "Comparative study of a structured neural network and an extended Kalman filter for state of health determination of lithium-ion batteries in hybrid electricvehicles," Engineering Applications of Artificial Intelligence, vol. 26, pp. 951-961, 2013.

[89] A. A. Hussein, "Kalman filters versus neural networks in battery state-of-charge estimation: A comparative study," International Journal of Modern Nonlinear Theory and Application, vol. 3, p. 199, 2014.

[90] M. A. Hannan, M. H. Lipu, A. Hussain, and A. Mohamed, "A review of lithium-ion battery state of charge estimation and management system in electric vehicle applications: Challenges and recommendations," Renewable and Sustainable Energy Reviews, vol. 78, pp. 834-854, 2017.

[91] J. Á. Antón, P. G. Nieto, F. de Cos Juez, F. S. Lasheras, M. G. Vega, and M. R. Gutiérrez, "Battery state-of-charge estimator using the SVM technique," Applied Mathematical Modelling, vol. 37, pp. 6244-6253, 2013.

[92] Y. Chen, B. Long, and X. Lei, "The battery state of charge estimation based weighted least squares support vector machine," in 2011 Asia-Pacific Power and Energy Engineering Conference, 2011, pp. 1-4.

[93] P. Singh, R. Vinjamuri, X. Wang, and D. Reisner, "Design and implementation of a fuzzy logic-based state-of-charge meter for Li-ion batteries used in portable defibrillators," Journal of Power Sources, vol. 162, pp. 829-836, 2006.

[94] H. Dai, P. Guo, X. Wei, Z. Sun, and J. Wang, "ANFIS (adaptive neuro-fuzzy inference system) based online SOC (State of Charge) correction considering cell divergence for the EV (electric vehicle) traction batteries," Energy, vol. 80, pp. 350-360, 2015.

[95] X. Lai, Y. Zheng, and T. Sun, "A comparative study of different equivalent circuit models for estimating state-of-charge of lithium-ion batteries," Electrochimica Acta, vol. 259, pp. 566-577, 2018.

[96] G. Liu, L. Lu, H. Fu, J. Hua, J. Li, M. Ouyang, Y. Wang, S. Xue, and P. Chen, "A comparative study of equivalent circuit models and enhanced equivalent circuit models of lithium-ion batteries with different model structures," in 2014 IEEE Conference and Expo Transportation Electrification Asia-Pacific (ITEC Asia-Pacific), 2014, pp. 1-6.

[97] H. He, R. Xiong, and J. Fan, "Evaluation of lithium-ion battery equivalent circuit models for state of charge estimation by an experimental approach," energies, vol. 4, pp. 582-598, 2011.

[98] C. Zhang, W. Allafi, Q. Dinh, P. Ascencio, and J. Marco, "Online estimation of battery equivalent circuit model parameters and state of charge using decoupled least squares technique," Energy, vol. 142, pp. 678-688, 2018.

[99] K. B. Hatzell, A. Sharma, and H. K. Fathy, "A survey of long-term health modeling, estimation, and control of lithium-ion batteries: Challenges and opportunities," in 2012 American Control Conference (ACC), 2012, pp. 584-591.

[100] S. J. Moura, N. A. Chaturvedi, and M. Krstic, "PDE estimation techniques for advanced battery management systems—Part I: SOC estimation," in 2012 American Control Conference (ACC), 2012, pp. 559-565.

[101] L. Zheng, "Development of lithium-ion battery state estimation techniques for battery management systems," Ph.D thesis, University of Technology Sydney, Australia, 2018.

[102] B. Tjaden, S. J. Cooper, D. J. Brett, D. Kramer, and P. R. Shearing, "On the origin and application of the Bruggeman correlation for analysing transport phenomena in electrochemical systems," Current Opinion in Chemical Engineering, vol. 12, pp. 44-51, 2016.

[103] S. J. Moura, M. Krstic, and N. A. Chaturvedi, "Adaptive PDE observer for battery SOC/SOH estimation," in 2012 ASME Dynamic Systems and Control Conference, 2012.

[104] B. Xiong, J. Zhao, Z. Wei, and M. Skyllas-Kazacos, "Extended Kalman filter method for state of charge estimation of vanadium redox flow battery using thermal-dependent electrical model," Journal of Power Sources, vol. 262, pp. 50-61, 2014.

[105] H. E. Perez, J. B. Siegel, X. Lin, A. G. Stefanopoulou, Y. Ding, and M. P. Castanier, "Parameterization and validation of an integrated electro-thermal cylindrical lfp battery model," in ASME 2012 5th Annual Dynamic Systems and Control Conference joint with the JSME 2012 11th Motion and Vibration Conference, 2012, pp. 41-50.

[106] A. A.-H. Hussein and I. Batarseh, "An overview of generic battery models," in 2011 IEEE Power and Energy Society General Meeting, 2011, pp. 1-6.

[107] A. R. Utomo, F. Husnayain, and P. S. Priambodo, "Analysis of Lead Acid battery operation based on Peukert formula," in 2014 International Conference on Electrical Engineering and Computer Science (ICEECS), 2014, pp. 345-348.

[108] S. Dorin, P. D. Dan, and R. Tirnovan, "Method for determining the effective capacity variation depending on the discharge current for lead-acid calcium batteries," in 2013 8TH INTERNATIONAL SYMPOSIUM ON ADVANCED TOPICS IN ELECTRICAL ENGINEERING (ATEE), 2013, pp. 1-6.

[109] H. He, X. Zhang, R. Xiong, Y. Xu, and H. Guo, "Online model-based estimation of state-of-charge and open-circuit voltage of lithium-ion batteries in electric vehicles," Energy, vol. 39, pp. 310-318, 2012.

[110] V. Johnson, "Battery performance models in ADVISOR," Journal of Power Sources, vol. 110, pp. 321-329, 2002.

[111] F. Altiparmak, M. Gen, L. Lin, and T. Paksoy, "A genetic algorithm approach for multi-objective optimization of supply chain networks," Computers & industrial engineering, vol. 51, pp. 196-215, 2006.

[112] J. Chiasson and B. Vairamohan, "Estimating the state of charge of a battery," in Proceedings of the 2003 American Control Conference, 2003., 2003, pp. 2863-2868.

[113] M. Daowd, N. Omar, B. Verbrugge, P. Van Den Bossche, and J. Van Mierlo, "Battery models parameter estimation based on MATLAB/Simulink®," in Proceedings of the 25th Electric Vehicle Symposium (EVS-25), Shenzhen, China, 2010.

[114] P. Nelson, I. Bloom, K. Amine, and G. Henriksen, "Design modeling of lithium-ion battery performance," Journal of Power Sources, vol. 110, pp. 437-444, 2002.

[115] X. Dang, L. Yan, K. Xu, X. Wu, H. Jiang, and H. Sun, "Open-circuit voltage-based state of charge estimation of lithium-ion battery using dual neural network fusion battery model," Electrochimica Acta, vol. 188, pp. 356-366, 2016.

[116] H. Wang, G. Li, M. Li, Z. Jiang, X. Wang, and Q. Zhao, "Third-order dynamic model of a lead acid battery for use in fuel cell vehicle simulation," in 2011 International Conference on Mechatronic Science, Electric Engineering and Computer (MEC), 2011, pp. 715-720.

[117] L. W. Yao, A. Wirun, J. Aziz, and T. Sutikno, "Battery state of charge estimation with extended Kalman filter using third order Thevenin model," Telkomnika, vol. 13, p. 401, 2015.

[118] S. Yuan, H. Wu, and C. Yin, "State of charge estimation using the extended Kalman filter for battery management systems based on the ARX battery model," energies, vol. 6, pp. 444-470, 2013.

[119] J. Gao, Y. Zhang, and H. He, "A real-time joint estimator for model parameters and state of charge of lithium-ion batteries in electric vehicles," energies, vol. 8, pp. 8594-8612, 2015.

[120] T. Ting, K. L. Man, E. G. Lim, and M. Leach, "Tuning of Kalman filter parameters via genetic algorithm for state-of-charge estimation in battery management system," The Scientific World Journal, vol. 2014, 2014.

[121] T. Ting, K. L. Man, C.-U. Lei, and C. Lu, "State-of-Charge for Battery Management System via Kalman Filter," Engineering Letters, vol. 22, 2014.

[122] L.-R. Dung, H.-F. Yuan, J.-H. Yen, C.-H. She, and M.-H. Lee, "A lithium-ion battery simulator based on a diffusion and switching overpotential hybrid model for dynamic discharging behavior and runtime predictions," energies, vol. 9, p. 51, 2016.

[123] B. Ristic, S. Arulampalam, and N. Gordon, "Beyond the Kalman filter," IEEE Aerospace and Electronic Systems Magazine, vol. 19, pp. 37-38, 2004.

[124] R. G. Brown and P. Y. Hwang, Introduction to random signals and applied Kalman filtering vol. 3: Wiley New York, 1992.

[125] Y. Guo, Z. Zhao, and L. Huang, "SoC estimation of lithium battery based on AEKF algorithm," Energy Procedia, vol. 105, pp. 4146-4152, 2017.

[126] Z.-L. Zhang, X. Cheng, Z.-Y. Lu, and D.-J. Gu, "SOC estimation of lithium-ion batteries with AEKF and wavelet transform matrix," IEEE Transactions on Power Electronics, vol. 32, pp. 7626-7634, 2016.

[127] X. Wang, J. Xu, and Y. Zhao, "Wavelet based denoising for the estimation of the state of charge for lithium-ion batteries," energies, vol. 11, p. 1144, 2018.

[128] B. Ning, S. Cheng, and Y. Qin, "Direct torque control of PMSM using sliding mode backstepping control with extended state observer," Journal of Vibration and Control, vol. 24, pp. 694-707, 2018.

[129] T. Floquet, "Contributions à la commande par modes glissants d'ordre supérieur," Lille 1, 2000.

[130] J. Liu and X. Wang, Advanced sliding mode control for mechanical systems: Springer, 2012.

[131] T. Li, S. Sun, and T. P. Sattar, "High-speed Sigma-gating SMC-PHD filter," Signal Processing, vol. 93, pp. 2586-2593, 2013.

[132] J.-J. E. Slotine and W. Li, Applied nonlinear control vol. 199: Prentice hall Englewood Cliffs, NJ, 1991.

[133] O. Assia, T. Riad, and D. Djalel, "Contribution to study Performance of the Induction Motor by Sliding Mode Control and Field Oriented Control," Proceedings-Copyright IPCO, pp. 26-31, 2014.

[134] D. Shevitz and B. Paden, "Lyapunov stability theory of nonsmooth systems," IEEE Transactions on automatic control, vol. 39, pp. 1910-1914, 1994.

[135] V. Srikanth and A. A. Dutt, "A comparative study on the effect of switching functions in SMO for PMSM drives," in 2012 IEEE International Conference on Power Electronics, Drives and Energy Systems (PEDES), 2012, pp. 1-6.

[136] Z. Xu and M. Rahman, "Comparison of a sliding observer and a Kalman filter for direct-torque-controlled IPM synchronous motor drives," IEEE Transactions on Industrial Electronics, vol. 59, pp. 4179-4188, 2012.

[137] A. Khlaief, "Contribution à la commande vectorielle sans capteur mécanique des machines synchrones à aimants permanents (MSAP)," PhD thesis, Aix-Marseille University, France, 2012.

[138] C.-M. Lin and Y.-J. Mon, "Decoupling control by hierarchical fuzzy sliding-mode controller," IEEE Transactions on Control Systems Technology, vol. 13, pp. 593-598, 2005.

[139] T. Kamel, D. Abdelkader, B. Said, S. Padmanaban, and A. Iqbal, "Extended Kalman filter based sliding mode control of parallel-connected two five-phase PMSM drive system," Electronics, vol. 7, p. 14, 2018.